Escola de Camins
Escola Tècnica Superior d'Enginyeria de Camins, Canals i Ports
UPC BARCELONATECH

PROJECTE O TESINA D'ESPECIALITAT

Títol

Study on the application of the CSM to stainless steel cross-sections under compression and biaxial bending

Autor/a

Antonio Sastre Segui

Tutor/a

Esther Real Saladrigas

Itsaso Arrayago Luquin

Departament

Enginyeria de la Construcció

Intensificació

Anàlisi i Projecte d'Estructures

Data

Juny 2014

Acknowledgements

First and foremost I offer my sincerest gratitude to my tutors, Professor Esther Real and Itsaso Arrayago, who have supported me throughout this research project with their patience and knowledge while allowing me the opportunity to awake my interest for research. Without them, this work would not have been possible. One simply could not wish better or friendlier tutors.

I also offer my sincerest gratitude to Marina Bock, for her enthusiasm, her persistence and her invaluable help during the elaboration of this document.

In the laboratory I have been aided by Tomàs Garcia and Carlos Hurtado, fine technicians whom taught me all about laboratories.

I would like to dedicate this work to my family, for their unconditional support along the journey which finally comes to an end.

Thank you very much, without you this work would not have been possible.

Antonio Sastre

Index

Abstract

Tittle: Study on the application of the CSM to stainless steel cross-sections under compression and biaxial bending

Autor: Antonio Sastre Seguí

Tutors: Esther Real Saladrigas, Itsaso Arrayago Luquin

Keywords: ferritic stainless steel, continuous strength method, combined loading, CSM

Stainless steel is nowadays being investigated as a structural material for construction, which presents a combination of good mechanical properties and excellent corrosion resistance. The price of ferritic stainless steel is stable due to its low nickel content whilst still maintaining good mechanical properties. New design methods and expressions, as the Continuous Strength Method (CSM), have been developed in order to consider the increase of resistance due to strain hardening presented in all the stainless steels. These new methods have been calibrated for the most common type of stainless steel: the austenitic. This research project wants to find out if these new analytical expressions could be used for the ferritic stainless steel and which of these existent expressions fits better its behaviour.

To tackle this problem, some stub-column experimental tests were performed and several numerical models developed in order to compare their results with the predicted ones from the existing standards and new proposals. This research project discusses the applicability of the existing European standards and new analytical proposals comparing the results obtained from some experimental tests conducted in ferritic stainless steel elements. It also compares analytical results with the ones obtained from numerical simulations. The loading cases that have been studied are: the resistant axial load, the resistant bending moment for both axis and the interaction between these three simple loading cases.

In conclusion, the CSM is the method that provides better results comparing to the numerical ones when talking about simple resistances: axial force and bending moment. When it comes to the interaction, the EN 1993-1-4 interaction expression, with the fundamental capacities derived from the CSM instead of the plastic ones, is the one that covers better each one of the twelve different cross-sections interaction results.

Resumen

El acero inoxidable está siendo actualmente investigado como material estructural para la construcción, el cual presenta una interesante combinación de buenas propiedades mecánicas y una excelente resistencia a la corrosión. El precio del acero inoxidable ferrítico es estable en el mercado debido a su bajo contenido en Níquel mientras que sus propiedades mecánicas siguen siendo más que aceptables. Nuevos métodos y expresiones de diseño, como el Continuous Strength Method (CSM), han sido desarrollados para poder considerar el incremento de resistencia debido al endurecimiento por deformación que se manifiesta en el acero inoxidable. Estos métodos han sido calibrados para el acero inoxidable más común: el austenítico. Este documento de investigación quiere averiguar si estos nuevos analíticos podrían ser usados para el acero inoxidable ferrítico y cuál de ellos se ajusta mejor a su comportamiento.

Para abordar este problema, se han realizado varios ensayos experimentales en laboratorio de compresión simple centrada, además de desarrollar un elevado número de modelos numéricos con el fin de comparar sus resultados con los que se predicen a partir de los métodos analíticos existentes en las actuales Normas y nuevas propuestas. De esta manera se podrán sacar conclusiones y decidir cuál de los métodos analíticos existentes reproducen mejor el comportamiento del acero inoxidable ferrítico. Los diferentes casos de carga estudiados en los modelos numéricos y métodos analíticos son los siguientes: compresión simple centrada, flexo-compresión en un eje, flexo-compresión en dos ejes, flexión simple y flexión compuesta.

En conclusión, el CSM es el método que proporciona los mejores resultados comparado con los resultados numéricos, cuando nos referimos a las resistencias básicas: compresión simple y flexión simple. Cuando nos referimos a la interacción de esfuerzos, la expresión de interacción que incluye EN 1993-1-4, evaluada a partir de las resistencias básicas calculadas por medio del CSM, es el método que cubre mejor la casuística de las diferentes secciones transversales que se estudian en este trabajo de investigación.

1. Introduction

Current situation

Stainless steel is a relatively new metallic material which presents a combination of good mechanical properties and excellent corrosion resistance. It has been used for several different purposes but not for structural applications due to its complex nonlinear behaviour, very different from carbon steel.

Ferritic stainless steels represent one of the five stainless steel families, with very low nickel content. Nickel is an element whose price is reaching unprecedented levels and suffers continuous fluctuations in market. This makes ferritic stainless steel an attractive material due to its lower and stable price against the austenitic ones, while preserving the mechanical and corrosion resistances.

The classical approach for the determination of the cross-section resistance due to local buckling of stocky cross-sections based on section classification underestimates real capacities when nonlinear metallic materials with high strain hardening are analysed. Alternatively, a more efficient design approach has been developed during last years, the Continuous Strength Method (CSM), based on the cross-section deformation capacity. The expressions for the determination of the axial and bending capacities of cross-sections according to the CSM have been widely analysed.

The use of stainless steel for structural purposes in construction has been continuously increasing due to its corrosion resistance, appropriate mechanical properties and aesthetic appearance. Considering that stainless steel needs a higher initial investment than carbon steel and is characterized by high nonlinear stress-strain behaviour with important strain hardening, the CSM can be considered a suitable design approach to exploit the features of this material.

The assessment of the CSM has already been studied for austenitic and duplex stainless steel stocky cross-sections subjected to either axial compression or bending moment, the corresponding expressions have been developed and recent research has also studied the assessment of these expressions to ferritic grades. In order to extend the applicability of the CSM to more general loading conditions, this work document presents a preliminary study on the determination of the ultimate resistance of ferritic stainless steel rectangular and square hollow sections (RHS and SHS) under combined axial compression and bending moment. Interaction equations proposed in EN 1993-1-4 [4] and the literature are analysed in order to determine the most appropriate approach.

Objectives

One part of the aforementioned work is focused on obtaining numerical results from ABAQUS finite element software. Four different numerical models are presented and analysed: stub-column (N), combined loading ($N+M_y+M_z$), uniaxial bending moment (M) and biaxial bending moment (M_y+M_z).

Another part is based on obtaining the analytical results. The expressions codified in EN 1993-1-4 and the CSM have been used to obtain the basic simple resistances: the ultimate axial load and the ultimate bending moment. Then, these basic resistances have been used to evaluate and verify the different interaction expressions presented and analysed in this research work: EN 1993-1-4[4], EN 1993-1-4 with Theofanous & Gardner[17] cross-section classification and the two expressions proposed by Theofanous [25] for austenitic stainless steel.

Finally, an experimental programme has been carried out during the elaboration of this work. The real dimensions of almost 70 specimens have been measured, and initial local imperfections of those elements have also been measured. Some tensile tests have been carried out in flat and corner coupons extracted from the cross-sections in order to accurately determine the stress-strain behaviour of the analysed sections. A detailed experimental programme consisting on stub column tests in rectangular and square hollow sections (RHS and SHS respectively) was developed in the "Laboratori de Tecnologia d'Estructures del Departament d'Enginyeria de la Construcció" for the determination of the ultimate axial compression resistances of the different cross-sections. These experimental results permit us to realize a more complete and robust analysis of the results and compare them with the numerical simulations for a better calibration of the models. The experimental ultimate capacities have also been compared with the EN 1993-1-4 and CSM predictions with the aim of assessing their applicability and accuracy for the analysed cross-sections.

Once all different types of results have been obtained, it is possible to proceed with the calculation of the comparison ratios. These dimensionless ratios are values that can be interpreted as how close the analytical expression is from the numerical one. In the case of stub-column test, the analytical expression can be compared to the experimental ones.

Besides these ratios, all numerical results have been plotted in their respective two dimensional graphs which include the different interaction expressions in order to have a visual comparison from where global conclusions can be extract, unlike ratios conclusions that are more punctual.

Content of the work

Section 2 presents a brief description of the literature review for stainless steel in general and ferritic stainless steel in particular and RHS & SHS profiles. It also provides a summary of the existing design standards and new interaction design expressions proposals as well as a complete description of the Continuous Strength Method (CSM).

Section 3 summarizes the numerical results obtained from ABAQUS numerical models. It also contains the explanation and presentation of the geometries and material chosen for the analysis. Furthermore, in this section the description of the main aspects that present numerical models for each loading case are included and have been calibrated against experimental results.

The main objectives and working plan are gathered in section 4, presenting the analytical results and the comparison between them and the numerical ones obtained along section 3, using ratios and graphs from where conclusions have been extracted and then presented.

Section 5 contains the explanation of the experimental programme of the stub-column test. It presents the material testing, the process followed when measuring the geometry, the instrumentation of the elements, the stub-column experimental test process explanation and finally, the experimental results and the comparison ratios in order to extract conclusions are shown.

All conclusions obtained along this research project are presented in section 6 in a more synthesized and compact way.

2. State of Art

In this section will be explained shortly what stainless steel is. As this research work is about ferritic stainless steel concretely, a more detailed explanation of it will be done in order to help to understand its behaviour and the reason of the analysis tools used herein.

2.1 Stainless steel

First of all will be described what stainless steel is, which elements are part of it and their contribution to the general behaviour of the material. This is necessary to understand where the ferritic category of stainless steel comes from and its properties.

Stainless steel is used to describe an extremely versatile family of engineering materials, which are selected primarily because of their corrosion and heat resistant properties. All stainless steels contain principally iron and a minimum of 10.5% chromium. Chromium reacts with oxygen and humidity in the environment to form a protective, adherent and coherent, oxide film that envelops the entire surface of the material. This oxide film (known as the passive or boundary layer) is very thin (2-3 nanometres).

The passive layer on stainless steels exhibits a truly remarkable property: when damaged (e.g. abraded), it self-repairs as chromium in the steel reacts rapidly with oxygen and humidity in the environment to reform the oxide layer. If the content of chromium is increased beyond the minimum (10.5%), a greater corrosion resistance will be achieved. Adding an 8% or more of nickel, this resistance may be further improved, and a wide range of properties provided. The addition of molybdenum further increases corrosion resistance (in particular, resistance to pitting corrosion), while nitrogen increases mechanical strength and enhances pitting resistance.

The selection of a particular type of stainless steel will depend on what requirements a particular application poses. Environment, expected part life and extent of acceptable corrosion all help determine what type of stainless steel to use. In most cases, the primary factor is corrosion resistance, followed by tarnish and oxidation resistance. Other factors include the ability to withstand pitting, crevice corrosion and intergranular attack. The austenitic/higher chromium stainless steel, usually required in very high or very low temperatures, are generally more corrosion resistant than the lower chromium ferritic or martensitic stainless steels.

2.1.1 Types of stainless steels

The stainless steel family has several branches, which may be differentiated in a variety of ways: in terms of their areas of application, by the alloying elements used in their production, or, perhaps the most accurate way, by the metallurgical phases present in their microscopic structures: ferritic, martensitic, austenitic and duplex steels (these last ones consist of mixture of ferrite and austenite crystalline structures).

Within each of these groups, there are several “grades” of stainless steel defined according to their compositional ranges. These compositional ranges are defined in European and USA standards (between others), and within the specified range, the stainless steel grade will

exhibit a wide range of properties (as can be corrosion resistance, heat resistance or machinability). More detail on standards and grades is given below.

Ferritic stainless steels (e.g. grades 1.4512, 1.4016 and 1.4003 which will be used in this research work) consist of chromium (typically 12.5% or 17%) and iron. Ferritic stainless steels are essentially nickel-free (this is an important advantage front the rest of stainless steel grades for structural use). These materials contain very little carbon and are non-heat treatable, but exhibit superior corrosion resistance than martensitic stainless steels and possess good resistance to oxidation. They are ferromagnetic and, although subject to an impact transition (i.e. become brittle) at low temperatures, possess adequate formability. Their thermal expansion and other thermal properties are similar to conventional steels, but with higher fire resistance in general (in fact, all types of stainless steel are better than carbon steel when talking about fire). Ferritic stainless steels are readily welded in thin sections, but suffer grain growth with consequential loss of properties when welded in thicker sections.

Martensitic stainless steels (e.g. grades 1.4006, 1.4028 and 1.4112) consist of carbon (0.2-1.0%), chromium (10.5-18%) and iron. These materials may be heat treated, in a similar manner to conventional steels, to provide a range of mechanical properties, but offer higher hardenability and have different heat treatment temperatures. Their corrosion resistance may be described as moderate (i.e. their corrosion performance is poorer than other stainless steels of the same chromium and alloy content). They are ferromagnetic, subject to an impact transition at low temperatures and possess poor formability. Their thermal expansion and other thermal properties are similar to conventional steels. They may be welded with caution, but cracking can be a feature when matching filler metals are used.

Austenitic stainless steels (e.g. grades 1.4301 and 1.4833) consist of chromium (16-26%), nickel (6-12%) and iron. Other alloying elements (e.g. molybdenum) may be added or modified according to the desired properties that are defined in the standards (e.g. 1.4404) to produce derivative grades. The austenitic group contains more grades that are used in greater quantities, than any other type of stainless steel. Austenitic stainless steels exhibit superior corrosion resistance to both ferritic and martensitic stainless steels. Corrosion performance may be varied to suit a wide range of service environments by careful alloy adjustment e.g. by varying the carbon or molybdenum content. These materials cannot be hardened by heat treatment and are strengthened by work-hardening. They offer excellent formability and their response to deformation can be controlled by chemical composition. They are not subject to an impact transition at low temperatures and possess high toughness to cryogenic temperatures. They exhibit greater thermal expansion and heat capacity, with lower thermal conductivity than other stainless or conventional steels. They are generally readily welded, but care is required in the selection of consumables and practices for more highly alloyed grades. Austenitic stainless steels are often described as non-magnetic, but may become slightly magnetic when machined or worked.

Duplex stainless steels (e.g. grade 1.4462) consist of chromium (18-26%) nickel (4-7%), molybdenum (0-4%), copper and iron. These stainless steels have a microstructure consisting of austenite and ferrite, which provides a combination of the corrosion resistance of austenitic stainless steels with greater strength. Duplex stainless steels are weldable, but care must be

exercised to maintain the correct balance of austenite and ferrite. They are ferromagnetic and subject to an impact transition at low temperatures. Their thermal expansion lies between that of austenitic and ferritic stainless steels, while other thermal properties are similar to plain carbon steels. Formability is reasonable, but higher forces than those used for austenitic stainless steels are required.

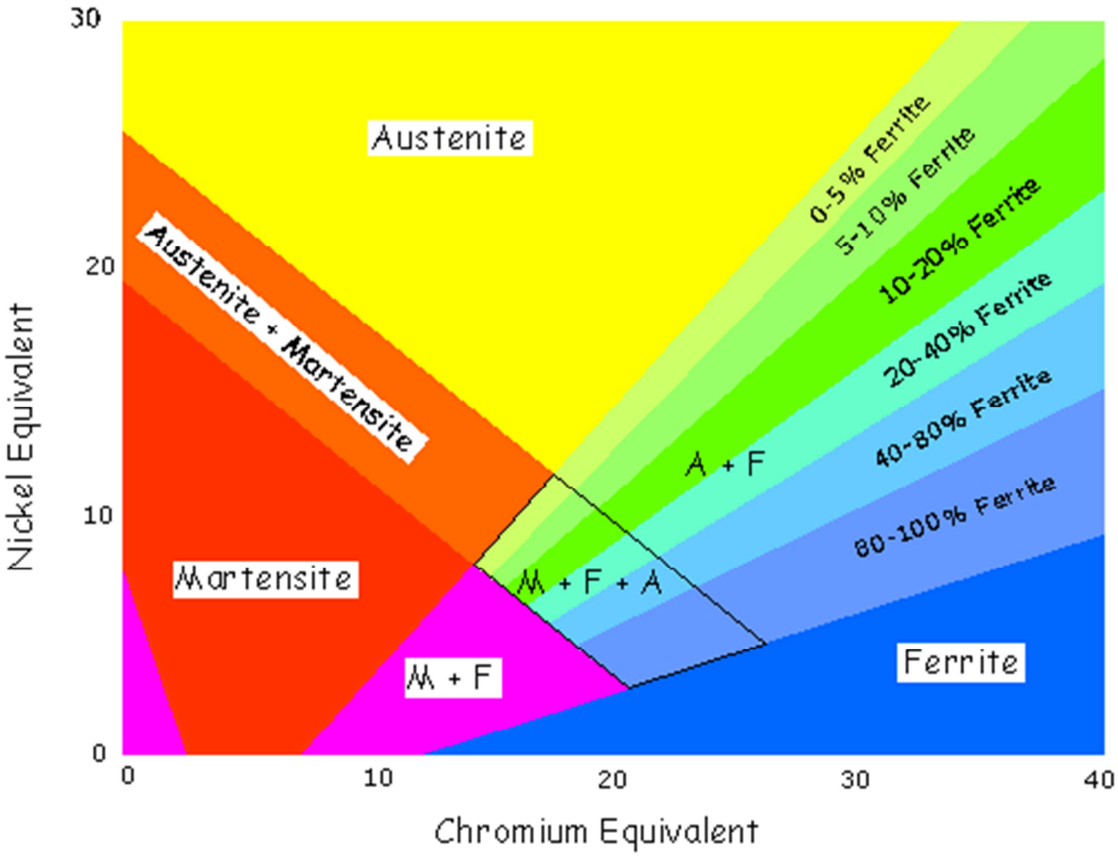

Figure 1. Stainless steel phase diagram[1]

2.1.2 Effect of each alloying element on structure and properties

In this section how each of the alloying elements contribute to the global behaviour of the stainless steel will be explained and what would happen if his content is varied.

CHROMIUM

Chromium is by far the most important alloying element in stainless steel production. A minimum of 10.5% chromium is required for the formation of a protective layer of chromium oxide on the steel surface. The strength of this protective (passive) layer increases with increasing chromium content. Chromium prompts the formation of ferrite within the alloy structure and is described as ferrite stabiliser.

NICKEL

Nickel improves general corrosion resistance and prompts the formation of austenite (i.e. it is an austenite stabiliser). Stainless steels with 8-9% nickel have a fully austenitic structure and exhibit superior welding and working characteristics to ferritic stainless steels. Increasing nickel

content beyond 8-9% further improves both corrosion resistance (especially in acid environments) and workability, as has been said before.

MOLYBDENUM (AND TUNGSTEN)

Molybdenum increases resistance to both local (pitting, crevice corrosion, etc.) and general corrosion. Molybdenum and tungsten are ferrite stabilisers which, when used in austenitic alloys, must be balanced with austenite stabilisers in order to maintain the austenitic structure. Molybdenum is added to martensitic stainless steels to improve high temperature strength.

NITROGEN

Nitrogen increases strength and enhances resistance to localised corrosion. It is austenite former.

COOPER

Cooper increases general corrosion resistance to acids and reduces the rate of work-hardening (e.g. it is used in cold-headed products such as nails and screws). It is an austenite stabiliser.

CARBON

Carbon enhances strength (especially, in hardenable martensitic stainless steels), but may have an adverse effect on corrosion resistance by the formation of chromium carbides. It is an austenite stabiliser.

TITANIUM (AND NIOBIUM & ZIRCONIUM)

Where it is not desirable or, indeed, not possible to control carbon at a low level, titanium or niobium may be used to stabilise stainless steel against intergranular corrosion. As titanium (niobium and zirconium) have greater affinity for carbon than chromium, titanium (niobium and zirconium) carbides are formed in preference to chromium carbide and thus localised depletion of chromium is prevented. These elements are ferrite stabilisers.

SULPHUR

Sulphur is added to improve the machinability of stainless steels. As a consequence, sulphur-bearing stainless steels exhibit reduced corrosion resistance.

CERIUM

Cerium, a rare earth metal, improves the strength and adhesion of the oxide film at high temperatures.

MANGANESE

Manganese is an austenite former, which increases the solubility of nitrogen in the steel and may be used to replace nickel in nitrogen-bearing grades.

SILICON

Silicon improves resistance to oxidation and is also used in special stainless steels exposed to highly concentred sulphuric and nitric acids. Silicon is a ferrite stabiliser.

2.1.3 Stainless Steel's used profiles

The applications for stainless cold formed such as rectangular hollow sections (RHS) and square hollow sections (SHS) are plenty, particularly in industrial, commercial and residential construction. There are also commonly used in the mechanical and fabricating industries, the agricultural industry, mining industry and simply for signage. Stainless steel RHS have such universal uses because they are durable and easy to prepare for welding or joining.

Stainless steel RHS are practical and aesthetic elements, what makes them highly sought after and a functional solution to modern building needs and requirements.

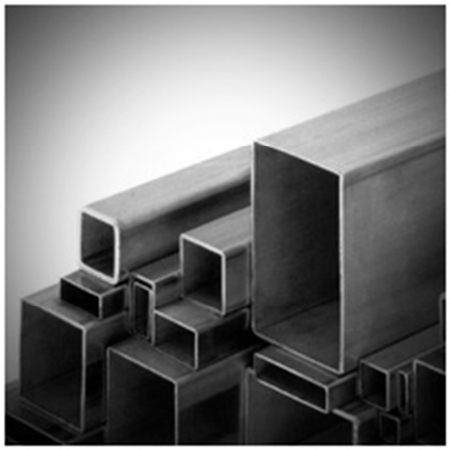

Figure 2. Stainless steel RHS & SHS [2]

2.1.4 Standards

American standards SEI/AISI "Specification for design of cold worked stainless structural members", [3] covers the three traditional ferritic steel grades, as well as South African standards and Australian standards. Eurocode corresponding to stainless steel, EN 1993-1-4 [4], is applicable for these three grades of feritic stainless steels: 1.4003, 1.4016 and 1.4512. Even so, in some cases the specifications have been obtained and contrasted only for austenitic and duplex stainless steel grades, and therefore in some cases specific guideline is missing for ferritic stainless steel. Besides, in many aspects EN 1993-1-4 [4] refers to part of Eurocode EN 1993-1-1 which has not been validated for ferritic stainless steels.

Even taking into account the past experience about ferritic steel in other areas, there is not enough information regarding to structural aspects, neither fire resistance, atmospherical corrosion resistance, welded and screwed unions resistance… for its use in construction. This work is presented as an attempt to cover part of the lack of information in order to develop appropriate design guidelines which can be incorporated to the corresponding EN 1993-1-4 and the rest of Standards and guidelines.

2.1.5 Life cycle cost

Although stainless steel is often considered as an expensive material, this is because only the initial cost is taken into account. Following the current trend considering lifecycle cost, operating costs should also be considered (e.i. maintenance) as well as the residual value of the material. In this case, stainless steel is presented as a competent material compared to others less resistant to corrosion as it can be in Fig. 3.

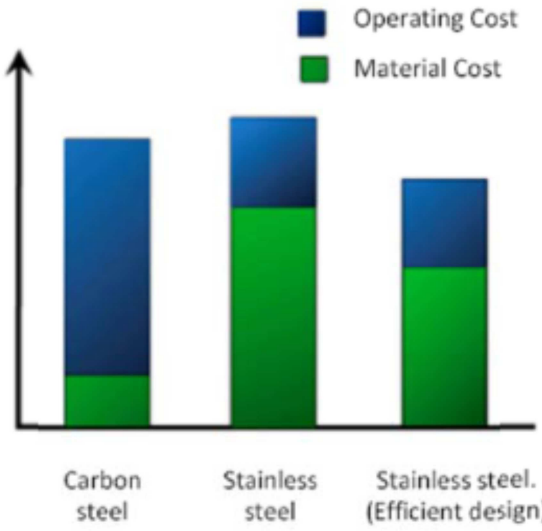

Figure 3. Comparison of the total costs between carbon steel and stainless steel [5]

2.1.6 Material models

The nonlinear stress-strain behaviour of stainless steel alloys, which differs from carbon steel's bilinear behaviour, required the development of several material models taking into account this characteristic in order to improve safety and economy of the design of structures. In fact, the increasing number of structural applications of stainless steel has shown the need of having more accurate models for the design process.

In the last decades, starting from the general Ramberg-Osgood proposal, several material models have been developed. Some of them are in the European, Australian and American standards already. All this models, with different levels of complexity and restrictions, are based in some material parameters generally obtained from experimental tests. Some of the existing models have shown a good adjustment with experimental stress-strain curve results for high strains, while others have focused on the expected behaviour for lowers strains.

The main material models developed for stainless steels are the following: Ramberg & Osgood model [6], Hill's modification of Ramberg & Osgood model [7], Mirambel & Real model [8], Rasmussen's modification of Mirambell & Real model [9] and Gardner's modification of Mirambell & Real model [10].

Mirambell & Real Model [8]

This model has been the chosen one for this research work. It combines good accuracy with simplicity and permits to adjust the tensile-deformational behaviour of stainless steel properly, even with high strains. When high strains occurred Ramberg-Osgood's model diverged from

experimental curve which was the main reason why Mirambell-Real improved it. Finally, the model is defined with a reasonable number of material parameters.

$$\varepsilon = \begin{cases} \frac{\sigma}{E_0} + 0.002\left(\frac{\sigma}{\sigma_{0.2}}\right)^n & for\ \sigma \le \sigma_{0.2} \\ \frac{\sigma - \sigma_{0.2}}{E_{0.2}} + {\varepsilon_{up}}^*\left(\frac{\sigma - \sigma_{0.2}}{\sigma_u - \sigma_{0.2}}\right)^m + \varepsilon_{0.2} & for\ \sigma \ge \sigma_{0.2} \end{cases} \quad \text{Eq. 1}$$

As has been said, this model was developed from the Ramberg-Osgood [6] formula. It includes 6 parameters. E is the Young's modulus, $\sigma_{0.2}$, conventionally considered as the yield stress, is the proof stress corresponding to a 0.2% plastic strain, n and m are the strain hardening exponents and σ_u and ε_u are the ultimate strength and its corresponding ultimate strain respectively.

Where $${\varepsilon_{up}}^* = \varepsilon_u - \varepsilon_{0.2} - \frac{\sigma_u - \sigma_{0.2}}{E_{0.2}}$$ *Eq. 2*

0,2% strain is $$\varepsilon_{0.2} = \frac{\sigma_{0.2}}{E_0} + 0.002$$ *Eq. 3*

The tangent modulus $$E_{0.2} = \frac{E_0}{1 + 0.002n\left(E_0/\sigma_{0.2}\right)}$$ *Eq. 4*

And strain hardening exponents are $$n = \frac{\ln(20)}{\ln\left(\frac{\sigma_{0.2}}{\sigma_{0.01}}\right)} \quad m = 1 + 3.5\frac{\sigma_{0.2}}{\sigma_u}$$ *Eq. 5*

The values of these parameters for 1.4003 ferritic stainless steel are the followings on table 1.

Table 1. Material properties values

E(MPa)	198000
$\sigma_{0.2}$(MPa)	330
σ_u(MPa)	480
ε_u	17%
n	11.5
m	2.8

2.2 Ferritic stainless steel

This section explains more accurately ferritic stainless steel by presenting its differents grades, economic advantages, and finally mechanical and physical properties. As has already been said, ferritic stainless steel presents a much higher resistance to corrosion than carbon steel does. Furthermore, it exhibits good ductility, formability and an excellent resistance to impact. The proportions range of its elements is: 0.02 to 0.06% of carbon and 10.5 to 29% of chrome. Certain ferritic grades contain additional alloying elements such as molybdenum (0 to 4%), to enhance properties. This material has a special resistance to certain types of corrosion.

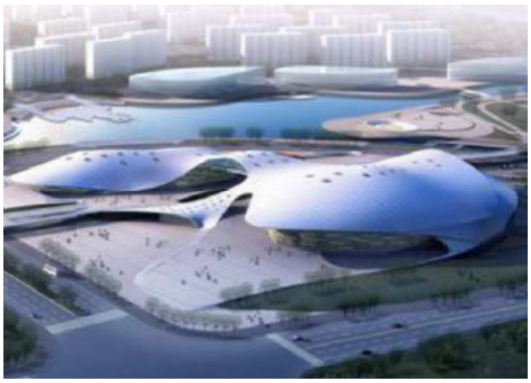

Figure 4. Guangzhou Multi-sports Arena's deck [11]

This material has been very successfully used in several applications as chassis, railway coaches, tanks, washing machine drums, exhaust systems and industrial conduits although it also exist recent structural applications as the one shown in Fig. 4 above. In many cases ferritic grades are emerging as a better choice than more expensive materials.

There are five groups of ferritic grades depending on the proportion range of its elements as shown in figure 5.

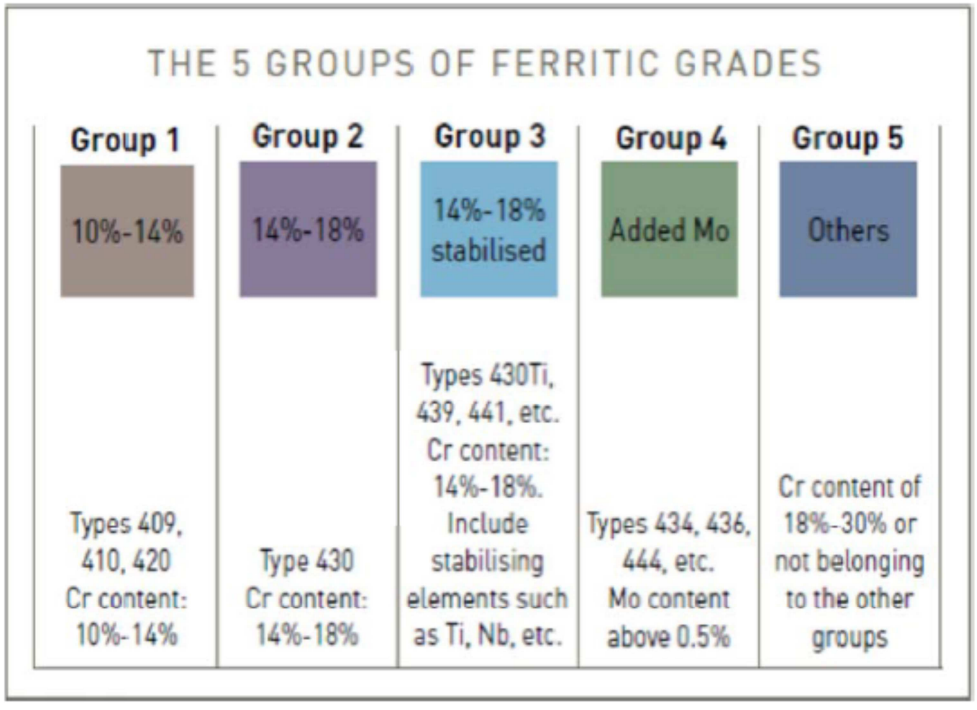

Figure 5. Groups of Ferritic Grades [12]

Some characteristics of these groups are mentioned as follows:

Group 1: This group of ferritic has the lowest chromium content and is the least expensive. It is perfect for non-corrosive conditions. In this context, it has a longer life than carbon steel (type 409/410L).

Group 2: It is the most widely used group, having higher content of chromium. It is appropriate to have an intermittent contact with water but in non-corrosive conditions (type 430).

Group 3: The difference between this group and group 2 is that this one presents better weldability and formability thanks to the stabilizers (includes types 430Ti, 439, 441, etc.). The quantity of chromium is similar to group 2.

Group 4: This group has added molybdenum for extra corrosion resistance. It is corrosion resistant and has a wide range of uses (includes types 434, 436, 444, etc.).

Group 5: These are grades with very high chromium content besides molybdenum, which makes them as corrosion resistant in highly corrosive environments as titanium metal (includes types 446, 445, 447 etc.).

Research on ferritic stainless steels became a priority when nickel prices increased to unprecedented levels, greatly affecting the cost of austenitic grades, and interest in more prices table grades increased. Because of the absence of nickel in ferritic grades, which is also subject to considerable price fluctuations, their cost is lower and more stable than austenitic stainless steels. Nickel price evolution in last few years is shown in Fig. 6.

Figure 6. Nickel Price evolution in $ [13]

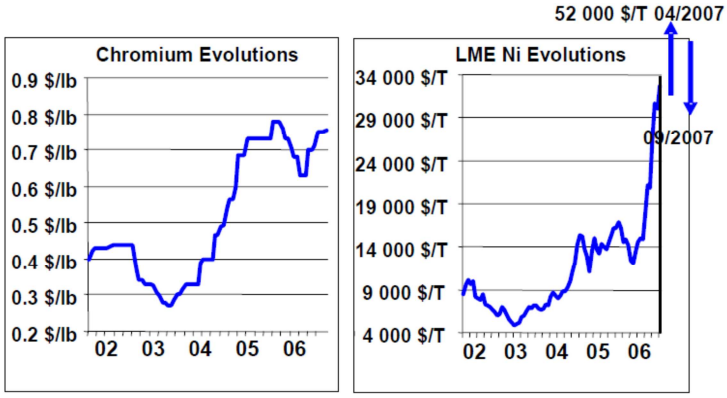

Figure 7. Cr and Ni Price evolution in '01-'07 period [14]

This is the main reason why it is interesting to develop and study a stainless steel alloy that presents a more constant price, so the expected project budget does not suffer cost variations

as far as concerns material. We can also see in Fig. 7 the price variation of chromium and nickel (taking into account that 1 lb is 0,45kg).

As we can appreciate, the range of prices of chromium is from 440 to 2000 $/T, and in nickel the variation occurs in a bigger wide range of prices from 4000 to 34000 $/T.

2.2.1 Mechanical properties

Mechanical properties of ferritic grades are presented in Fig. 8. Ferritics have generally lower elongation and strain hardening properties than austenitics. As for plain carbon steels, ferritic stainless steels in the annealed state present a kind of "yield point" (is not a real yield point because is a non-linear material) followed by a stress drop on the stress/strain curves. This behaviour is caused by the breakaway of pinned dislocations and enables a "true yield stress" to be defined. It is accompanied by the formation of localized deformation bands named "Piobert-Lüders" bands. As a result, after plastic deformation on annealed samples, surface defects may be observed. In the case of deep drawing, they are called "stretcher strains" or "worms". It can be avoided partially by stabilisation or by a skin pass operation which introduce "fresh" dislocations in the structure. Beware with 304 (Fig. 8), which is not a ferritic stainless steel grade.

MECHANICAL PROPERTIES (COLD ROLLED)

ASTM A 240				JIS G 4305				EN 10088-2				
	R_m min	R_{p02} min	A_5 min		R_m min	R_{p02} min	A_5 min			R_m	R_{p02} min	A_{80} min
409	380	170	20	--	--	--	--	X2CrTi12	1.4512	380-560	220	25
410S	415	205	22	SUS 410	440	205	20	X2CrNi12	1.4003	450-650	320	20
430	450	205	22	SUS 430	420	205	22	X6Cr17	1.4016	450-600	280	18
434	450	240	22	SUS 434	450	205	22	X6CrMo17-1	1.4113	450-630	280	18
436	450	240	22	SUS 436	410	245	20	X6CrMoNb17-1	1.4526	480-560	300	25
439	415	205	22	--	--	--	--	X2CrTi17	1.4520	380-530	200	24
439	415	205	22	--	--	--	--	X2CrTi17	1.4510	420-600	240	23
441	415	205	22	--	--	--	--	X2CrMoNb18	1.4509	430-630	250	18
S44400 (444)	415	275	20	SUS 444	410	245	20	X2CrMoTi18-2	1.4521	420-640	320	20
304	515	205	40	SUS 304	520	205	40	X5CrNi1-80	1.4301	540-750	230	45

Figure 9. Typical mechanical properties of some ferritic stainless grades[14]

2.2.2 Physical properties

The most obvious difference between ferritic stainless and austenitic properties is their ferromagnetic behaviour at room temperature and up to a critical temperature known as the Curie point, temperature typically in the range of 650-750°C at which the magnetic order disappears. Magnetism has nothing to do with corrosion resistance which is closely linked to

chemical composition (Cr, Mo ...). Moreover, corrosion resistance is almost independent from the microstructure (not considering the specific case of stress corrosion cracking where ferritic structure is an advantage or crevice corrosion propagation rate where nickel plays a beneficial role). The popular link between magnetism and poor corrosion resistance results from an inappropriate comparison i.e. comparing a ferritic grade with lower Cr content (13-16%) with the austenitic 304 grade (18%).

In fact, the magnetism of ferritic grades is one of the material's major assets in some applications. This includes advantages ranging from the ability to stick memos on the refrigerator door to storing knives and other metallic implements. Indeed, it is also an essential property for ferritic stainless uses in applications dealing with induction heating such as the familiar pans and other cookware for "induction" cooking. In those applications, magnetic materials are requested to generate heat from magnetic energy.

PHYSICAL PROPERTIES

Type of stainless steel	Density	Electric resistance	Specific heat	Thermal conductivity	Thermal expansion coefficient		Young's modulus x10³
	g/cm³	Ω mm²/m	0 – 100°C J/kg • °C	100°C W/m • °C	0–200°C 10⁻⁶/°C	0–600°C 10⁻⁶/°C	N/mm²
409/410 10%-14% Cr	7.7	0.58	460	28	11	12	220
430 14%-17% Cr	7.7	0.60	460	26	10.5	11.5	220
Stabilised 430Ti, 439, 441	7.7	0.60	460	26	10.5	11.5	220
Mo > 0,5% 434, 436, 444	7.7	0.60	460	26	10.5	11.5	220
Others 17%-30% Cr	7.7	0.62	460	25	10.0	11.0	220
304	7.9	0.72	500	15	16	18	200
Carbon steel	7.7	0.22	460	50	12	14	215

The modulus of elasticity of ferritic grades (at 20°C) is superior to that of 304 austenitic. IS units: g/cm³ = kg/dm³ – J/kg • °C = J/kg • °K – W/m • C = W/m • K –10-6/°C = 10-6/°K – N/mm³ = MPa.

Figure 8. Physical properties of some ferritic stainless steel grades[14]

Ferritics' lower thermal expansion coefficient combined with their improved thermal conductivity often provides a key advantage to ferritics over austenitics when considering applications involving heat transfer. Typical physical properties of ferritic stainless compared to austenitics are presented in Fig. 9. Beware with 441 and 444 (Fig. 9), which are not ferritic stainless steel grades.

Ferritic stainless exhibits a non-uniform texture which leads to heterogeneous mechanical behaviour. Phenomena such as "earing" as well as "roping" (sometimes called "ridging") are observed. Roping generally occurs during deep drawing and involves the formation of small undulations elongated in the tensile direction. Those defects must be eliminated during finishing. The stabilized ferritic steels are less sensitive to roping than basic AISI 430 grade. In

practice, optimization of process parameters makes it possible to significantly attenuate this phenomenon. Deep drawing performance is determined by the limit drawing ratio (LDR), which is well correlated with the mean strain ratio. Ferritics have higher LDR values than austenitics, which makes them particularly suitable for deep drawing applications. The main stress ratio may be optimized in ferritic stainless steels by process cycle parameters including slab microstructure control and cold rolling parameters preceding the final heat treatment. In industrial practice, for a single cycle cold rolling process, values of 1.8-1.9 LDR are obtained for a conventional 430 grade.

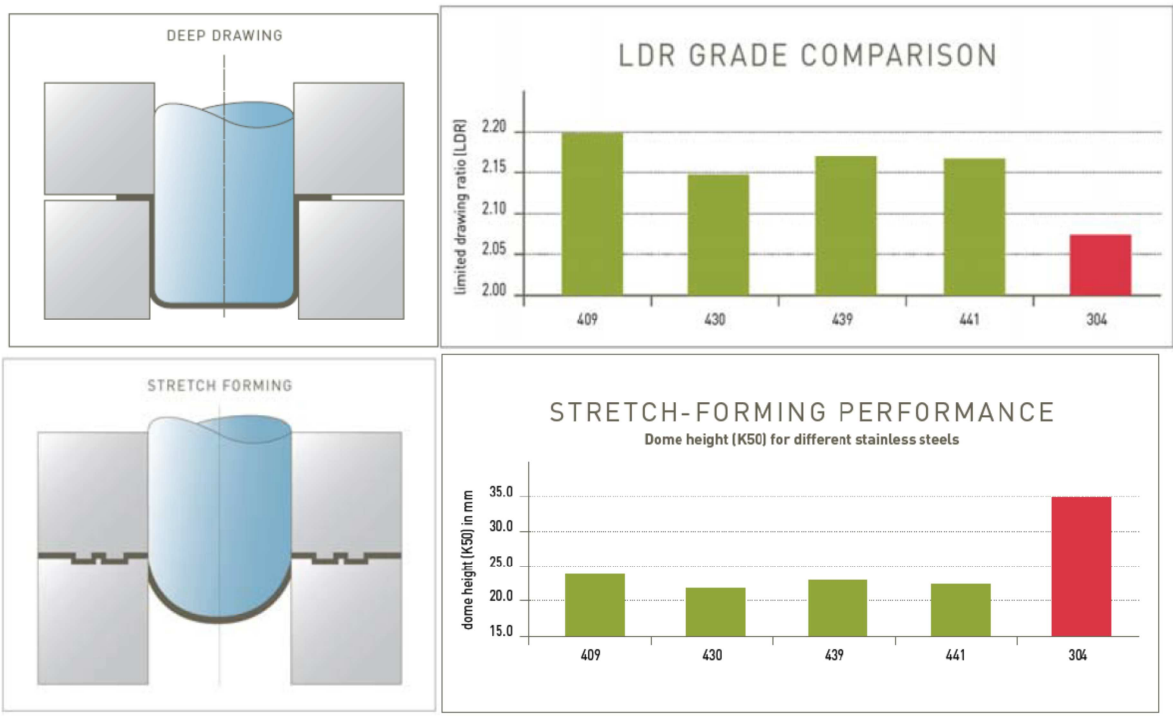

Figure 10. LDR and dome height values of several ferritic and 304 austenitic grades [14]

The LDR may reach values higher than 2.1 for optimized process including a two steps cold rolling process (Fig. 10, above). Stabilization (by Ti, Nb addition…) of ferritic stainless steel induces a significant modification in the crystalline texture leading to a sharp improvement of the strain ratio. Improved LDR values are observed. The performance regarding pure deep drawing aside, ferritic grades are inferior to austenitics in pure stretch forming. “Dome height” refers to the maximum degree of deformation – of a blank undergoing stretching – before “necking”. Dome height (K50, in mm) values of ferritic and 304 austenitic grades are presented (Fig. 10, down).

In practice, industrial forming operations involve a combination of both drawing and stretch-forming deformation, in a series of “passes”. Forming limit curves are a useful guide to assess maximum deformation before failure, in both deep drawing and stretching processes. These curves define local deformations during and after forming in terms of two principal “true strains”: longitudinal (“major strain”) and transverse (“minor strain”). The curves plot the effects of the various combinations of these two strains, up to the point of fracture. Typical results obtained for ferritics and 304 grades are presented (Fig. 11). Ferritics clearly have less combined forming properties than austenitics. For the most severe forming conditions, the

switch from austenitics to ferritics may need some design optimisation with shape modifications of the most critical areas.

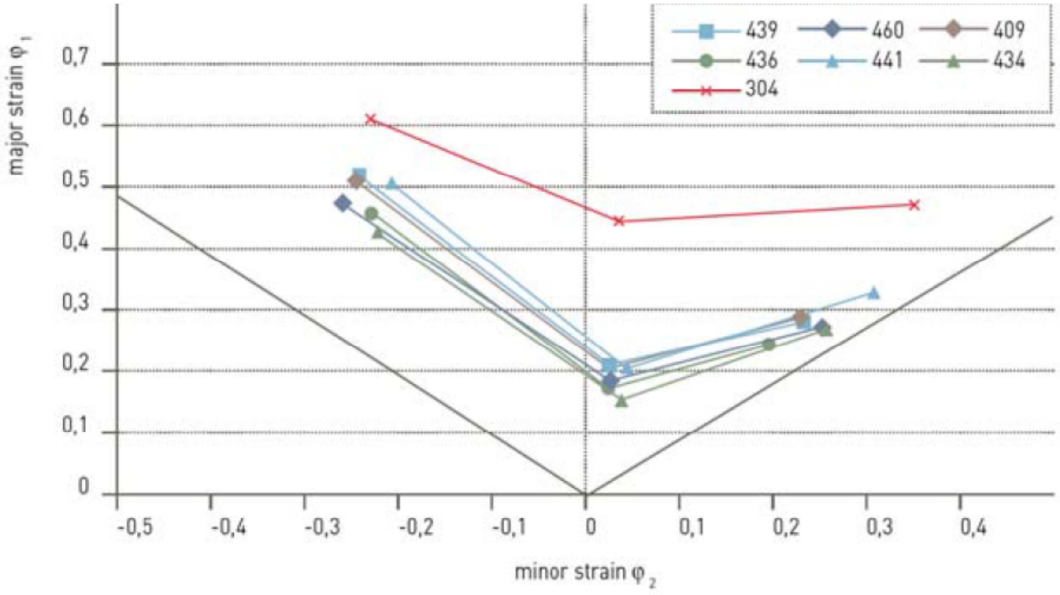

Figure 11. Forming limit curves of ferritic and 304 stainless grades [14]

2.3 Cross-sectional resistance of stainless steel: analytical expressions

This section will present and explain different analytical expressions that will be used to calculate ultimate resistances of the cross-sections (axial forces and/or bending moments, N_u and M_u, respectively). These values will be needed when analysing the behaviour of ferritic stainless steel cross-sections to combined loading conditions, in order to identify the expressions that fits better to the safety region defined by N_u and/or M_u (simple or combined loading). Furthermore, different analytical expressions for interaction from standards and investigation papers will be studied too.

On the one hand, one of the ways to determine these ultimate resistances of the cross-sections is by attending EN 1993-1-4 [4], which is the specific standard for stainless steel. This Standard refers to part of Eurocode (EN 1993-1-1 [15] and 1993-1-3 [16]) that in many aspects has not been validated for ferritic stainless steel (e.g. when interaction is being studied, EN 1993-1-4 refers to EN 1993-1-1).This method requires a cross-section classification in order to evaluate properly the different expressions presented in this Standard.

On the other hand, there is a new and more accurate way to determine these ultimate resistances of the cross-sections: Continuous Strength Method (CSM). This method is not included in any standard but is used for research. Because of this, CSM will be included in the analysis of this research project. The CSM will be evaluated for each cross-section and loading case to see whether the final result can be improved taking advantage of the stainless steel's strain hardening.

2.3.1 EN 1993-1-4 analytical expressions for combined loading

This section will present firstly the cross-section classification method, and secondly the expressions for simple and combined loadings (interaction expressions) in order to be able to evaluate all of the ultimate loading cases being studied.

2.3.1.1 Classification of compression elements

The equation to obtain the resisting moment for normal bending, combined loading, buckling or simple compression depends on the Class of the cross-section that is being studied. The classification given by EN 1993-1-4 for stainless-steel cross-sections follows the criteria presented on the table 2 below.

Table 2. Maximum width-to-thickness ratios for compression parts [4]

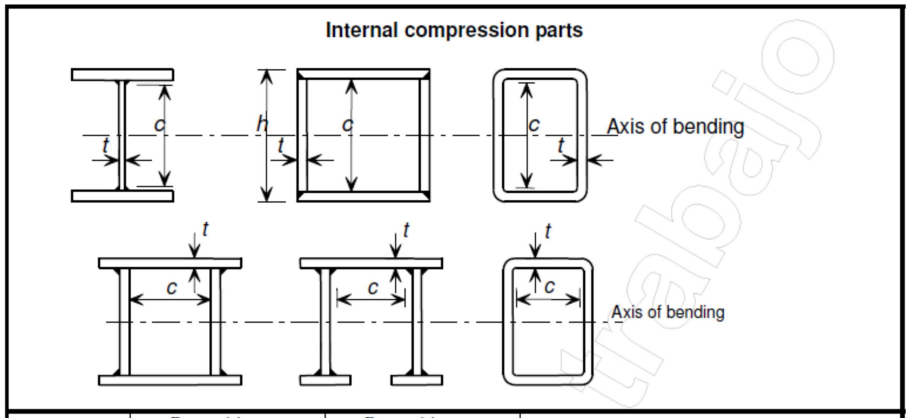

Class	Part subject to bending	Part subject to compression	Part subject to bending and compression
Stress distribution in parts (compression positive)	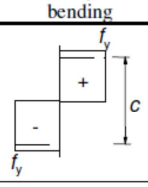	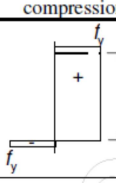	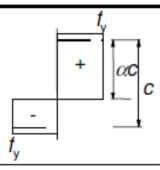
1	$c/t \le 56{,}0\varepsilon$	$c/t \le 25{,}7\varepsilon$	when $\alpha > 0{,}5$: $c/t \le \frac{308\varepsilon}{13\alpha - 1}$ when $\alpha \le 0{,}5$: $c/t \le \frac{28\varepsilon}{\alpha}$
2	$c/t \le 58{,}2\varepsilon$	$c/t \le 26{,}7\varepsilon$	when $\alpha > 0{,}5$: $c/t \le \frac{320\varepsilon}{13\alpha - 1}$ when $\alpha \le 0{,}5$: $c/t \le \frac{29{,}1\varepsilon}{\alpha}$
Stress distribution in parts (compression positive)	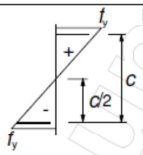	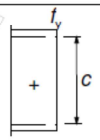	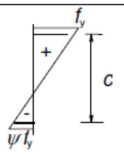
3	$c/t \le 74{,}8\varepsilon$	$c/t \le 30{,}7\varepsilon$	$c/t \le 15{,}3\varepsilon\sqrt{k_\sigma}$ For k_σ see EN 1993-1-5

$$\varepsilon = \left[\frac{235}{f_y}\frac{E}{210\,000}\right]^{0,5}$$

Grade	1.4301	1.4401	1.4462
f_y (N/mm^2)	210	220	460
ε	1,03	1,01	0,698

Note: For hollow sections, c may conservatively be taken as (h-2t) or (b-2t).

However, recent research conducted by Gardner and Theofanous in [17]recent researches have demonstrated that these slenderness limits are overly conservative. Because of it, new limits have been proposed and will maybe be included in the next revision of EN 1993-1-4, which is expected to be soon published. As the analysed section are all rectangular and square hollow section, they do not have any outstand flanges, so only need the information that is referred to internal elements under compression. As it can be appreciated on table 3, where appears the new T&G [17] cross-section classification criteria, limit values of slenderness for

each Class are different from those proposed for carbon steel and the ones presented in EN1993-1-4[4] or T&G [17] for stainless steels.

Table 3. Carbon and stainless Steel slenderness limits for compression elements in EN 1993 and other proposals

Element	Class 2 limit			Class 3 limit		
	Carbon steel EN	Stainless steel EN	Stainless steel T&G	Carbon steel EN	Stainless steel EN	Stainless steel T&G
Internal element in compression	38ε	26.7ε	35ε	42ε	30.7ε	37ε
Internal element in bending	83ε	58.2ε	76ε	124ε	74.8ε	90ε

Note: ε has the same expression as in EN 1993-1-4 (table 2).

As this work is focused on the behaviour of class 1, 2 and 3, is not necessary to include in this paper the way to procedure to obtain the value of the effective values of section properties (effective inertial moment and effective areas) that are needed to evaluate the expressions presented for Class 4 sections.

2.3.1.2 Resistance of cross-sections, Ultimate Limit States [4 and 15]

After classifying the cross-section depending on the slenderness of the elements that shape the cross-section being studied, we are able to proceed applying the correct expression for the calculation of the ultimate capacities of the cross-section subjected to each case of loading.

-Traction

The resistant value of the traction force $N_{t,Rd}$ at each cross section is:

$$N_{t,Rd} = \frac{Af_y}{\gamma_{M0}} \qquad Eq.6$$

A cross sectional area

f_y yield stress, for stainless-steel is considered $\sigma_{0.2}$

γ_{M0} partial factor for resistance of cross-sections whatever the Class is

In this case we will not have to check the class of the section, only when the member is under compression actions.

-Compression

The resistant value of the compression force $N_{c,Rd}$ at each cross section is:

$$N_{c,Rd} = \frac{Af_y}{\gamma_{M0}} \qquad \text{for Class 1,2 or 3 cross} - \text{sections} \qquad Eq.7$$

$$N_{c,Rd} = \frac{A_{eff}f_y}{\gamma_{M0}} \qquad \text{for Class 4 cross} - \text{sections} \qquad Eq.8$$

A cross sectional area

A_{eff} effective area, we can find how to calculate it in 4.3 (EN 1993-1-5)

f_y yield stress, for stainless-steel is considered $\sigma_{0.2}$

γ_{M0} partial factor for resistance of cross-sections whatever the Class is

-Bending moment

The resistant value of the bending moment M_{Rd} at each cross section is:

$$M_{Rd} = \frac{W_{pl} f_y}{\gamma_{M0}} \quad \text{for Class 1or 2 cross} - \text{sections} \qquad Eq.9$$

$$M_{Rd} = \frac{W_{el,min} f_y}{\gamma_{M0}} \quad \text{for Class 3 cross} - \text{sections} \qquad Eq.10$$

$$M_{Rd} = \frac{W_{eff,min} f_y}{\gamma_{M0}} \quad \text{for Class 4 cross} - \text{sections} \qquad Eq.11$$

W_{pl} cross-section plastic resistant modulus

$W_{el,min}$ cross-section elastic resistant modulus referred to the fibre with the maximum elastic stress

$W_{eff,min}$ cross-section elastic resistant modulus referred to the fibre with the maximum elastic stress calculated with the effective properties of the cross-section , see 4.3 (EN 1993-1-5)

f_y yield stress, for stainless-steel is considered $\sigma_{0.2}$

γ_{M0} partial factor for resistance of cross-sections whatever the Class is

-Bending and axial force (interaction EN 1993-1-1)

For Class 1 and 2 rectangular or square hollow sections of uniform thickness the following approximations may be followed:

$$M_{N,y,Rd} = \frac{M_{pl,y,Rd}(1-n)}{1-0.5a_w} \quad but\ M_{N,y,Rd} \leq M_{pl,y,Rd} \qquad Eq.12$$

$$M_{N,z,Rd} = \frac{M_{pl,z,Rd}(1-n)}{1-0.5a_f} \quad but\ M_{N,z,Rd} \leq M_{pl,z,Rd} \qquad Eq.13$$

Where $a_w=(A-2bt)/A$ but $a_w \leq 0.5$ for hollow sections

$a_f=(A-2ht)/A$ but $a_f \leq 0.5$ for hollow sections

$n=N_{Ed}/N_{pl,Rd}$ where N_{Ed} is the design value of the axial force and $N_{pl,Rd}$ the design plastic resistance to normal forces of the cross-section

A, area; h, depth; b, width

$M_{pl,i,Rd}$ design plastic value of the resistance to bending moments, i-i axis

When a bi-axial verification is needed, the following criterion may be used:

$$\left[\frac{M_{y,Ed}}{M_{N,y,Rd}}\right]^{\alpha} + \left[\frac{M_{z,Ed}}{M_{N,z,Rd}}\right]^{\beta} \leq 1 \qquad Eq.14$$

Where $M_{N,y,Rd}$ and $M_{N,z,Rd}$ are defined in Eq. 12 and 13 above.

$M_{y,Ed}\ and\ M_{z,Ed}$ are the design bending moments, for y-y and z-z axis, respectively.

α and β are constants, which may be conservatively be taken as unity, otherwise as follows:

$$\alpha = \beta = \frac{1{,}66}{1 - 1{,}13n^2} \quad \text{but } \alpha = \beta \leq 6$$

$$\text{and } n = N_{Ed}/M_{Ed}$$

For class 3 cross-sections, a linear criterion is applied as follows:

$$\frac{N_{Ed}}{Af_y/\gamma_{M0}} + \frac{M_{y,Ed}}{W_{el,y}f_y/\gamma_{M0}} + \frac{M_{z,Ed}}{W_{el,z}f_y/\gamma_{M0}} \leq 1 \qquad Eq.15$$

Where A cross sectional area

γ_{M0} partial factor for resistance of cross-sections whatever the Class is

$W_{el,y}$ and $W_{el,z}$ are the cross-section elastic resistant modulus referred to the fibre with the maximum elastic, each one referred to y-y and z-z axis, respectively

f_y yield stress, for stainless-steel is considered $\sigma_{0.2}$

N_{Ed}, $M_{y,Ed}$ and $M_{z,Ed}$ are the design values for: the normal force, y-y bending moment and z-z bending moment, respectively.

For class 4 cross-sections, the criterion used is the following:

$$\frac{N_{Ed}}{A_{eff}f_y/\gamma_{M0}} + \frac{M_{y,Ed} + N_{Ed}e_{Ny}}{W_{eff,y}f_y/\gamma_{M0}} + \frac{M_{z,Ed} + N_{Ed}e_{Nz}}{W_{eff,z}f_y/\gamma_{M0}} \leq 1 \qquad Eq.16$$

Where e_{Ny} and e_{Nz} are the shifts of the relevant centroidal axis when the cross-section is subjected to compression only

N_{Ed}, $M_{y,Ed}$ and $M_{z,Ed}$ are the design values for: the normal force, y-y bending moment and z-z bending moment, respectively.

f_y yield stress, for stainless-steel is considered $\sigma_{0.2}$

$W_{eff,y}$ and $W_{eff,z}$ are the cross-section elastic resistant modulus referred to the fibre with the maximum elastic stress stress calculated with the effective properties of the cross-section , (see 4.3, EN 1993-1-5[18]), each one referred to y-y and z-z axis, respectively

NOTE: this research work will not take into account the interaction with shear force.

2.4 Continuous strength method - CSM

The Continuous Strength Method (CSM) is a novel approach to the treatment of local buckling in metallic cross-sections, which does not utilize the effective width concept, does not assume the traditional bilinear material behaviour and allows for better exploitation of the material. It is based on the deformation capacity of the cross-section in question, as predicted by an experimentally derived design curve relating the strain at which local buckling occurs, denoted ε_{LB}, to the cross-section slenderness. This deformation capacity is utilized in conjunction with an accurate stress–strain law to obtain the maximum attainable stress σ_{LB} corresponding to the local buckling strain ε_{LB}. Additional features of the method include explicit allowance for the beneficial influence of strain hardening incurred during the forming process on the strength of the corner regions of cold-formed cross-sections and generalizations of the method to cover member instabilities and interaction of various loading conditions. The method has also been successfully applied to aluminium alloy, high strength steel and carbon steel design. It should be noted that the Continuous Strength Method deals primarily with the fundamental loading cases associated with normal stresses (i.e. pure compression, bending and interaction of compression and bending). The shear buckling resistance of stainless steel cross-sections has been examined elsewhere.

2.4.1 Development of the continuous strength method

The continuous strength method (CSM) is a strain based design approach featuring two key components: a base curve that defines the level of strain that a cross-section can carry in a normalised form and a material model, which allows for strain hardening and, in conjunction with the strain measure, can be used to determine the cross-section resistance.

2.4.2 Design base curve

A fundamental feature of the CSM is relating the cross-section resistance to the cross-section deformation capacity, which is controlled by the cross-section slenderness and its susceptibility to local buckling effects. The cross-section deformation capacity determines the ability of the section to advance into the strain hardening region and hence sustain increased loading. A design base curve, providing a continuous relationship between the normalised cross-section deformation capacity and the cross- section slenderness, has been established on the basis of both stub column test data and beam test data.

2.4.2.1 Cross-section slenderness definition

Within the CSM, the cross-section slenderness is defined in non-dimensional form as the square root of the ratio of the yield stress f_y to the elastic buckling stress of the section. For structural sections consisting of a series of interconnected plates, the elastic buckling stress of the full cross-section $\sigma_{cr,cs}$, allowing for element interaction, may be determined by means of

existing numerical [19] or approximate analytical methods[20]. This cross-section slenderness definition is given by Eq. 27 and will initially relate to the centreline dimensions. To maintain consistency with the codified slenderness definitions [4 and 18], which is based on the flat element widths, the resulting slenderness values can be multiplied by the maximum flat to centreline width ratio (c_{flat}/c_{cl}) max of the section as given by Eq. 28.

Alternatively, as recommended in EN1993-1-4 and EN 1993-1-5 [4 and 18], the section elastic buckling stress may be taken as the lowest of those of its individual plate elements $\sigma_{cr,cs,min}$, resulting in the section slenderness definition given in Eq. 29. In Eq. 29, b is element width, t is the thickness, ε is the material factor and k_σ is the appropriate buckling coefficient, taking due account of the plate support conditions and the applied stress distribution, as outlined inEN1993-1-5, of the plate element with the lowest elastic buckling stress.

$$\lambda_p = \sqrt{\frac{f_y}{\sigma_{\mathrm{cr,cs}}}} \qquad \text{based on centreline dimensions} \qquad Eq.27$$

$$\lambda_p = \sqrt{\frac{f_y}{\sigma_{\mathrm{cr,cs}}}\left(\frac{c_{flat}}{c_{cl}}\right)_{max}} \qquad \text{based on flat widths} \qquad Eq.28$$

$$\lambda_{cs} = \lambda_p = \sqrt{\frac{f_y}{\sigma_{\mathrm{cr,p,min}}}} = \frac{b/t}{28.4\varepsilon\sqrt{k_\sigma}} \qquad Eq.29$$

2.4.2.2 Cross-section deformation capacity definition

Cross-section deformation capacity is defined in a normalised format and is taken for stocky sections as the strain at the ultimate load divided by the yield strain. This normalised deformation capacity, referred to as the strain ratio $\varepsilon_{csm}/\varepsilon_y$, can be determined from both stub column and beam test results.

First, the limiting slenderness defining the transition between slender cross-sections (i.e., those that fail due to local buckling below the yield load) and non-slender cross-section (i.e., those that benefit from strain hardening and fail by inelastic local buckling above the yield load) should be defined. This limit may be determined with reference to the material's test data (stainless steel in our case).

A linear regression fit to the test data of Fig. 12 indicates that, the point on the line where $N_{u,test}/A\sigma_{0.2}$ equals unity occurs at λ_p= 0.68; a similar value is obtained from equivalent carbon steel and aluminium alloy test data. A range of slenderness limits appear in different design standards and research papers. The existing slenderness limits corresponding to the Class 3–4 width-to-thickness ratio are: for internal compression elements, 0.739 (42ε) [15] for carbon steel, 0.540 (30.7ε) [4] for stainless steel; for outstand elements (not needed in our study), 0.756 (14 ε) [15] for carbon steel, 0.642 (11.9ε) [4] and 0.594 (11ε) [17] for cold-formed and welded stainless steel, respectively (where ε is the coefficient defined in the end of table 2 of cross-section classification). Considering the available information, to make the transition between slender and non-slender sections a common limit for stainless steel, carbon steel and aluminium alloys, λ_p= 0.68 is adopted. This slenderness value also marks the limit of

applicability of the CSM (i.e., $\lambda_p \leq 0.68$), since beyond this limit there is no significant benefit to be derived from strain hardening, and slender sections may be adequately treated by means of the existing effective width method[4 and 18] or the Direct Strength Method (DSM)[21].

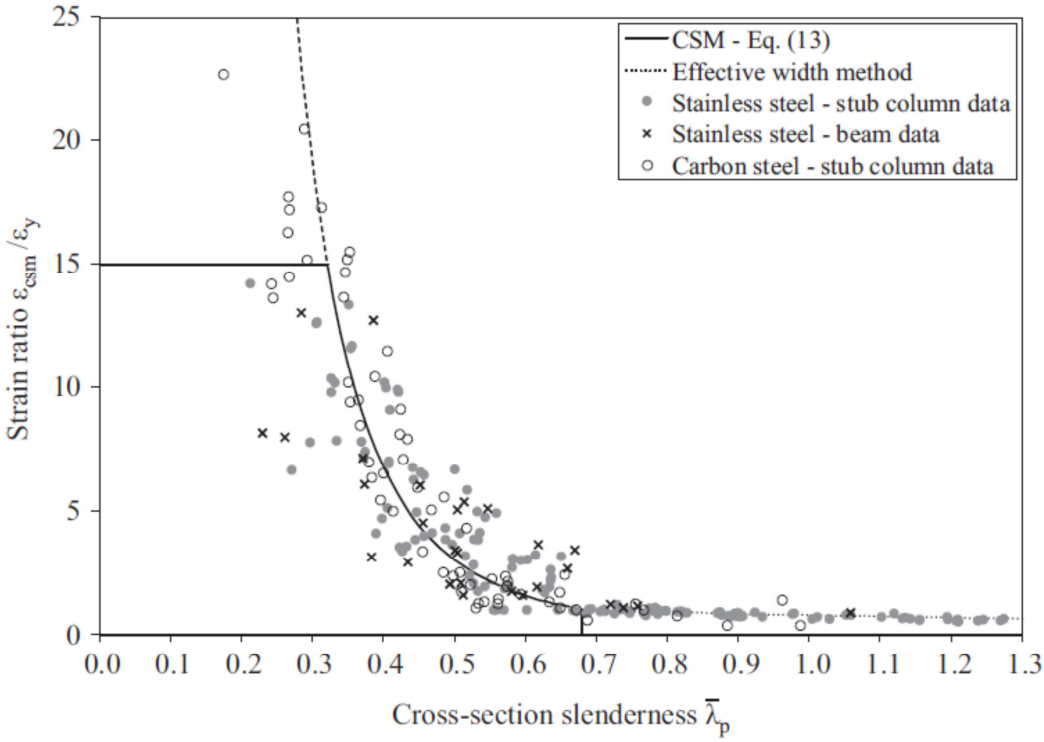

Figure 12. Base curve-relationship between strain ratio and slenderness [22]

For stub columns where the ultimate test load N_u exceeds the section yield load N_y, the end shortening at the ultimate load δ_u divided by the stub column length L is used to define the failure strain of the cross-section ε_{lb} due to inelastic local buckling.

In bending, assuming plane sections remain plane and normal to the neutral axis, there is a linear relationship between strain ε and curvature κ as given by $\varepsilon = \kappa \cdot y$, where *y* is the distance from the neutral axis. Hence, analogous to the use of stub column tests data, similar definitions of normalised cross-section deformation capacity may be established based on beam test results.

2.4.2.3 Experimental database and proposed base curve

Test data on stainless steel stub columns and 4 point bending tests from a broad spectrum of existing testing programs were gathered and combined with equivalent carbon steel data [23] for the development of the design base curve. Using the criteria described above, the test data were plotted on a graph of normalised deformation capacity $\varepsilon_{csm}/\varepsilon_y$ versus cross- section slenderness λ_p, as shown in Fig. 12 from previous section. A continuous function of the general form given by Eq. 30 was then fitted to the test data. Two upper bounds have been placed on the predicted cross-section deformation capacity; the first limit of 15 corresponds to the material ductility requirement expressed in EN 1993-1-1 and the second limit of 0.1 $\varepsilon_u/\varepsilon_y$, where ε_u is the strain corresponding to the ultimate tensile stress, is related to the adopted

stress–strain material model, and ensures no significant over-predictions of the cross-section resistance can occur.

$$\frac{\varepsilon_{csm}}{\varepsilon_y} = \frac{0.25}{\lambda_p{}^{3.6}} \quad but \quad \frac{\varepsilon_{csm}}{\varepsilon_y} \leq min\left(15, \frac{0.1\varepsilon_u}{\varepsilon_y}\right) \qquad Eq.30$$

2.4.3 Material model in CSM

The CSM employs an elastic, linear hardening material model (bilinear, see Fig. 13). The origin of the adopted material model starts at 0.2% off-set plastic strain, which combined with the strain ratio definitions, predicts the correct corresponding stress. The yield stress point is defined as (f_y, ε_y), where f_y is taken as the material 0.2% proof stress and ε_y is the corresponding elastic strain $\varepsilon_y = f_y/E$, where E is the slope of the elastic region and is taken as the material's Young's modulus. The strain hardening slope (E_{sh}) is determined as the slope of the line passing through the 0.2% proof stress point (f_y, ε_y). E_{sh} value will be chosen in order to fit properly to the stress-strain curve defined for the the material model chosen before (Mirambell-Real [8]).

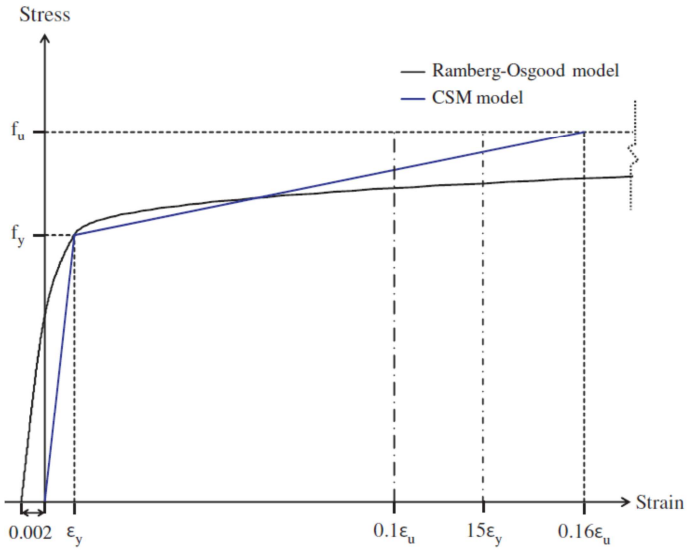

Figure 13. CSM elastic, linear hardening material model. [22]

2.4.4 Cross-section compression and bending resistance

Having established the normalised deformation capacity of the cross-section $\varepsilon_{csm}/\varepsilon_y$ from the design base curve (Eq. 30), the limiting strain ε_{csm} may now be used in conjunction with the proposed elastic, linear hardening material model to determine the cross-section resistances in compression and bending. For sections with For $\lambda_p \leq 0.68$, the cross-section compression resistance $N_{c,Rd}$ is given by Eq. 31, where A is the gross cross-sectional area, f_{csm} is the limiting stress determined from the strain hardening material model, resulting in Eq. 32 and γ_{M0} is the material partial safety factor as recommended in EN1993-1-4 [4] (for stainless steel) .

$$N_{c,Rd} = N_{csm,Rd} = \frac{Af_{csm}}{\gamma_{M0}} \qquad Eq.31$$

$$f_{csm} = f_y + E_{sh}\varepsilon_y\left(\frac{\varepsilon_{csm}}{\varepsilon_y} - 1\right) \quad Eq.32$$

E_{sh} is determined as the slope of the line passing through the 0.2% proof stress point (f_y, ε_y).

Assuming that plane sections remain plane and normal to the neutral axis in bending, the corresponding linearly-varying strain distribution may be used in conjunction with the material model to determine the cross-section in-plane bending resistance M_{csm} through Eq. 33, where f is the stress in the section with a maximum outer fibre value of f_{csm}, *y* is the distance from the neutral axis and dA is the incremental cross-sectional area.

$$M_{csm} = \int_A fydA \quad Eq.33$$

For sections with $\lambda_p \leq 0.68$, the cross-section bending resistance $M_{c,Rd}$ is given by Eqs. 33 and 34 for major axis and minor axis bending, respectively, where W_{pl} is the plastic section modulus, W_{el} is the elastic section modulus and α is 2.0 for SHS/ RHS and 1.2 for I-sections. In this study we will use α = 2.0, as we have RHS & SHS.

$$M_{y,csm,Rk} = W_{pl,y} \cdot \sigma_{csm}\left[1 + \frac{E_{sh}}{E}\frac{W_{el,y}}{W_{pl,y}}\left(\frac{\varepsilon_{csm}}{\varepsilon_y} - 1\right) - \left(1 - \frac{W_{el,y}}{W_{pl,y}}\right)\Big/\left(\frac{\varepsilon_{csm}}{\varepsilon_y}\right)^2\right] \quad Eq.33$$

$$M_{z,csm,Rk} = W_{pl,z} \cdot \sigma_{csm}\left[1 + \frac{E_{sh}}{E}\frac{W_{el,z}}{W_{pl,z}}\left(\frac{\varepsilon_{csm}}{\varepsilon_y} - 1\right) - \left(1 - \frac{W_{el,z}}{W_{pl,z}}\right)\Big/\left(\frac{\varepsilon_{csm}}{\varepsilon_y}\right)^{\alpha}\right] \quad Eq.34$$

Where

W_{pl} cross-section plastic resistant modulus

$W_{el,min}$ cross-section elastic resistant modulus referred to the fibre with the maximum elastic stress

σ_{csm} is the part of the total stress that belongs to the strain hardening part of the stress-strain curve of the material

ε_{csm} is the part of the total strain that belongs to the strain hardening part of the stress-strain curve of the material

E_{sh} strain hardening slope, which is determined as the slope of the line passing through the 0.2% proof stress point (f_y, ε_y). The value adopted that fits better the reference material stress-strain curve is 2000 MPa.

E is the material young's modulus, which in the case of stainless-steel is the slope of the line that conects the coordinate origin and the 0.2% proof stress point

2.5 Interaction proposals for stainless steel

The CSM expressions above are only useful if we only want to obtain the basic resistant capacities: ultimate axial force and ultimate bending moment. Both ultimate axial force and ultimate bending moment can only be compared with design value of axial force and bending moment, respectively, when there is no interaction between these two types of actions. Habitual loading cases always have interaction between axial force and bending moments, so it is important to develop interaction expressions in order to cover a more wide casuistry of loading cases.

Currently there are some research projects regarding interaction design expressions in order to improve the final results obtained from the interaction expression from EN 1993-1-4. As is already known, EN 1993-1-4 gives quite conservative results and what would be very interesting is to be as closer as possible to the real ones. It is more important it for materials with high initial costs as the one that is being studied: ferritic stainless-steel. This research project will include a study of two recent interaction proposals, which will be explained in sections below.

2.5.1 Liew & Gardner: interacion expression proposal [24]

The aim of this research project was to find an interaction expression to improve the actual EN 1993-1-4 results that would be obtained for the ultimate cross-section resistance of I-sections and box sections under combined loading. A strain based numerical model was used to perform the final expression using an equation in which each member is pondered by its power and its value taking into account where the axil force is applied and the proportion of web area of the total. The obtained expression was compared with experimental results and the conclusions extracted were good.

The design equations Eq. 36 and Eq. 37 trace bi-axial bending interaction curves that are anchored by reduced moments $M_{R,y}$ and $M_{R,z}$, which are functions of the axial load $n = N/N_{csm}$. Eq. 35 contains reduced moment normalised terms, raised to powers α and β, and are of a similar format to the design provisions in EN 1993-1-1 for combined axial load and bending moments. The equations provide smooth curves between $M_{R,y}$ and $M_{R,z}$, and map surfaces that conform well to the numerical model surfaces.

$$\left(\frac{M_y}{M_{R,y}}\right)^{\alpha} + \left(\frac{M_z}{M_{R,z}}\right)^{\beta} \leq 1 \qquad Eq.35$$

$$M_{R,y} = M_{csm,y}(1 - n^{a_y})^{\frac{1}{b_y}} \quad and \quad M_{R,z} = M_{csm,z}(1 - n^{a_z})^{\frac{1}{b_z}} \qquad Eq.36\ and\ 37$$

The design equations collapse to all loading states, combined or otherwise, when the appropriate terms are taken as zero. For example, when there is no axial load (n = 0), the reduced moments in Eq. 26 and 37 collapse to the CSM moments and convert Eq. 35 into a bi-axial bending design equation. When either M_y or M_z are zero, the equations collapse into the simple axial load and uni-axial bending forms of $M_z \leq M_{R,z}$ and $M_y \leq M_{R,y}$ respectively. Finally, when both the axial load and minor axis bending components are zero, Eq. 35 returns $M_y = M_{csm,y}$.

The powers a_y, a_z, b_y, b_z, α and β are all defined in table 4. The tabulated powers were found via a non-linear least squares fitting regime, and are based on the ratio of the cross-section web area to gross area a = Aw/A, and the ratio of the major to minor axis plastic section moduli $W_r = W_{pl,y}/W_{pl,z}$. A strain ratio of 5 is required before the convergence of the powers for I- sections, compared to that of 3 needed for box sections. The powers a_y, a_z, b_y, b_z, α and β are all unity when $\varepsilon_{csm}/\varepsilon_y < 3$.

Table 4. CSM design a_y, a_z, b_y, b_z, α and β powers for combined loading[24]

	$3 \leq \frac{\epsilon_{csm}}{\epsilon_y} < 5$	$5 \leq \frac{\epsilon_{csm}}{\epsilon_y} \leq 15$	$3 \leq \frac{\epsilon_{csm}}{\epsilon_y} < 5$
	I-sections		Box sections
a_y	a+1.2		
b_y	0.8		
a_z	2	8a+1.2	a+1.2
b_z	1	0.8-0.5a	0.8
α	$2 - 1.5n \geq 1$	$2 + 0.15W_r - 5n^{1.5} \geq 1.3$	$1.75 + W_r(2n^2 - 0.15) \leq 1.7 + W_r$
β	$0.8 + 5n^{2.2} \leq 4$	$0.8 + (15 - W_r)n^{2.2} \leq 8$	$1.6 + (3.5 - 1.5W_r)n^{2.2} \leq 3.7 - W_r$

2.5.2 Theofanous: interaction expression proposal [25]

This research project's aim was to find novel interaction equations for stainless steel RHS and SHS under combined loading. To do this was used numerical models of two different hollow sections, (100x100 SHS and 200x100 RHS) with 5 different wall thicknesses (3, 4, 5, 6 and 8mm) for each one, undergoing combined loading. The analysis was non-linear and the numerical failure loads data obtained were normalized by the respective capacities and utilized to derive a suitable interaction curve that fit the data.

Two new equations have been proposed in [25]:

$$\left(\frac{N_{Ed}}{N_{csm}}\right)^2 + \sqrt{\left(\frac{M_{y,Ed}}{M_{csm,y}}\right)^2 + \left(\frac{M_{z,Ed}}{N_{csm,z}}\right)^2} \leq 1 \qquad Eq.38$$

$$\frac{N_{Ed}}{N_{csm}} + \sqrt{\left(\frac{M_{y,Ed}}{M_{csm,y}}\right)^2 + \left(\frac{M_{z,Ed}}{N_{csm,z}}\right)^2} \leq 1 \qquad Eq.39$$

This research project was done for austenitic stainless steel and results conducted to the following conclusions: Eq. 38 provides an excellent fit to the numerical predictions for SHS whereas Eq. 39 provides a more safe interaction surface for RHS. However, both interaction equations will try to be validated for both RHS and SHS.

The CSM has been shown to offer significant advantages over alternative design methods in ultimate capacity predictions, both in terms of design efficiency as well as in terms of consistency of the predictions. To obtain these two interaction expressions a non-bilinear

material has been used and it makes more complex the development of the expressions (see the reference if is wanted more detailed information).

2.6 Previous work

This is the first research work regarding interaction ultimate loadings for ferritic stainless steel. It's true, though, that this research work would not have been possible without other actual research papers referred to CSM calibration using another type of stainless steel (austenitic [22]) and interaction expressions proposals.

The aim of this work is to validate which of the different existing analytical design methods fits better to ferritic stainless steel. New equations for ferritic stainless steel will not be performed.

3. Cross-Section Analysis: Numerical Simulation

A numerical simulation consists on obtaining results of the behaviour of a virtual system designed in a computer's software that is put down to external actions that modify the initial state. In this research project, the system is the beam or column and its boundary conditions; and the external actions are the different types of loading proposed. There are many different computer programs that are able to do this type of simulations. The advantage of these simulations is that it is possible to conduct a lot of them without any additional economic cost and it is easy to modify aspects from the model and recalculate again.

To carry out the numerical simulation has been used the following computer software: ABAQUS. This software uses the Finite Element Method (FEM) to obtain the numerical results. To get these results is needed to: design properly a virtual model; define the shape, size and the grade of nodal interpolation that is desired of the finite elements (mesh creation and element characteristics); specify the type of analysis that is required (static risks, buckle…) and finally run it.

In this research project 4 different test types are analysed numerically:

- stub-column test (N): this test consists on compressing an element without eccentricities in order to analyse the maximum compressive axial force that resists the element

- combined loading test (N+M): in this test is applied a compression with different eccentricities to know what combination of axial force and bending moment resists the element

- simple bending test (M): this test analyses the resistant bending moment when it is acting only to one axis.

- biaxial bending test (M_y+M_z): this test analyses the combination of bending moments (one for each axis) that can resist the element.

After explaining common specifications for each test, particular calibrations will be explained.

3.1 Common Specifications

Each test has its own model but there are several specifications that are common. These common specifications are presented in: defining the model, steps, external actions, meshing the model, running the model and finally obtaining data results.

3.1.1 Model

The virtual model includes the geometry of the element being studied, the material properties, the boundary conditions and the sequence of them.

a) To define the geometry model a tool called sketcher that allows to draw easily the shape of the cross-section can be used. The geometry is designed as a closed shell.
b) To assign the material to the geometric model is required to define a generic cross-section that includes: the thickness, the Young's Modulus, the Poisson's ratio (which is assumed as 0.3) and the plastic part of the material model (plastic strain).

c) The boundary conditions are referred to both constrains and external actions (loads, displacements). When defining them, is required to put in which step of the global sequence will be placed and the type of analysis that is wanted.

3.1.2 Steps

ABAQUS uses steps to order the different boundary conditions and external actions that follow the global sequence of the numerical simulation. For example, when having "prestressed concrete" as material, firstly would be introduced boundary conditions, secondly the "prestressed" charge and afterwards the external action. The analysis type or time discretization, are examples of options that can be personalized for each step.

In all models the global sequence followed during the analysis is separated in 3 steps (the words in italics are referred to the real name in ABAQUS of the analysis's type):

- Initial: in this step all constrains that act on the beam or column are definde(i.e. the element supports).
- Buckle: this step permits to carry out an eigenvalue analysis. It contains the external actions. The type of analysis that will follow the external actions in this step is: *Linear Perturbation; Buckle*. As can be guessed from the name, is a linear analysis that gives us a simulation of the geometry with imperfections of the element.
- Analysis: this step contains the same external actions that Buckle step has, but it will only be enabled when the eigenvalue results have already been calculated. This step will give us the simulation results. The type of analysis that will follow the external actions in this step is: *General; Static, Riks*. It uses the geometry imperfections obtained from the Buckle analysis. The analysis carried out is non-linear for the geometry and the material.

3.1.3 External action

As it is not known the ultimate response of the element, what has been done is to apply a big displacement. ABAQUS applies this external action with small increments until reaching the value imposed. From the post-process ABAQUS tools it will be possible to extract the values in which we are interested. The value of the displacement applied varies from 20 to 50 mm, depending on the size of the member, for larger element, larger displacement.

3.1.4 Mesh

Before running the analysis is required to define the mesh that will be applied to the model. This mesh is the way that the whole model is separated in smaller elements (is possible to define how to do this separation, not necessarily all elements will have the same size and shape). After this, is required to choose the type of element that is wanted. In all of the simulations the cross section has been modelled by using a four node (quadrilateral) shell element with reduced integration S4R, which has been widely utilised when modelling cold-formed stainless steel cross-sections. After a mesh convergence study, and in order to guarantee computational efficiency, the analyses have been conducted with 5mm long shell elements for stub-column and combined loading simulations but for simple and biaxial bending simulations the elements have been defined with 10mm length due to the larger length of these last ones.

The S4R (Fig. 14) is an element that uses uniformly reduced integration to avoid shear and membrane locking. The element has several hourglass modes that may propagate over the mesh. S4R converges to shear flexible theory for thick shells and classical theory for thin shells. Is a robust, general-purpose element that is suitable when the 3D model can be simplified by plane elements where each one of them has an assigned thickness (this thickness tends to be small, when thickness is bigger will be necessary 3D discretization elements for the FEM: hexahedral and tetahedra).

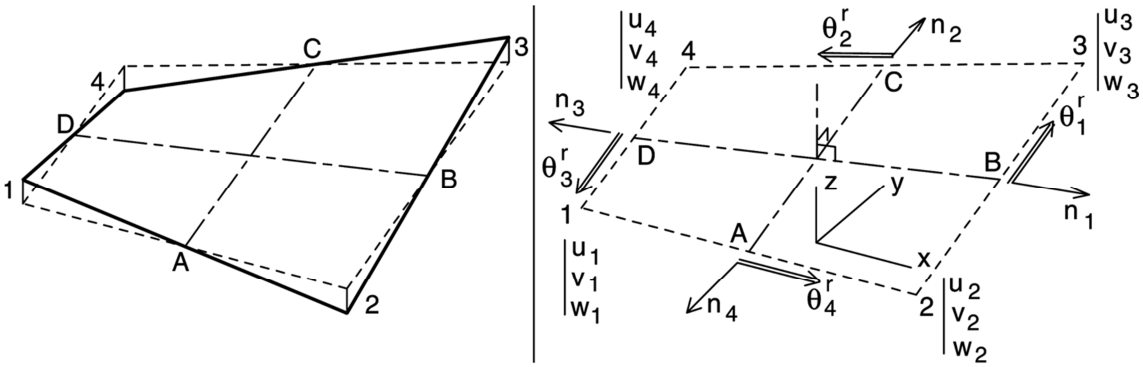

Figure 14. S4R mesh element [26]

3.1.5 Running the model

After being defined the mesh, it will be possible to run the model. The first linear analysis is due to obtain the initial imperfection shapes of the member. Once done this, a new file is created (.fil) which will be used to modify the input file of the non-linear analysis *Static, Riks* in order to introduce the initial imperfection's information and get the final results properly. The initial deformation considered is related to the first buckling mode with a 1% of the thickness as amplitude value.

3.1.6 Obtaining the results

After running the non-linear analysis, the next step it to analyse the post-process. Results can be shown with different variables, for instance: comparing the evolution of the displacement versus the reaction force, or the moment that appears versus the rotation manifested. It is possible to get a graph to show the relationship between these two couples of parameters. With this graphs, ultimate efforts and displacements will be easily obtained.

3.2 Model: Calibrations and Particular specifications

Each model needs to be calibrated with an experimental test in order to guaranty that the reality is simulated properly. To do this, some papers of experimental tests were used [29 and 30]. The aim was to emulate the effort-deformation/rotation real curve as good as possible.

The next subsections explain particular specifications that each model has, apart from the calibration.

3.2.1 Stub-column/Combined loading tests

The following table 5 presents the length for each cross-section, which will be 3 times the value of the larger side of the cross-section.

Table 5. Element length for stub-column numerical simulations

Section	SC-Length(mm)	Section	SC-Length(mm)
S1-120x80x4	360	S7-60x60x3	180
S2-80x40x4	240	S8-70x50x2	210
S3-80x80x4	240	S9-100x100x3	300
S4-60x60x4	180	S10-100x100x3.5	300
S5-100x100x4	300	S11-120x120x5.5	360
S6-120x80x3	360	S12-80x80x2.5	240

The boundary conditions are defined with two constraint-coupling points placed 35mm perpendicularly to both faces in each extreme of the element (Fig. 15). Each constraint is referred to each extreme face of the element. The position of this point referred to the face will depend on the bending moment that will be required, as the axial load will be introduced with an eccentricity that will cause an additional bending moment (N·e=M). When the position of the point is on the centre of the section, it will mean stub-column test.

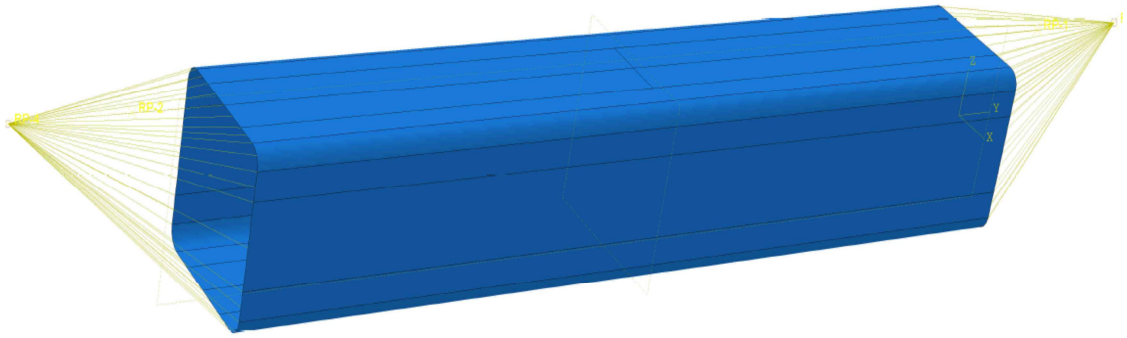

Figure 15. Stub-column boundary conditions

These two points were fixed in all of their 3 displacements and torsional rotation (2 free rotations) but one of these two points has an imposed longitudinal displacement which is the external action applied. Rotation restrictions depend on the axis that is required to be studied: normally the rotation that is restricted is the one that belongs to the strong bending axis.

3.2.1.1 Calibration

Good agreement between the experimental results and FEM has been observed as it can be appreciated at Fig.16, where load-deflection curves are presented for the experimental test and numerical analysis. The experimental test was done for a SHS 60x60x5 and 400mm long.

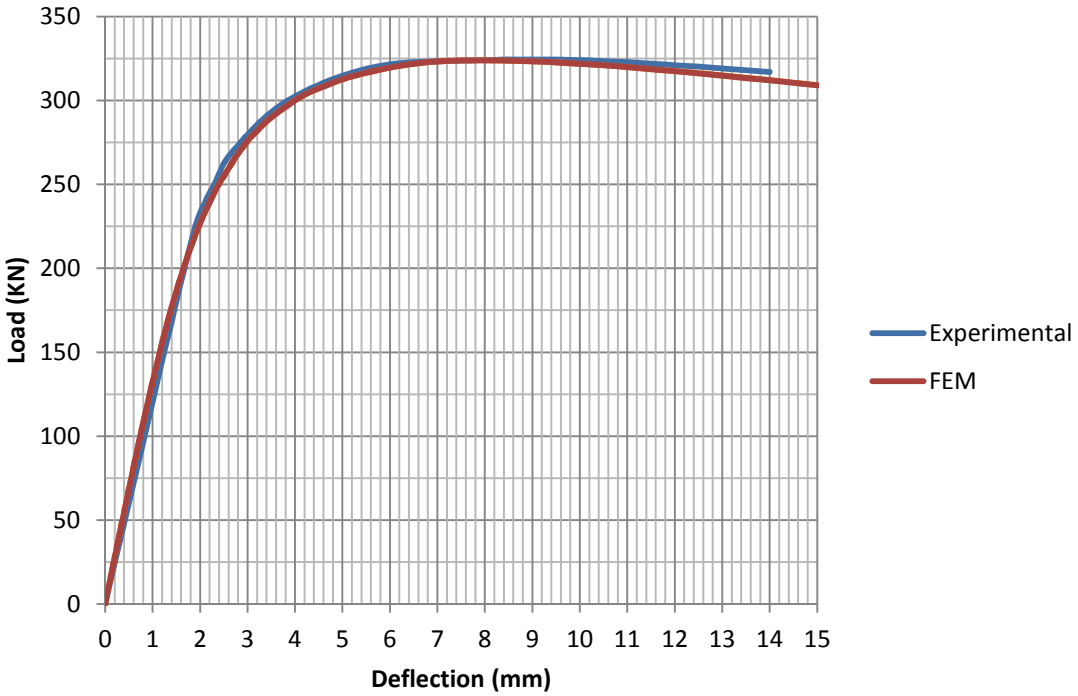

Figure 16. Stub-column/combined load-deflection calibration curve

The error between the maximum resisting load between the experimental case and the one simulated can be appreciated in table 6.

Table 6. Error between experimental results and simulation for stub-column test

	Experimental Results	Simulated Results
Ultimate Load(KN)	325	323.9
Displacement(mm)	9	7.7
Relative Error in Ultimate Load(%)	-	0.4
Relative Error in Displacement (%)	-	14.4

With these results, not only the simulated load-deflection curve fits well, but an important parameters as the maximum load is accurately predicted. However, the displacement has larger error but assumable.

3.2.2 Bending tests

The length of the element will be 1600mm for all of the different cross-sections. The boundary conditions are defined in 3 different constraint-coupling points. Each constraint is referred to a surface, which depend on the test being analysed:

a) Uniaxial bending test:

The surface measures 50xbmm^2, if we want to obtain the ultimate M_y or 50xhmm^2, if we want to obtain the ultimate M_z, where *b* and *h* are the width and depth of the cross-section respectively. An example is shown in Fig. 17.

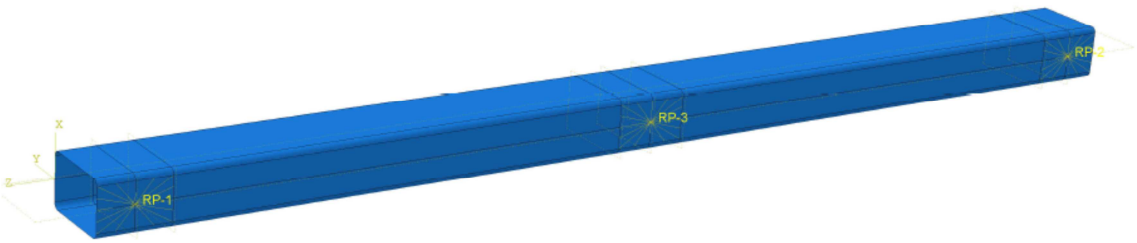

Figure 17. Boundary conditions of uniaxial bending test

The middle point is placed where the external action will be applied action in terms of a displacement. The direction of this displacement will be normal towards the exterior referring to the surface which is placed in the middle of the beam (no more degrees of freedom are modified).

b) Biaxial bending test:

The surface coincides with the cross-sections that are placed at 50, 800 and 1550mm (extremes and middle of the beam). An example is shown in Fig. 18.

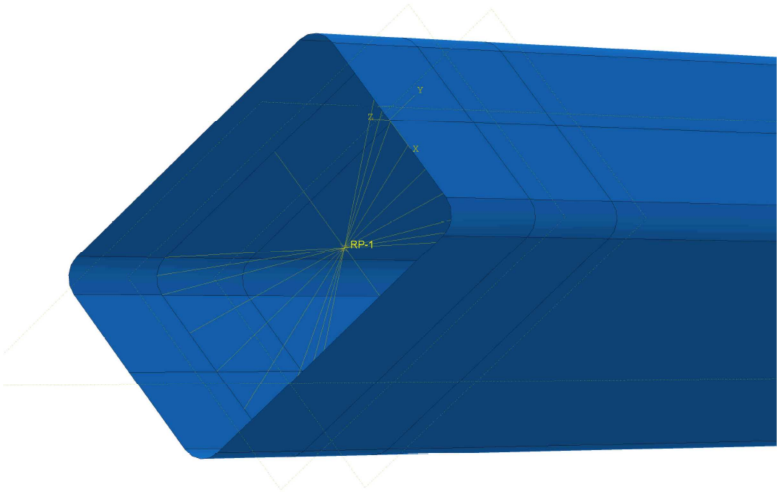

Figure 18. Boundary conditions of biaxial bending test

The middle point is placed where the external action will be applied which is applied to the central cross-section and consists of a displacement in “y” and “z” directions (x displacement is free). The values for these combined displacements will be a combination of the values associated to each direction, depending on the combination of the ultimate M_y+M_z that is wanted to be obtained.

For both tests, the position of each constrained point is in the centre of each surface. These 3 surfaces are placed in: one in the middle of the beam (referred to the longitudinal dimension) and the last two in each extreme of the beam (at 50, 800 and 1550mm, extremes of the beam and the midspan section, see Fig. 17).

The rest two boundary conditions define the supports of the beam. These supports only restrict torsional rotation, and when talking about displacements, all will be restricted in one of the supports but the other one will permit the longitudinal displacement.

As it can be appreciated, the span length between supports is 1500mm (distance between centres of both extreme boundary condition surfaces) and this will be the value to use when calculating analytical results.

3.2.2.1 Calibration

The experimental test was done for a RHS 60x60x3 and 1600mm length. As well as for the stub-column test, a parameters comparison has been done too (table 7).

Table 7. Error between experimental results and simulation for Uniaxial Bending test

	Experimental Results	Simulated Results
Ultimate Load(KN)	615	638.7
Displacement(mm)	4	3.7
Relative Error in Ultimate Load (%)	-	3.8
Relative Error in Displacement (%)	-	7.5

As it can be appreciated, both errors are near 5% and it can be concluded that the numerical model simulates properly the real test. The result of the calibration is shown in Fig. 19, in which good agreement between the experimental results and FEM simulation is presented.

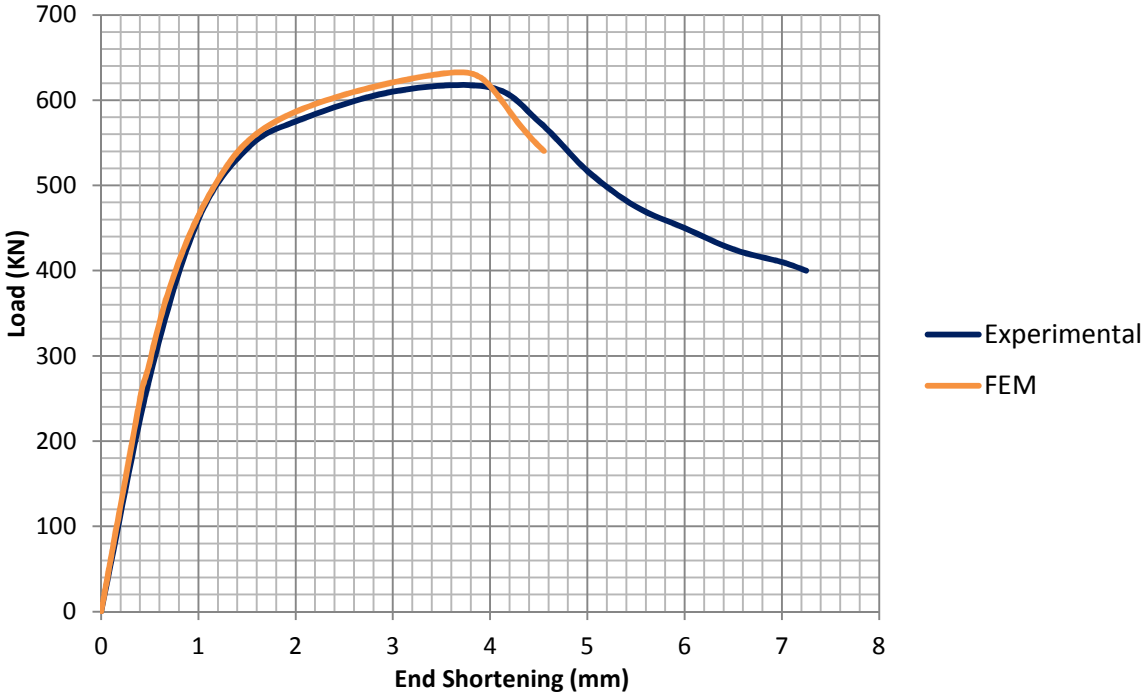

Figure 19. Uniaxial bending test calibration

3.3 Geometry and material

This section will justify the different cross-section and material that have been chosen for this numerical analysis.

3.3.1 Geometry

It is very important to define the cross-section geometry properly in order to obtain results that will be easier to analyse and extract conclusions about. If the geometry would be chosen randomly, surely the obtained results would not represent the wide whole casuistry of cross-sections commercially available.

While choosing the cross-section geometry, the parameter that is being looked for is the cross-sectional slenderness. This parameter is the one used, for Eurocode 1993-1-4, when classifying a stainless-steel cross-section with the aim of identifying the extent to which resistance and rotation capacity of the cross section is limited by its local buckling resistance. It is an important parameter for the CSM too.

This base curve has to important slenderness values:

- $\varepsilon_{csm}/\varepsilon_y \leq 15 \rightarrow \lambda_p = 0.32$ (corresponds to the material ductility requirement ex
- pressed in EN 1993-1-1) it does not depend on the cross-section.
- $\varepsilon_{csm}/\varepsilon_y = 1 \rightarrow \lambda_p = 0.68$ This limit is the transition from class 3 to class 4 cross-sections in EN 1993-1-3 and EN 1993-1-4 classification.

When the slenderness is lower than 0.32, the base curve is a straight line and for slenderness higher than 0.68 cross-sections begin to undergo local buckling problems. As this research project is for stocky members, slenderness higher than 0.68 will have no interest herein. The straight line for slenderness lower than 0.32 is due to a material maximum ductility requirement (a material with too high ductility will fail with considerably high deformation and because of this, when the designing process takes place, its ultimate strain is limited virtually).

Said this, the different geometries that will be analysed will present slenderness between 0 (does not exists) and 0.68. After consulting some ferritic stainless steel cross-section catalogues [27 and 28], the ones chosen are presented on table 8. This table includes the slenderness of each cross-section calculated by the EN 1993-1-1 method (Eq. 29).

Table 8. Analysed cross-sections and their slenderness

Dimensions	$\lambda_{cs,min}$ EN expression	Dimensions	$\lambda_{cs,min}$ EN expression
S1-120x80x4	0.54	S7-60x60x3	0.35
S2-80x40x4	0.34	S8-70x50x2	0.64
S3-80x80x4	0.34	S9-100x100x3	0.65
S4-60x60x4	0.26	S10-100x100x3.5	0.55
S5-100x100x4	0.45	S11-120x120x5.5	0.40
S6-120x80x3	0.76	S12-80x80x2.5	0.60

As it can be seen on Fig. 20, there are cross-sections with the slenderness very close to each other, but the reason to choose them was because in this research project are analysed both RHS and SHS cross-sections. A total of 12 different RHS and SHS will be analysed, trying to cover all the casuistry of stocky cross-sections.

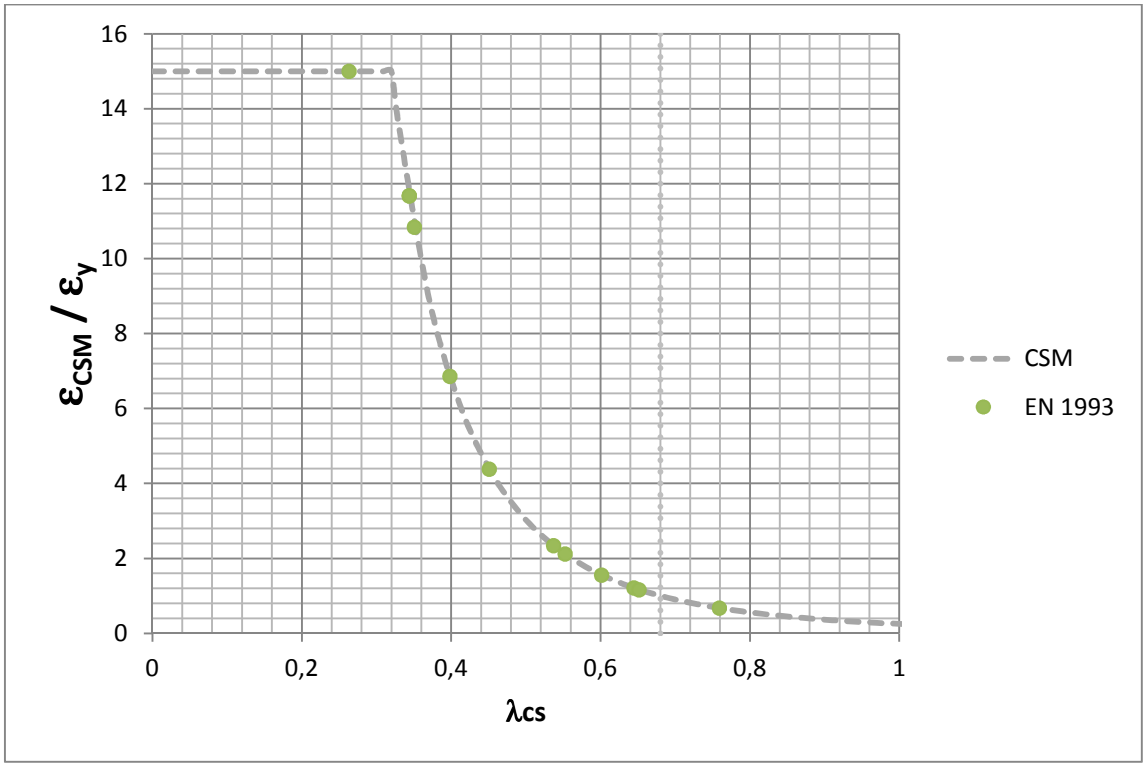

Figure 20. Analysed cross-section slenderness

The parameters that will define our RHS or SHS will be the following ones:

-b: width, which refers to the width of the average perimeter

-h: depth, which refers to the depth of the average perimeter

-t: thickness

-r: radius, which refers to the radius of the average perimeter

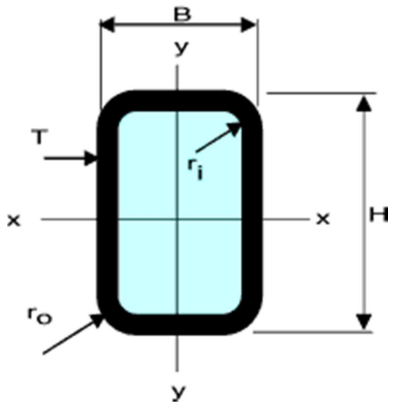

Figure 21. RHS & SHS geometry parameters

In this research work has been assumed that when parameters are with small letter refers to average perimeter, and when are with capitals refers to the external perimeter (Fig. 21).

The different cross-section values for all the geometry parameters are gathered in the following table 9.

Table 9. Cross-section parameters values

Cross-Section	b(mm)	h(mm)	t(mm)	r(mm)
S1-120x80x4	116	76	4	8
S2-80x40x4	76	36	4	6
S3-80x80x4	76	76	4	6
S4-60x60x4	56	56	4	3.5
S5-100x100x4	96	96	4	6
S6-120x80x3	117	77	3	5.5
S7-60x60x3	57	57	3	4
S8-70x50x2	68	48	2	4
S9-100x100x3	97	97	3	3
S10-100x100x3.5	96.5	96.5	3.5	3.25
S11-120x120x5.5	114.5	114.5	5.5	6.25
S12-80x80x2.5	77.5	77.5	2.5	3.75

The radius hardly ever appears in catalogues and is the most difficult parameter to measure. To define the radius of each cross-section an experimental database which contained different cross-section's geometries has been used. Areas and second moments of inertia have been deduced using a graphic design program.

3.3.2 Material

The material chosen for the preliminary study has been the ferritic stainless-steel grade 1.4003. The typical values for the parameters that will be used to define the stress-strain curve of this steel are specified in the following table 10.

Table 10. Adopted material properties

E(MPa)	198000
$\sigma_{0.2}$(MPa)	330
σ_u(MPa)	480
ε_u	17%
n	11.5
m	2.8

Where E is the Young's Modulus, $\sigma_{0.2}$ is the proof stress corresponding to a 0.2% plastic strain, σ_u is the ultimate strength of the material and ε_u the % of deformation that corresponds to this ultimate strength. Parameters n and m are the strain hardening exponents for Mirambell&Real [8] material model, as defined in section 2.1.6. This model has been chosen because it has two tiers that arrive to ε_u and gives very good results for ferritic stainless-steels as it takes into account the strain hardening.

With these values, applying the proposed material model in 2.1.6, the stress-strain curve has been obtained (Fig. 22).

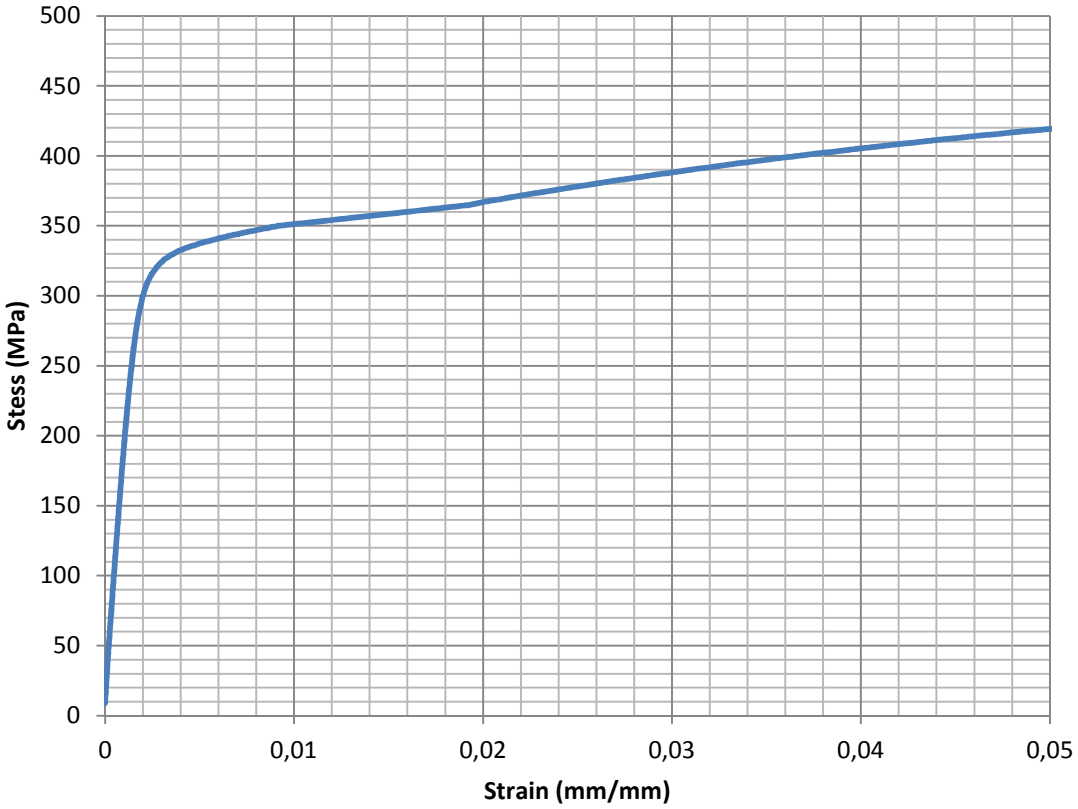

Figure 22. Basic 1.4003 ferritic stainless steel stress-strain curve

We will assume that this is the real stress-strain curve for the material being studied. This material model is going to be used for the numerical models. As it has been seen in section 2.4.3, CSM requires a bilinear model in order to simplify the calculations. Mirambell&Real [8]

material model is a two stage material model and is the one that will be used for analytical expressions.

After applying the material parameter values from table 10 to the CSM material model presented in [22] the resulting curve did not fit with the reference one. The problem was that the E_{sh} (strain hardening modulus) was too large. In fact, given that ferritic and austenitic stainless steels present such different material behaviour between them and that the CSM material [22] model was calibrated for austenitic stainless steels, it was not a surprise that this CSM material model did not fit well to the reference model.

What has been done is to find out what value of E_{sh} fits better the target material model. The value that fit better was 2000 MPa (see Fig. 23).

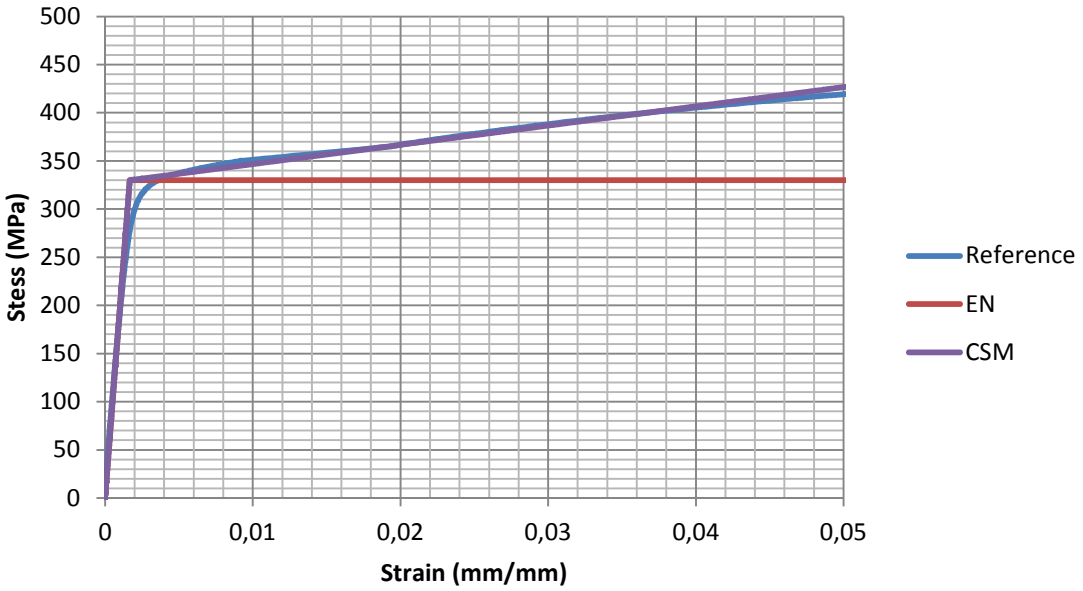

Figure 23. Comparison of the different material models

As can be appreciated, EN 1991-1-1 material model (carbon steel) is the elastic perfectly plastic material behaviour, noted as EN in Fig. 23, which differs from the CSM one in the plastic tier of the stress-strain curve: EN 1993-1-1 does not take into account the stain hardening (it is like considering E_{sh}=0, slope of the plastic part of the curve). The CSM considers that the material is able to admit more strength while gaining strain, which does not happen with an elastic perfectly plastic material. Thereby, it has been adopted a bilinear model with a branch of hardening of E_{sh}=E/100.

3.4 Numerical Results

In the following sections are presented the results of the numerical simulations obtained from each type of test: stub-column tests, combined loading tests, uniaxial and biaxial bending tests. For each type of test it will be shown a deformed shape as a prime example for both buckle and non-linear analysis. Moreover, tables with the numerical results of the ultimate loads and/or moments that have been reached will be included.

3.4.1 Stub-column

As it has been said before, in order to obtain the numerical results, two different types of analysis have to be done: "*Buckle"* and "*Static, Riks"*. The model used is the one explained in section 3.2.1: stub-column/combined loading test. The displacement will be applied in the centre of the cross section, this way no bending moment is introduced into the member.

Following EN 1993-1-1 recommendations, the length of the elements for this type of test will be 3 times the larger dimension of the cross-section, so the length will depend on the cross-section being analysed.

On table 11 is shown a comparison between the analytical (EN 1993-1-1) and the numerical (ABAQUS) results for the slenderness. The analytical slenderness is calculated with Eq. 29. However, the numerical one is calculated using Eq. 27, where f_y is known (material parameter) and it is only missed the critical stress. To calculate this critical stress is required the numerical eigenvalue of the deformed shape for the first mode of buckling (ABAQUS). Multiplying the eigenvalue for the imposed displacement, it gives us the critical displacement. Given the critical displacement is easy to calculate the critical axial load (for stub-column tests) or critical bending moment (for bending tests) that produces this displacement. Then only lasts the calculation of the critical stress and finally apply Eq. 27.

Table 11. Comparison of analytical and numerical slenderness

Section	$\lambda_{cs,min}$		Section	$\lambda_{cs,min}$	
	EN expression	ABAQUS		EN expression	ABAQUS
S1-120x80x4	0.54	0.54	S7-60x60x3	0.35	0.4
S2-80x40x4	0.34	0.35	S8-70x50x2	0.64	0.71
S3-80x80x4	0.34	0.4	S9-100x100x3	0.65	0.67
S4-60x60x4	0.26	0.3	S10-100x100x3.5	0.55	0.58
S5-100x100x4	0.45	0.5	S11-120x120x5.5	0.40	0.44
S6-120x80x3	0.76	0.71	S12-80x80x2.5	0.60	0.64

As it can be appreciated, obtained numerical slendernesses are very close to the analytical ones. The difference between both methods is that analytical slendernesses only take into account the most slender element of the cross-section (being more conservative) while the numerical one takes into account the interaction of this element (the more slender one) with the rest of the cross-section elements (giving higher slenderness).

In order to give an idea of the deformed shapes for the first mode of "Buckle" and the "Static, Riks" analysis, an example of each one, for S1 cross-section, are shown on Fig. 24 and Fig. 25, respectively.

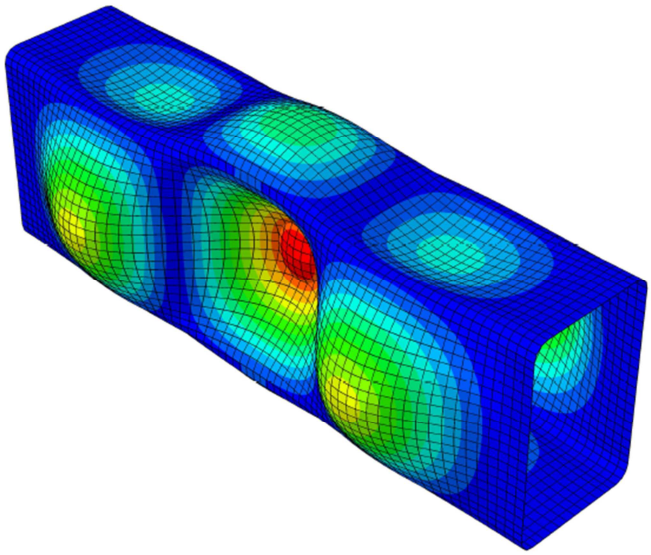

Figure 24. S1 stub-column test first mode shape of “Buckle” analysis

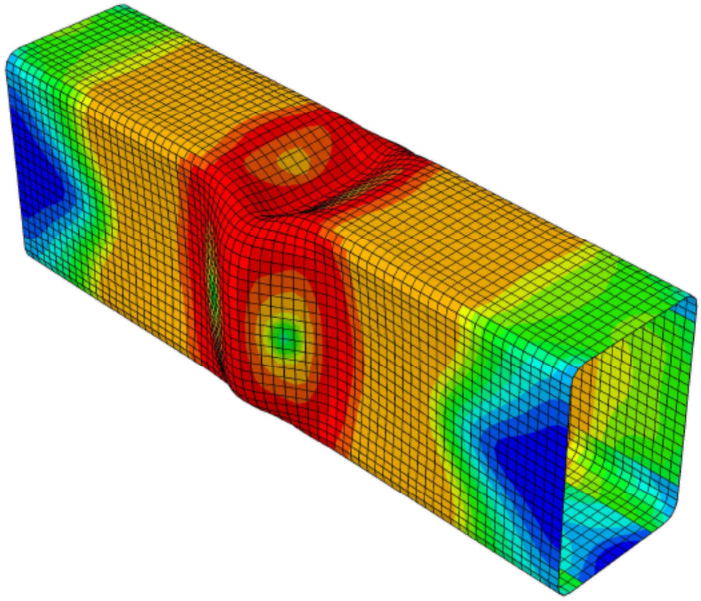

Figure 25. S1 stub-column test deformed shape of “Static, Riks” analysis

The following table 12 shows the numerical results of all of the ultimate loads for the different cross-sections for stub-column test simulations.

Table 12. Numerical stub-column results

Cross-section	$N_{u,FEM}$ (kN)
S1-120x80x4	583.5
S2-80x40x4	351.4
S3-80x80x4	458.2
S4-60x60x4	398.7
S5-100x100x4	521.1
S6-120x80x3	419.1
S7-60x60x3	257.5

Table 12. Numerical stub-column results

Cross-section	$N_{u,FEM}$ (kN)
S8-70x50x2	165.2
S9-100x100x3	439.3
S10-100x100x3.5	520.1
S11-120x120x5.5	995.4
S12-80x80x2.5	250.3

3.4.2 Combined loading

The model used is the one explained in section 3.2.1: stub-column/combined loading test. The displacement will be applied to a reference point, which will be placed with different eccentricities in order to obtain different N, $M_{y,}$and M_z combinations (axial force, "y" bending moment and "z" bending moment, respectively) . The positions chosen to apply the displacement are shown on Fig. 26.

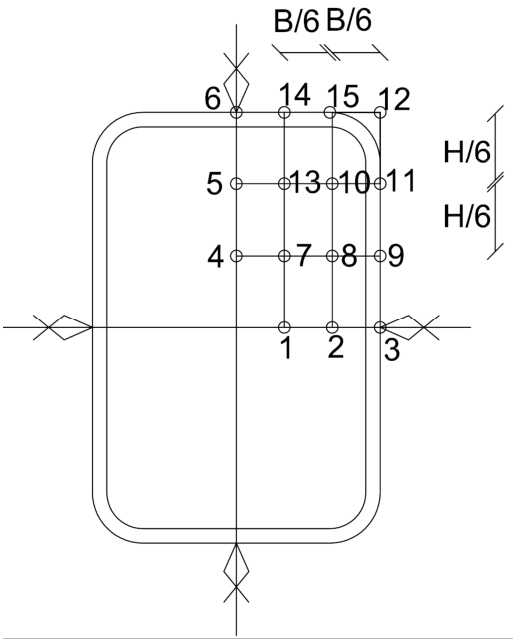

Figure 26. Positions of different reference points for combined loading test

Where B and H are the width and depth of the average perimeter, respectively. Given these different positions, results can be separated between: uniaxial combined loading (1, 2, 3, 4, 5 and 6 positions) and biaxial combined loading (7, 8, 9, 10, 11, 12, 13, 14 and 15). A total of 15 simulations have to be done for each RHS, but the diagonal symmetry that exists for SHS will mean a reduction in the number of simulations required to cover all the different cases: 3 for uniaxial combined loading (1=4, 2=5, 3=6) and 6 for biaxial combined loading (8=13, 9=14, 10, 11=15 and 12).

The first mode shape of "Buckle" and deformed shape of "Static, Riks" analysis for S1 cross-section are shown on Fig. 27 and Fig. 28, respectively.

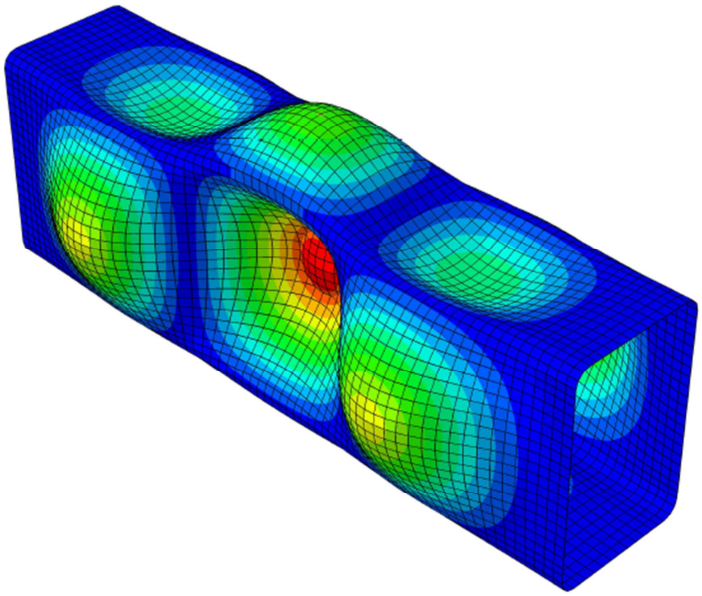

Figure 27. S1 combined loading test first mode shape of "Buckle" analysis (2nd reference point)

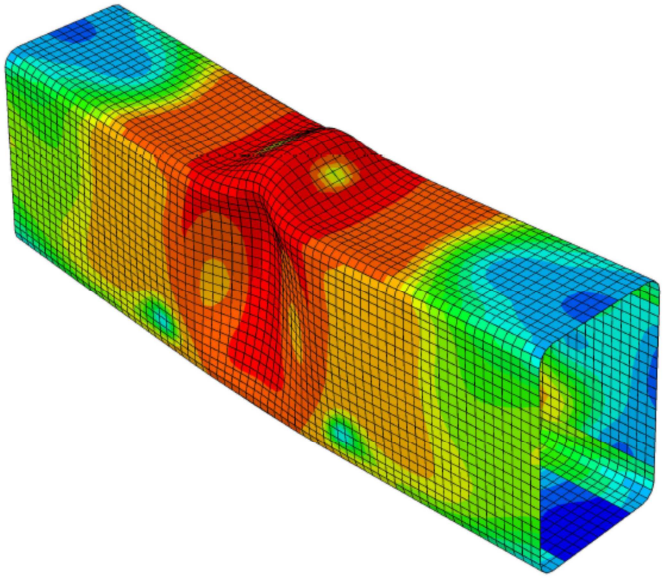

Figure 28. S1 combined loading test deformed shape of "Static, Riks" analysis (2nd reference point)

As the model used is the same as the one used for stub-column test, the "*Buckle*" analysis results are similar, the bigger imperfections are on the larger face of the member. The axis of buckling depends on the load case. In this 2nd reference point case, the axis of buckling has been the strong one but it could happen the buckling in the weak axis of bending. For example, if is shown the results for the 12th reference point (Fig. 29), the buckle occurs in the weak axis (in this case, the buckling has not taken place in the middle of the element).

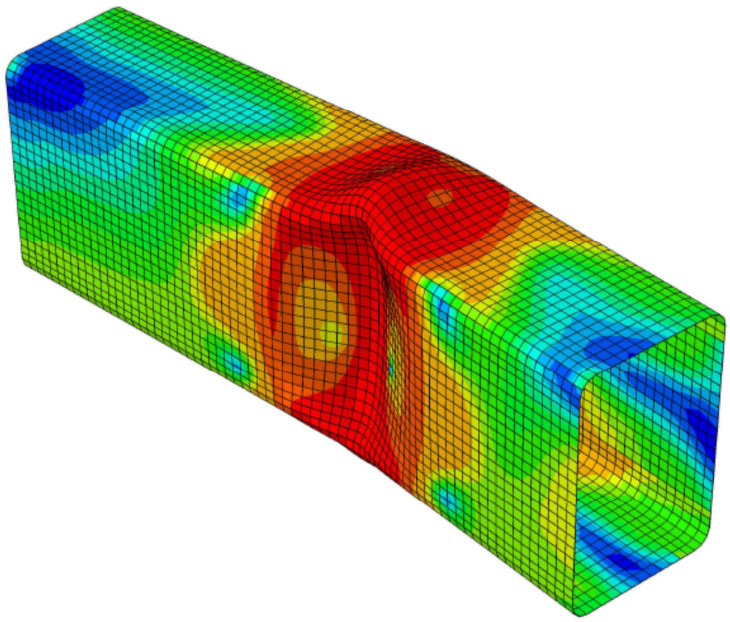

Figure 29. S1 combined loading test deformed shape of "Static, Riks" analysis (12th reference point)

Uniaxial combined loading results are shown in the following table 13. The position of each reference point has been defined in the beginning of this section. The following tables 13 and 14 present the results for uniaxial and biaxial combined loading tests, respectively.

Table 13. Uniaxial combined loading numerical results

Cross-section	Ref. Point	e_z(mm)	e_y(mm)	N_u(kN)	$M_{u,y}$(kNm)	$M_{u,z}$(kNm)
S1-120x80x4	1	12.7	0	421.5	0	5.3
	2	25.3	0	334.1	0	8.5
	3	38.0	0	276.8	0	10.5
	4	0	19.33	438.1	8.5	0
	5	0	38.7	351.3	13.6	0
	6	0	58	289.7	16.8	0
S2-80x40x4	1	6.0	0	216.9	0	1.3
	2	12.0	0	176.7	0	2.1
	3	18.0	0	148.9	0	2.7
	4	0	12.7	247.6	3.1	0
	5	0	25.3	194.5	4.9	0
	6	0	38.0	157.5	6.0	0
S3-80x80x4	1=4	12.7	0	327.9	0	4.2
	2=5	25.3	0	264.0	0	6.7
	3=6	38.0	0	219.4	0	8.3
S4-60x60x4	1=4	9.3	0	248.7	0	2.3
	2=5	18.7	0	202.2	0	3.8
	3=6	28	0	168.1	0	4.7
S5-100x100x4	1=4	16.0	0	391.8	0	6.3
	2=5	32	0	313.5	0	10.0
	3=6	48	0	260.9	0	12.5

Table 13. Uniaxial combined loading numerical results

Cross-section	Ref. Point	e_z(mm)	e_y(mm)	N_u(kN)	$M_{u,y}$(kNm)	$M_{u,z}$(kNm)
S6-120x80x3	1	12.7	0	347.6	0	4.5
	2	25.3	0	272.9	0	7.0
	3	38.0	0	224.0	0	8.6
	4	0	38.7	358.3	7.0	0
	5	0	38.7	281.6	11.0	0
	6	0	58	235.8	13.8	0
S7-60x60x3	1=4	9.5	0	177.3	0	1.7
	2=5	19	0	142.9	0	2.7
	3=6	28.5	0	118.8	0	3.4
S8-70x50x2	1	0	8.0	124.5	0	1.0
	2	0	16.0	100.2	0	1.6
	3	0	24.0	82.6	0	2.0
	4	11.3	0	126.9	1.4	0
	5	22.7	0	102.7	2.3	0
	6	34	0	86.1	2.9	0
S9-100x100x3	1=4	16.2	0	324.2	0	5.2
	2=5	32.3	0	253.0	0	8.2
	3=6	48.5	0	205.1	0	9.9
S10-100x100x3.5	1=4	16.1	0	384.2	0	6.2
	2=5	32.2	0	304.5	0	9.8
	3=6	48.3	0	250.7	0	12.1
S11-120x120x5.5	1=4	19.1	0	752.7	0	14.4
	2=5	38.2	0	602.8	0	23.0
	3=6	57.3	0	502.2	0	28.8
S12-80x80x2.5	1=4	12.9	0	215.0	0	2.8
	2=5	25.8	0	168.2	0	4.3
	3=6	38.75	0	136.3	0	5.3

Table 14. Biaxial combined loading numerical results

Cross-section	Ref. Point	e_z(mm)	e_y(mm)	N_u(kN)	$M_{u,y}$(kNm)	$M_{u,z}$(kNm)
S1-120x80x4	7	19.3	12.7	397.0	7.7	5.0
	8	19.3	25.3	323.8	6.3	8.2
	9	19.3	38.0	271.2	5.2	10.3
	10	38.7	25.3	292.7	11.3	7.4
	11	38.7	38.0	252.6	9.8	9.6
	12	58	38.0	227.7	13.2	5.8
	13	38.7	12.7	327.3	12.7	4.1
	14	58	12.7	276.4	16.0	3.5
	15	58	25.3	253.1	14.7	6.4

Table 14. Biaxial combined loading numerical results

Cross-section	Ref. Point	e_z(mm)	e_y(mm)	N_u(kN)	$M_{u,y}$(kNm)	$M_{u,z}$(kNm)
S2-80x40x4	7	12.7	6.0	209.7	2.7	1.3
	8	12.7	12.0	172.2	2.2	2.1
	9	12.7	18.0	145.5	1.8	2.6
	10	25.3	12.0	156.1	4.0	1.9
	11	25.3	18.0	135.1	3.4	2.4
	12	38.0	18.0	121.0	4.6	2.2
	13	25.3	6.0	181.1	4.6	1.1
	14	38.0	6.0	151.5	5.8	0.9
	15	38.0	12.0	135.6	5.2	1.6
S3-80x80x4	7	12.7	12.7	309.1	3.9	3.9
	8=13	12.7	25.3	256.3	3.2	6.5
	9=14	12.7	38.0	213.5	2.7	8.1
	10	25.3	25.3	229.1	5.8	5.8
	11=15	25.3	38.0	198.4	5.0	7.5
	12	38.0	38.0	177.7	6.8	6.8
S4-60x60x4	7	9.3	9.3	231.4	2.2	2.2
	8=13	9.3	18.7	192.6	1.8	3.6
	9=14	9.3	28.0	162.0	1.5	4.5
	10	18.7	18.7	170.2	3.2	3.2
	11=15	18.7	28.0	148.2	2.8	4.1
	12	28.0	28.0	132.8	3.7	3.7
S5-100x100x4	7	16.0	16.0	370.4	5.9	5.9
	8=13	16.0	32.0	306.6	4.9	9.8
	9=14	16.0	48.0	255.9	4.1	12.3
	10	32.0	32.0	277.2	8.9	8.9
	11=15	32.0	48.0	240.3	7.7	11.5
	12	48	48.0	216.3	10.4	10.4
S6-120x80x3	7	19.3	12.7	315.2	6.1	4.0
	8	19.3	25.3	259.9	5.1	6.7
	9	19.3	38.0	215.4	4.2	8.3
	10	38.7	25.3	233.6	9.1	6.0
	11	38.7	38.0	203.9	8.0	7.8
	12	58	38.0	178.6	10.5	6.9
	13	38.7	12.7	257.5	10.0	3.3
	14	58	12.7	226.2	13.2	2.9
	15	58	25.3	197.5	11.6	5.1
S7-60x60x3	7	9.3	9.3	166.9	1.6	1.6
	8=13	9.3	18.7	137.9	1.3	2.6
	9=14	9.3	28.0	115.3	1.1	3.3
	10	18.7	18.7	123.0	2.3	2.3
	11=15	18.7	28.0	106.5	2.0	3.0
	12	28.0	28.0	95.3	2.7	2.7

Table 14. Biaxial combined loading numerical results

Cross-section	Ref. Point	e_z(mm)	e_y(mm)	N_u(kN)	$M_{u,y}$(kNm)	$M_{u,z}$(kNm)
8-70x50x2	7	11.3	8.0	115.2	1.3	0.9
	8	11.3	16.0	97.1	1.1	1.6
	9	11.3	24.0	81.2	0.9	1.9
	10	22.7	16.0	88.2	2.0	1.4
	11	22.7	24.0	77.0	1.7	1.8
	12	34	24.0	67.7	2.3	1.6
	13	22.7	8.0	97.3	2.2	0.8
	14	34	8.0	83.3	2.8	0.7
	15	34	16.0	74.2	2.5	1.2
S9-100x100x3	7	16.0	16.0	293.8	4.7	4.7
	8=13	16.0	32.0	243.1	3.9	7.9
	9=14	16.0	48.0	203.7	3.3	9.9
	10	32.0	32.0	214.3	6.9	6.9
	11=15	32.0	48.0	188.6	6.1	9.1
	12	48	48.0	169.4	8.2	8.2
S10-100x100x3.5	7	16.0	16.0	355.4	5.7	5.7
	8=13	16.0	32.0	295.8	4.8	9.5
	9=14	16.0	48.0	246.4	4.0	11.9
	10	32.0	32.0	266.3	8.6	8.6
	11=15	32.0	48.0	231.0	7.4	11.1
	12	48	48.0	208.1	10.0	10.0
S11-120x120x5.5	7	19.3	12.7	712.5	13.6	13.6
	8=13	19.3	25.3	589.9	11.3	22.5
	9=14	19.3	38.0	491.5	9.4	28.1
	10	38.7	25.3	529.7	20.2	20.2
	11=15	38.7	38.0	459.5	17.5	26.3
	12	58	38.0	411.4	23.6	23.6
S12-80x80x2.5	7	12.7	12.7	196.6	2.5	2.5
	8=13	12.7	25.3	162.2	2.1	4.2
	9=14	12.7	38.0	134.7	1.7	5.2
	10	25.3	25.3	142.5	3.7	3.7
	11=15	25.3	38.0	126.1	3.3	4.9
	12	38.0	38.0	112.8	4.4	4.4

As it can be appreciated, more eccentricity means less axial effort endured by the member. Due to this eccentricity, the axial force produces a moment, which is translated as more stresses acting on the member. These bending stresses consume part of the capacity of the beam, which will not be able to resist the same axial force as without eccentricity.

3.4.3 Uniaxial Bending

The model used is the one explained in section 3.2.2: uniaxial bending test. Fig 30 and 31 show: the first mode shape of “Buckle” and deformed shape of “Static, Riks” analysis for S1 cross-section, respectively.

The biggest imperfections are in the middle of the beam. The final result is logical as the displacement is applied to central point of the 50xbmm^2 central reference surface.

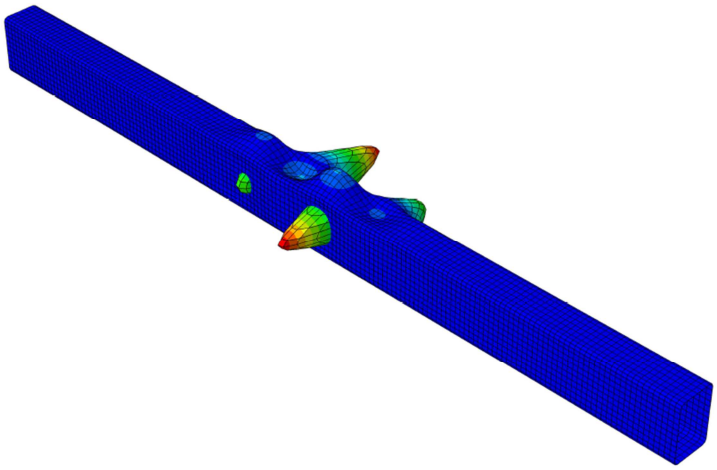

Figure 30. S1 uniaxial bending test first mode shape of “Buckle” analysis

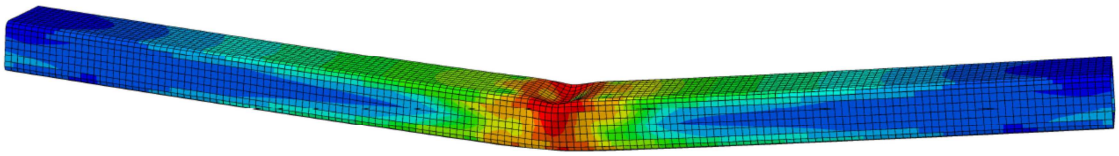

Figure 31. S1 uniaxial bending test deformed shape of “Static, Riks” analysis

The numerical ultimate capacities are shown in tables 15 and 16 below.

Table 15. Uniaxial Bending M_y numerical results

Cross-section	$M_{u,FEM,y}$ (kNm)
S1-120x80x4	29.4
S2-80x40x4	11.4
S3-80x80x4	14.8
S4-60x60x4	8.8
S5-100x100x4	22.2
S6-120x80x3	20.5
S7-60x60x3	6.1
S8-70x50x2	5.7
S9-100x100x3	17.7
S10-100x100x3.5	20.9
S11-120x120x5.5	50.6
S12-80x80x2.5	9.4

Table 16. Uniaxial Bending M_z numerical results

Cross-section	$M_{u,FEM,z}$ (kNm)
S1-120x80x4	19.7
S2-80x40x4	5.6
S3-80x80x4	14.8
S4-60x60x4	8.8
S5-100x100x4	22.2
S6-120x80x3	11.1
S7-60x60x3	6.1
S8-70x50x2	4.4
S9-100x100x3	17.7
S10-100x100x3.5	20.9
S11-120x120x5.5	50.6
S12-80x80x2.5	9.4

The more cross-section area, the larger is the resisting bending moment. It can be appreciated that the weaker axis of bending is “z” and the resisting bending moments are smaller than the ones for the “y” axis, the strong axis.

3.4.4 Biaxial Bending

The model used is the one explained in section 3.2.2: bending test. Fig 32 and 33 show: the first mode shape of “Buckle” and deformed shape of “Static, Riks” analysis for S1 cross-section, respectively.

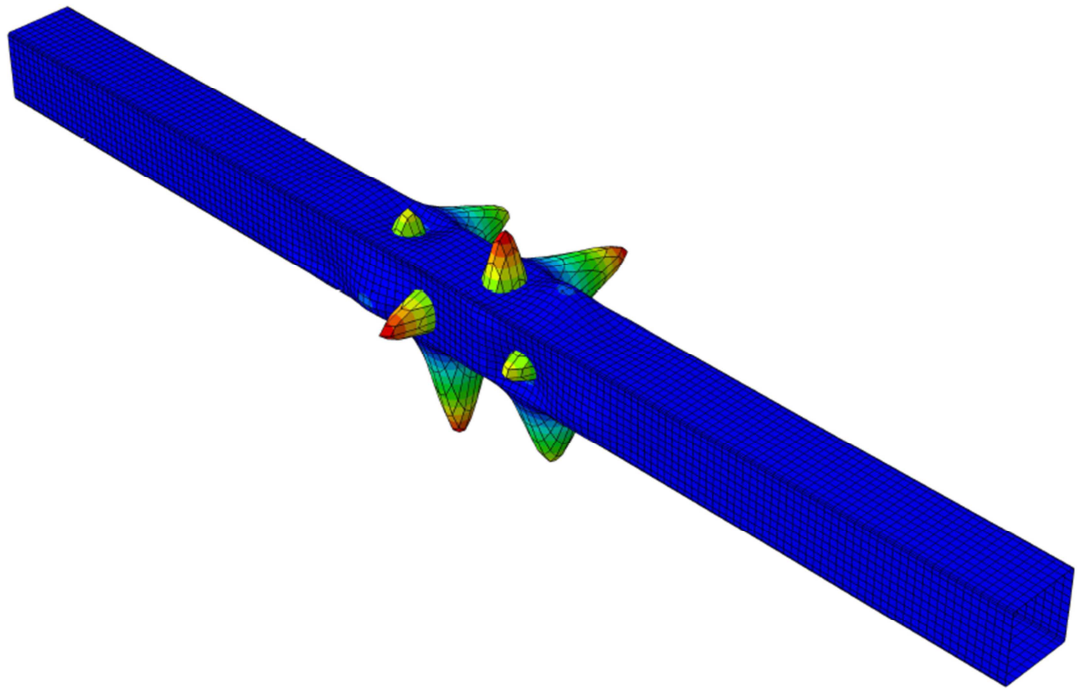

Figure 32. S1 biaxial bending test first mode shape of “Buckle” analysis

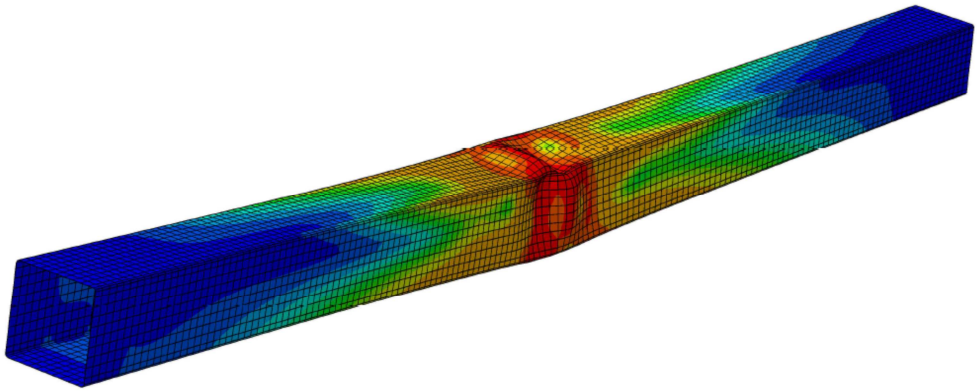

Figure 33. S1 biaxial bending test deformed shape of "Static, Riks" analysis

The following table 17 presents the numerical ultimate pare of bending moments that resists the element. The aim of this test was obtaining pair of M_y + M_z values that define the safety region of the space on the plane N_u=0. Three pairs of each cross-section have been obtained: one for uy=uz, another one for uy=2uz and a last one for 2uy=uz. Obviously, when is being simulated a SHS would only be needed to do two pairs (result from 2uy=uz is the same as uy=2uz because of the symmetry). Instead of only obtaining two simulations (2 pairs), another third pair was done.

Table 17. Biaxial Bending numerical results

Cross-section	$M_{u,FEM,y}$ (kN)	$M_{u,FEM,z}$ (kN)
S1-120x80x4	25.8	6.3
	7.7	18.3
	17.8	13.3
S2-80x40x4	7.4	3.2
	3.2	5.1
	7.7	2.9
S3-80x80x4	14.1	3.9
	2.9	14.5
	7.3	12.0
S4-60x60x4	5.9	5.8
	1.8	8.7
	8.5	2.6
S5-100x100x4	21.0	6.0
	4.3	21.5
	9.1	19.3
S6-120x80x3	17.6	4.7
	5.5	12.7
	15.0	7.6
S7-60x60x3	4.1	4.1
	1.2	6.0
	5.9	1.8
S8-70x50x2	4.1	2.5
	1.4	4.3
	5.4	1.3

Table 17. Biaxial Bending numerical results

Cross-section	$M_{u,FEM,y}$ (kN)	$M_{u,FEM,z}$ (kN)
S9-100x100x3	11.7	11.7
	5.2	16.6
	9.8	13.3
S10-100x100x3.5	13.4	13.4
	9.6	16.7
	4.9	19.7
S11-120x120x5.5	33.2	32.8
	22.7	41.1
	11.1	47.7
S12-80x80x2.5	6.1	6.2
	4.5	7.7
	2.3	9.0

One observation that can be done is that if there is a bending moment actuating in one axel it will affect the capacity to bend in the other axis by reducing it.

4. Cross-Section Analysis: Analytical Results and its Comparison versus FEM Results

This section summarises the analytical results that have been obtained from standards, EN 1993-1-4 and the new design method CSM. It will also be compared these analytical results with the numerical ones presented along the section 3 below.

4.1 Method for the comparison of the results

In order to compare results, ratios $d_{analytical}/d_{numerical}$ ("d" represents a distance) have been calculated following different criterions depending on the test being studied. The aim of this method is to know how close each interaction equation is to the point that represents a numerical solution.

When the element undergoes one unique type of external action: axial force or bending moment (*stub-column* or *uniaxial bending moment* tests); the method followed is to calculate directly the ratio between the analytical result and the numerical one by using as $d_{analytical}$ the analytical result of the external action obtained and as $d_{numerical}$ the numerical result of the external action obtained. Note that in this case we are in a one dimension space and this is the reason why ratios are calculated directly.

The two tests types whose results can be compared using a one dimension space are: stub-column test and uniaxial bending test. Fig. 34 and 35 illustrate what has been explained in the paragraph above referring to stub-column test and uniaxial bending test, respectively.

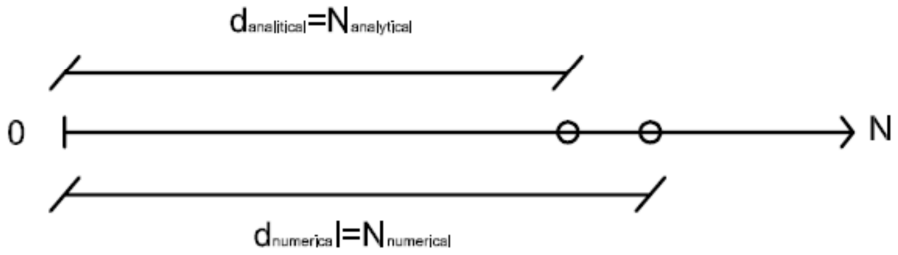

Figure 34. $d_{analytical}/d_{numerical}$ ratio for stub-column test

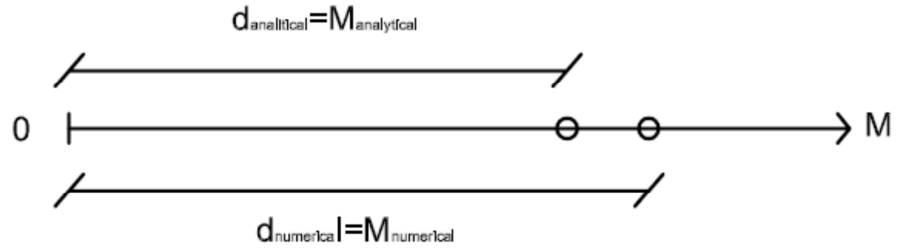

Figure 35. $d_{analytical}/d_{numerical}$ ratio for uniaxial bending test

When the element undergoes two types of external actions: axial force plus bending moment (y-y or z-z, *uniaxial combined loading*) or y-y bending moment plus z-z bending moment; the

method followed to calculate the ratio is not direct. In this case we are in a two dimensional space (M-N, or M_y-M_z). Our interaction equation is defined in this space, and what we are going to do to compare results is to measure the distances between the coordinate origin and the point that represents the combination of both external actions for each case: numerical (OA) and analytical (OB). Then, it is possible to calculate the ratio OA/OB (see Fig. 36, M-N example). Point B it's a numerical result ($M_{numercial}$, $N_{numerical}$), and point A is the analytical result ($M_{analitycal}$, $N_{analytical}$) obtained by intersecting the line that connects the numerical result with the coordinate origin and the interaction equation.

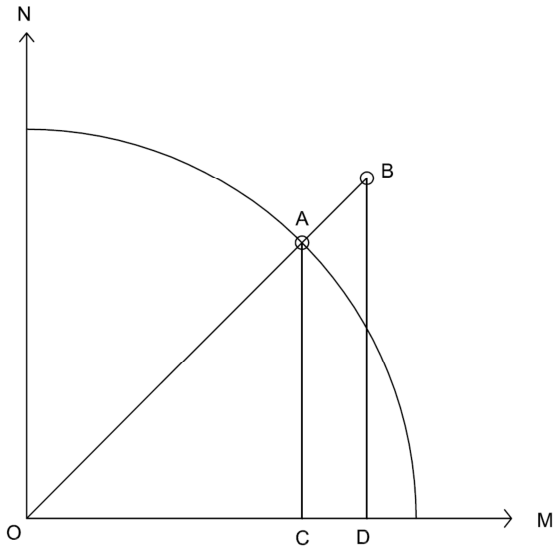

Figure 36. $d_{analytical}/d_{numerical}$ ratio for uniaxial combined loading

Note that if the ratio would have been calculated as CA/DB (one dimension ratio), the result would be more conservative as it only would have compared one of the two external action's results. The M_y-M_z case is analogous to the M-N one.

When the element undergoes three types of external actions: axial force, y-y bending moment and z-z bending moment (*biaxial combined loading*); the method followed can be extrapolated from the one used when two types of external actions were actuating on the element.

4.2 Stub-column

The following table 17 presents the values of the resistant axial force, for the different cross-sections, calculated with Eq. 7 (N_{EN1993}) and 31 (N_{CSM}). N_{EN1993} is the resistant axial force calculated by using EN 1993-1-4 and N_{CSM} is the resistant axial force calculated with the CSM. Both use the EN 1993-1-4 analytical slenderness (Eq 29).

$$N_{EN1993} = \frac{Af_y}{\gamma_{M0}} \qquad \text{for Class 1,2 or 3 cross} - \text{sections} \qquad Eq.7$$

$$N_{CSM} = \frac{Af_{csm}}{\gamma_{M0}} \qquad Eq.31$$

Where:

$$f_{csm} = f_y + E_{sh}\varepsilon_y\left(\frac{\varepsilon_{csm}}{\varepsilon_y} - 1\right) \qquad Eq.\,32$$

A cross sectional area

A_{eff} effective area, we can find how to calculate it in 4.3 (EN 1993-1-5)

f_y yield stress, for stainless-steel is considered $\sigma_{0.2}$

γ_{M0} partial factor for resistance of cross-sections whatever the Class is

E_{sh} strain hardening slope, which is determined as the slope of the line passing through the 0.2% proof stress point (f_y, ε_y). The value adopted that fits better the reference material stress-strain curve is 2000 MPa.

Table 17. Predicted stub-column test analytical results

Cross-section	N_{EN1993} (kN)	N_{CSM} (kN)
S1-120x80x4	488.8	495.4
S2-80x40x4	282.1	312.6
S3-80x80x4	387.7	429.6
S4-60x60x4	218.9	249.9
S5-100x100x4	502.3	519.6
S6-120x80x3	374.8	373.5
S7-60x60x3	218.9	240.7
S8-70x50x2	148.6	148.9
S9-100x100x3	379.0	379.7
S10-100x100x3.5	439.4	444.4
S11-120x120x5.5	811.8	860.0
S12-80x80x2.5	250.4	251.9

The following table 18 presents a comparison between the analytical and the numerical results. In this case is easy to define the comparison ratio, as the unique external action actuating is an axial force.

Table 18. Numercial vs analitycal ratios for stub-column test

Element Cross-Section	EN 1993 d_{EN1993}/d_{FEM}	CSM (EN) d_{CSM}/d_{FEM}
S1-120x80x4	0.84	0.85
S2-80x40x4	0.80	0.89
S3-80x80x4	0.85	0.94
S4-60x60x4	0.56	0.64
S5-100x100x4	0.96	1.00
S6-120x80x3	0.89	0.89
S7-60x60x3	0.85	0.93
S8-70x50x2	0.90	0.90
S9-100x100x3	0.86	0.86
S10-100x100x3.5	0.84	0.85
S11-120x120x5.5	0.82	0.86
S12-80x80x2.5	0.88	0.88

Table 18. Numercial vs analitycal ratios for stub-column test

Element Cross-Section	EN 1993	CSM (EN)
	d_{EN1993}/d_{FEM}	d_{CSM}/d_{FEM}
Average	0.84	0.88
COV	0.116	0.097

As it can be appreciated, CSM approaches better the numerical solution (3% better). S4 is the cross-section that presents worse analytical results. This is due to being the only section that does not accomplish the restriction on the normalised deformation capacity: $\varepsilon_{CSM}/\varepsilon_y<\min(15,0.45\varepsilon_u/\varepsilon_y)$, and needs to be applied an ε_{csm} modification. In other words, its slenderness is too low (λ_p=0.26, EN 1993-1-4 [4] slenderness).

The COV (coefficient of variation) is defined as the standard deviation divided by the average value. It's a kind of normalised value for the variation that shows a sample. The COV result is lower for CSM(EN) method.

4.3 Uniaxial bending test

The table 19 below shows ultimate resistant moments calculated with EN 1993-1-4 (Eq. 9 and 10) and CSM [22] (Eq. 33 and 34). Both are obtained using EN 1993-1-4 slenderness.

The resistant bending moment for uniaxial bending test defined in EN 1993-1-4 is:

$$M_{Rd} = \frac{W_{pl} f_y}{\gamma_{M0}} \quad \text{for Class 1or 2 cross} - \text{sections} \qquad Eq.9$$

$$M_{Rd} = \frac{W_{el,min} f_y}{\gamma_{M0}} \quad \text{for Class 3 cross} - \text{sections} \qquad Eq.10$$

Where:

W_{pl} cross-section plastic resistant modulus

$W_{el,min}$ cross-section elastic resistant modulus referred to the fibre with the maximum elastic stress

f_y yield stress, for stainless-steel is considered $\sigma_{0.2}$

γ_{M0} partial factor for resistance of cross-sections whatever the Class is

The CSM resistant bending moment for uniaxial bending test defined in [22] is:

$$M_{y,csm,Rk} = W_{pl,y} \cdot \sigma_{csm} \left[1 + \frac{E_{sh}}{E} \frac{W_{el,y}}{W_{pl,y}} \left(\frac{\varepsilon_{csm}}{\varepsilon_y} - 1 \right) - \left(1 - \frac{W_{el,y}}{W_{pl,y}} \right) \Big/ \left(\frac{\varepsilon_{csm}}{\varepsilon_y} \right)^2 \right] \qquad Eq.33$$

$$M_{z,csm,Rk} = W_{pl,z} \cdot \sigma_{csm} \left[1 + \frac{E_{sh}}{E} \frac{W_{el,z}}{W_{pl,z}} \left(\frac{\varepsilon_{csm}}{\varepsilon_y} - 1 \right) - \left(1 - \frac{W_{el,z}}{W_{pl,z}} \right) \Big/ \left(\frac{\varepsilon_{csm}}{\varepsilon_y} \right)^{\alpha} \right] \qquad Eq.34$$

Where

W_{pl} cross-section plastic resistant modulus

$W_{el,min}$ cross-section elastic resistant modulus referred to the fibre with the maximum elastic stress

σ_{csm} is the part of the total stress that belongs to the strain hardening part of the stress-strain curve of the material

ε_{csm} is the part of the total strain that belongs to the strain hardening part of the stress-strain curve of the material

E_{sh} strain hardening slope, which is determined as the slope of the line passing through the 0.2% proof stress point (f_y, ε_y). The value adopted that fits better the reference material stress-strain curve is 2000 MPa.

E is the material young's modulus, which in the case of stainless-steel is the slope of the line that conects the coordinate origin and the point of 0.2% strain

Table 19. Uniaxial Bending Test M_y analitycal results

Cross-section	$M_{y,CSM}$ (kNm)	$M_{y,EN}$ (kNm)	$M_{z,CSM}$ (kNm)	$M_{z,EN}$ (kNm)
S1-120x80x4	24.6	19.4	14.4	14.7
S2-80x40x4	8.7	6.9	5.1	4.2
S3-80x80x4	13.1	10.9	13.1	10.9
S4-60x60x4	5.9	4.6	5.9	4.6
S5-100x100x4	19.1	18.0	19.1	18.0
S6-120x80x3	15.7	15.1	4.8	8.5
S7-60x60x3	5.5	4.6	5.5	4.6
S8-70x50x2	3.8	3.5	2.3	2.8
S9-100x100x3	12.3	13.7	12.3	13.7
S10-100x100x3.5	15.6	15.8	15.6	15.8
S11-120x120x5.5	38.3	34.6	38.3	34.6
S12-80x80x2.5	6.8	7.2	6.8	7.2

Once all analytical results have been presented, the following table 20 shows the ratios that compare these analytical results with the numerical ones. As it has been explained in section 4.1, for uniaxial bending test is only required a one dimension distance (M) to define the comparative ratio.

Table 20. Numercial vs analitycal ratios for uniaxial bending test

Element Cross-Section	EN 1993 d_{EN1993}/d_{FEM}	CSM (EN) d_{CSM}/d_{FEM}
S1-120x80x4	0.66	0.84
S2-80x40x4	0.60	0.76
S3-80x80x4	0.74	0.89
S4-60x60x4	0.52	0.67
S5-100x100x4	0.81	0.86
S6-120x80x3	0.74	0.77
S7-60x60x3	0.76	0.90

Table 20. Numercial vs analitycal ratios for uniaxial bending test

Element Cross-Section	EN 1993	CSM (EN)
	d_{EN1993}/d_{FEM}	d_{CSM}/d_{FEM}
S8-70x50x2	0.62	0.66
S9-100x100x3	0.78	0.70
S10-100x100x3.5	0.76	0.75
S11-120x120x5.5	0.68	0.76
S12-80x80x2.5	0.77	0.73
Average	0.70	0.77
COV	0.125	0.106

As it can be appreciated, CSM approaches better the numerical solution (7% better). S4 is the cross-section that presents worse analytical results, it might be because this sections presents a slenderness very low (0.26). As it also happens for stub-column tests, it could be due to being the only section that does not accomplish the restriction on the normalised deformation capacity: $\varepsilon_{CSM}/\varepsilon_y<\min(15,0.45\varepsilon_u/\varepsilon_y)$, and needs to be applied an ε_{csm} modification. The COV is lower for CSM(EN) method.

4.4 Uniaxial combined loading

The next table 21 shows the ultimate load calculated using Eq. x and x. To calculate this expression $N_{pl,Rd}$ and $M_{pl,Rd}$ (simple axial resistant force and simple bending resistant moment, respectively) are required. These two values are obtained by applying Eurocode formulas under EN 1993-1-4 proposed classification criteria which has been presented in section 2.3.1.1. Each one of the reference points are defined in 3.4.2.

For Class 1 and 2:

$$M_{N,y,Rd} = \frac{M_{pl,y,Rd}(1-n)}{1-0.5a_w} \quad but\ M_{N,y,Rd} \leq M_{pl,y,Rd} \qquad Eq.12$$

$$M_{N,z,Rd} = \frac{M_{pl,z,Rd}(1-n)}{1-0.5a_f} \quad but\ M_{N,z,Rd} \leq M_{pl,z,Rd} \qquad Eq.13$$

Where $a_w=(A-2bt)/A$ but $a_w\leq 0.5$ for hollow sections

$a_f=(A-2ht)/A$ but $a_f\leq 0.5$ for hollow sections

$n=N_{Ed}/N_{pl,Rd}$ where N_{Ed} is the design value of the axial force and $N_{pl,Rd}$ the design plastic resistance to normal forces of the cross-section

A, area; h, depth; b, width

$M_{pl,i,Rd}$ design plastic value of the resistance to bending moments, i-i axis

Table 21. Predicted uniaxial combined loading test analytical results: EN 1993-1-4 classification proposal

Cross-section	Ref. Point	e_z(mm)	e_y(mm)	$N_{EN1993\text{-}1\text{-}4}$(kN) EN 1993-1-4 Classification
S1-120x80x4	1	12.7	0	314.5
	2	25.3	0	231.9
	3	38.0	0	183.6
	4	0	19.33	302.8
	5	0	38.7	219.4
	6	0	58	172.0
S2-80x40x4	1	6.0	0	208.8
	2	12.0	0	165.7
	3	18.0	0	137.4
	4	0	12.7	130.3
	5	0	25.3	158.8
	6	0	38.0	130.3
S3-80x80x4	1=4	12.7	0	287.7
	2=5	25.3	0	228.7
	3=6	38.0	0	189.8
S4-60x60x4	1=4	9.3	0	158.6
	2=5	18.7	0	124.3
	3=6	28	0	102.2
S5-100x100x4	1=4	16.0	0	374.9
	2=5	32	0	299.0
	3=6	48	0	248.7
S6-120x80x3	1	12.7	0	239.0
	2	25.3	0	175.4
	3	38.0	0	138.5
	4	0	38.7	235.5
	5	0	38.7	171.6
	6	0	58	135.0
S7-60x60x3	1=4	9.5	0	162.6
	2=5	19	0	129.3
	3=6	28.5	0	107.3
S8-70x50x2	1	0	8.0	95.0
	2	0	16.0	69.8
	3	0	24.0	55.2
	4	11.3	0	93.5
	5	22.7	0	68.2
	6	34	0	53.7
S9-100x100x3	1=4	16.2	0	249.1
	2=5	32.3	0	185.5
	3=6	48.5	0	135.0
S10-100x100x3.5	1=4	16.1	0	288.1
	2=5	32.2	0	214.3
	3=6	48.3	0	147.7
S11-120x120x5.5	1=4	19.1	0	603.9
	2=5	38.2	0	480.8
	3=6	57.3	0	399.4

Table 21. Predicted uniaxial combined loading test analytical results: EN 1993-1-4 classification proposal

Cross-section	Ref. Point	e_z(mm)	e_y(mm)	$N_{EN1993-1-4}$(kN) EN 1993-1-4 Classification
S12-80x80x2.5	1=4	12.9	0	163.8
	2=5	25.8	0	121.7
	3=6	38.8	0	96.8

$N_{EN1993-1-4}$ is the analytical predicted load result obtained using EN 1993-1-4 classification criteria.

The table 22 below shows the ultimate loading force that can be applied calculated by the same interaction expression used before to obtain table 21 values (Eq. 12 and 13). To calculate this expression $N_{pl,Rd}$ and $M_{pl,Rd}$ (simple axial resistant force and simple bending resistant moment, respectively) are required. These values are obtained by applying Eurocode formulas (the same that have been used for the results from EN 1993-1-4 classification criteria) under Theofanous and Gardner proposed classification criteria presented in section 2.3.1.1. Each one of the reference points are defined in 3.4.2.

Table 22. Predicted uniaxial combined loading test analytical results EN T&G classification proposal

Cross-section	Ref. Point	e_z(mm)	e_y(mm)	$N_{T\&G}$(kN) T&G Classification Proposal
S1-120x80x4	1	12.7	0	363.1
	2	25.3	0	288.8
	3	38.0	0	239.8
	4	0	19.33	358.2
	5	0	38.7	219.4
	6	0	58	172.0
S2-80x40x4	1	6.0	0	208.8
	2	12.0	0	165.7
	3	18.0	0	137.4
	4	0	12.7	203.2
	5	0	25.3	158.8
	6	0	38.0	130.3
S3-80x80x4	1=4	12.7	0	287.7
	2=5	25.3	0	228.7
	3=6	38.0	0	189.8
S4-60x60x4	1=4	9.3	0	158.6
	2=5	18.7	0	124.3
	3=6	28	0	102.2
S5-100x100x4	1=4	16.0	0	374.9
	2=5	32	0	299.0
	3=6	48	0	248.7

Table 22. Predicted uniaxial combined loading test analytical results EN T&G classification proposal

Cross-section	Ref. Point	e_z(mm)	e_y(mm)	$N_{T\&G}$(kN) T&G Classification Proposal
S6-120x80x3	1	12.7	0	239.0
	2	25.3	0	175.4
	3	38.0	0	138.5
	4	0	38.7	235.5
	5	0	38.7	171.6
	6	0	58	135.0
S7-60x60x3	1=4	9.5	0	162.6
	2=5	19	0	129.3
	3=6	28.5	0	107.3
S8-70x50x2	1	0	8.0	95.0
	2	0	16.0	69.8
	3	0	24.0	55.2
	4	11.3	0	93.5
	5	22.7	0	68.2
	6	34	0	53.7
S9-100x100x3	1=4	16.2	0	249.1
	2=5	32.3	0	185.5
	3=6	48.5	0	147.7
S10-100x100x3.5	1=4	16.1	0	288.1
	2=5	32.2	0	214.3
	3=6	48.3	0	170.6
S11-120x120x5.5	1=4	19.1	0	603.9
	2=5	38.2	0	480.8
	3=6	57.3	0	399.4
S12-80x80x2.5	1=4	12.9	0	163.8
	2=5	25.8	0	121.7
	3=6	38.8	0	96.8

$N_{T\&G}$ is the analytical predicted ultimate load result obtained by using the T&G classification criteria.

Table 23 shows the predicted loads according to the interaction expressions codified in EN 1993-1-4 (Eq. 40 and 41). To calculate this expression N_{csm} and M_{csm} (simple axial resistant force and simple bending resistant moment calculated with the CSM, respectively; as it has been defined in section 2.4.4) values are required, with EN 1993-1-4 slenderness (Eq. 29). Each one of the reference points are defined in 3.4.2.

For class 1 and 2 cross-sectios:

$$M_{N,y,csm} = \frac{M_{y,csm}(1-n)}{1-0.5a_w} \quad but\ M_{N,y,csm} \leq M_{y,csm} \qquad Eq.40$$

$$M_{N,z,csm} = \frac{M_{z,csm}(1-n)}{1-0.5a_f} \quad but\ M_{N,z,csm} \leq M_{z,csm} \qquad Eq.41$$

Where $a_w=(A-2bt)/A$ but $a_w \leq 0.5$ for hollow sections

$a_f=(A-2ht)/A$ but $a_f \leq 0.5$ for hollow sections

$n=N_{Ed}/N_{csm}$ where N_{Ed} is the design value of the axial force and N_{csm} the design resistant value obtained using the CSM

A, area; h, depth; b, width

$M_{i,csm}$ design value of the resistance to bending moments, i-i axis

Table 23. Predicted uniaxial combined loading test analytical results: EN 1993-1-4 interaction with CSM values

Cross-section	Ref. Point	e_z(mm)	e_y(mm)	N_{CSM}(kN) EN 1993-1-4
S1-120x80x4	1	12.7	0	364.8
	2	25.3	0	288.6
	3	38.0	0	238.8
	4	0	19.33	383.3
	5	0	38.7	312.6
	6	0	58	263.9
S2-80x40x4	1	6.0	0	236.8
	2	12.0	0	190.6
	3	18.0	0	159.5
	4	0	12.7	232.9
	5	0	25.3	185.7
	6	0	38.0	154.3
S3-80x80x4	1=4	12.7	0	325.5
	2=5	25.3	0	262.0
	3=6	38.0	0	219.2
S4-60x60x4	1=4	9.3	0	186.4
	2=5	18.7	0	148.6
	3=6	28	0	123.5
S5-100x100x4	1=4	16.0	0	389.8
	2=5	32	0	311.9
	3=6	48	0	260.0
S6-120x80x3	1	12.7	0	205.4
	2	25.3	0	141.7
	3	38.0	0	108.1
	4	0	38.7	277.1
	5	0	38.7	220.2
	6	0	58	182.7
S7-60x60x3	1=4	9.5	0	182.3
	2=5	19	0	146.6
	3=6	28.5	0	122.7
S8-70x50x2	1	0	8.0	105.4
	2	0	16.0	81.6
	3	0	24.0	66.5
	4	11.3	0	111.5
	5	22.7	0	89.2
	6	34	0	74.3

Table 23. Predicted uniaxial combined loading test analytical results: EN 1993-1-4 interaction with CSM values

Cross-section	Ref. Point	e_z(mm)	e_y(mm)	N_{CSM}(kN) EN 1993-1-4
S9-100x100x3	1=4	16.2	0	275.2
	2=5	32.3	0	215.8
	3=6	48.5	0	177.5
S10-100x100x3.5	1=4	16.1	0	329.4
	2=5	32.2	0	261.7
	3=6	48.3	0	217.1
S11-120x120x5.5	1=4	19.1	0	647.0
	2=5	38.2	0	518.6
	3=6	57.3	0	432.7
S12-80x80x2.5	1=4	12.9	0	184.8
	2=5	25.8	0	145.9
	3=6	38.8	0	120.6

N_{CSM} is the analytical predicted ultimate load result obtained with Eq. 40 and 41.

Table 24 shows the ultimate predicted load calculated by one of the interaction equation proposed in [25] (the one that is linear at N_{Ed}/N_{csm} term: Eq. 39). To calculate this expression is needed to have N_{csm} and M_{csm} and (simple axial resistant force and simple bending resistant moment calculated with the CSM, respectively; as it has been defined in section 2.4.4) values, with EN 1993-1-4 slenderness (Eq. 29). Each one of the reference points are defined in 3.4.2.

$$\frac{N_{Ed}}{N_{csm}} + \sqrt{\left(\frac{M_{y,Ed}}{M_{csm,y}}\right)^2 + \left(\frac{M_{z,Ed}}{N_{csm,z}}\right)^2} \leq 1 \qquad Eq.39$$

Where

N_{Ed}, $M_{y,Ed}$ and $M_{z,Ed}$ are the design values for: the normal force, y-y bending moment and z-z bending moment, respectively

N_{csm}, $M_{csm,y}$ and $M_{csm,z}$ are the simple resistant: axial force, y-y bending moment and z-z bending moment, respectively, calculated with the CSM

Table 24. Predicted uniaxial combined loading test analytical results: CSM lineal N_{Ed}/N_{csm} interaction

Cross-section	Ref. Point	e_z(mm)	e_y(mm)	$N_{u,RHS1}$(kN) Linear N_{Ed}/N_{csm} term
S1-120x80x4	1	12.7	0	345.32
	2	25.3	0	265.0
	3	38.0	0	215.0
	4	0	19.33	356.4
	5	0	38.7	278.4
	6	0	58	228.3

Table 24. Predicted uniaxial combined loading test analytical results: CSM lineal N_{Ed}/N_{csm} interaction

Cross-section	Ref. Point	e_z(mm)	e_y(mm)	$N_{u,RHS1}$(kN) Linear N_{Ed}/N_{csm} term
S2-80x40x4	1	6.0	0	228.9
	2	12.0	0	180.5
	3	18.0	0	149.0
	4	0	12.7	214.7
	5	0	25.3	163.5
	6	0	38.0	132.0
S3-80x80x4	1=4	12.7	0	303.8
	2=5	25.3	0	235.0
	3=6	38.0	0	191.6
S4-60x60x4	1=4	9.3	0	179.1
	2=5	18.7	0	139.5
	3=6	28	0	114.3
S5-100x100x4	1=4	16.0	0	361.7
	2=5	32	0	277.5
	3=6	48	0	225.0
S6-120x80x3	1	12.7	0	186.6
	2	25.3	0	124.4
	3	38.0	0	93.3
	4	0	38.7	255.1
	5	0	38.7	193.7
	6	0	58	156.2
S7-60x60x3	1=4	9.5	0	170.0
	2=5	19	0	131.4
	3=6	28.5	0	107.1
S8-70x50x2	1	0	8.0	98.7
	2	0	16.0	73.8
	3	0	24.0	58.9
	4	11.3	0	102.9
	5	22.7	0	78.6
	6	34	0	63.6
S9-100x100x3	1=4	16.2	0	253.4
	2=5	32.3	0	190.1
	3=6	48.5	0	152.1
S10-100x100x3.5	1=4	16.1	0	304.9
	2=5	32.2	0	232.0
	3=6	48.3	0	187.3
S11-120x120x5.5	1=4	19.1	0	602.0
	2=5	38.2	0	463.1
	3=6	57.3	0	376.3
S12-80x80x2.5	1=4	12.9	0	170.7
	2=5	25.8	0	129.1
	3=6	38.8	0	103.8

$N_{u,RHS1}$ defines the predicted ultimate load analytical result obtained from Eq. 39.

Table 25 shows the predicted ultimate load calculated by the other equation of the interaction equations that are proposed in [25] (the one that is square at N_{Ed}/N_{csm} term: Eq. 38). To calculate this expression N_{csm} and M_{csm} (simple axial resistant force and simple bending resistant moment calculated with the CSM, respectively; as it has been defined in section 2.4.4) values are required, with EN 1993-1-4 slenderness. Each one of the reference points are defined in 3.4.2.

$$\left(\frac{N_{Ed}}{N_{csm}}\right)^2 + \sqrt{\left(\frac{M_{y,Ed}}{M_{csm,y}}\right)^2 + \left(\frac{M_{z,Ed}}{N_{csm,z}}\right)^2} \leq 1 \qquad Eq.38$$

Where

N_{Ed}, $M_{y,Ed}$ and $M_{z,Ed}$ are the design values for: the normal force, y-y bending moment and z-z bending moment, respectively

N_{csm}, $M_{csm,y}$ and $M_{csm,z}$ are the simple resistant: axial force, y-y bending moment and z-z bending moment, respectively, calculated with the CSM

Table 25. Predicted uniaxial combined loading test analytical results: CSM square N_{Ed}/N_{csm} interaction

Cross-section	Ref. Point	e_z(mm)	e_y(mm)	$N_{u,RHS2}$(kN) Square N_{Ed}/N_{csm} term
S1-120x80x4	1	12.7	0	399.30
	2	25.3	0	324.9
	3	38.0	0	268.4
	4	0	19.33	408.2
	5	0	38.7	338.6
	6	0	58	284.2
S2-80x40x4	1	6.0	0	260.6
	2	12.0	0	218.5
	3	18.0	0	185.0
	4	0	12.7	249.4
	5	0	25.3	201.0
	6	0	38.0	164.9
S3-80x80x4	1=4	12.7	0	349.7
	2=5	25.3	0	287.1
	3=6	38.0	0	238.9
S4-60x60x4	1=4	9.3	0	205.3
	2=5	18.7	0	169.9
	3=6	28	0	142.3
S5-100x100x4	1=4	16.0	0	418.4
	2=5	32	0	340.2
	3=6	48	0	280.9
S6-120x80x3	1	12.7	0	230.7
	2	25.3	0	154.6
	3	38.0	0	113.0
	4	0	38.7	296.8
	5	0	38.7	238.5
	6	0	58	195.1

Table 25. Predicted uniaxial combined loading test analytical results: CSM square N_{Ed}/N_{csm} interaction

Cross-section	Ref. Point	e_z(mm)	e_y(mm)	$N_{u,RHS2}$(kN) Square N_{Ed}/N_{csm} term
S7-60x60x3	1=4	9.5	0	195.8
	2=5	19	0	160.6
	3=6	28.5	0	133.5
S8-70x50x2	1	0	8.0	115.8
	2	0	16.0	91.3
	3	0	24.0	73.7
	4	11.3	0	119.3
	5	22.7	0	96.6
	6	34	0	79.5
S9-100x100x3	1=4	16.2	0	296.6
	2=5	32.3	0	235.0
	3=6	48.5	0	190.2
S10-100x100x3.5	1=4	16.1	0	354.2
	2=5	32.2	0	285.4
	3=6	48.3	0	234.0
S11-120x120x5.5	1=4	19.1	0	695.3
	2=5	38.2	0	567.1
	3=6	57.3	0	469.6
S12-80x80x2.5	1=4	12.9	0	199.0
	2=5	25.8	0	159.1
	3=6	38.8	0	129.7

$N_{u,RHS2}$ defines the predicted ultimate load analytical result obtained from Eq. 38.

Once all analytical results have been presented, the following table 26 shows the ratios that compare these analytical results with the numerical ones. As it has been explained in section 4.1, a two dimensional distance has been defined for these ratios in order to do the comparisons as reliable as possible.

As we are calculating the relative distance that exists between the numerical result point and its projection to the interaction expression, this results only depend on the type of interaction equation and on the values of the simple resistances: axial force and bending moment. Hence, for uniaxial combined loading test there are three different interaction equations: one for RHS1 (Eq. 39), one for RHS2 (Eq. 38) and the one contained in EN 1993-1-4 (Eq. 12 and 13, or 40 and 41); and there are two different ways to obtain these simple resistances values: EN 1993-1-4 (section 2.3.1.2) and CSM (section 2.4.4). In conclusion, joining all these information, for uniaxial combined loading, there are 4 different possible comparisons:

- CSM(RHS^1): uses RHS1 interaction equation and CSM values for the simple resistances

- CSM(RHS^2): uses RHS2 interaction equation and CSM values for the simple resistances

- CSM(EN): uses EN1993-1-4 interaction equation and CSM values for the simple resistances

-EN1993-1-4 and T&G: both use EN 1993-1-4 interaction equation and EN 1993-1-4 values for the resistances, which means that the ratios for each case do not depend on the classification criteria and is the reason why both share the same column in table 26

Table 26. Numerical vs Analytical results: uniaxial combined loading test ratios

Cross-section	Ref. Point	$d_{analytical}/d_{numerical}$			
		CSM(RHS[1])	CSM(RHS[2])	CSM(EN)	EN 1993-1-4 and T&G
S1	1	0.82	0.95	0.86	0.86
	2	0.79	0.97	0.86	0.86
	3	0.78	0.97	0.86	0.87
	4	0.81	0.93	0.87	0.82
	5	0.79	0.96	0.89	0.80
	6	0.79	0.98	0.91	0.81
S2	1	1.13	1.20	1.06	0.96
	2	1.09	1.24	1.04	0.94
	3	1.06	1.24	1.02	0.92
	4	0.87	1.01	0.94	0.84
	5	0.84	1.03	0.95	0.82
	6	0.84	1.05	0.98	0.82
S3	1=4	0.93	1.07	0.97	0.88
	2=5	0.89	1.09	0.95	0.87
	3=6	0.87	1.09	0.95	0.87
S4	1=4	0.72	0.83	0.72	0.64
	2=5	0.69	0.84	0.69	0.61
	3=6	0.68	0.85	0.69	0.61
S5	1=4	0.92	1.07	0.99	0.96
	2=5	0.89	1.09	0.98	0.95
	3=6	0.86	1.08	0.98	0.95
S6	1	0.54	0.66	0.59	0.80
	2	0.46	0.57	0.52	0.82
	3	0.42	0.50	0.48	0.83
	4	0.71	0.83	0.77	0.77
	5	0.69	0.85	0.78	0.77
	6	0.66	0.83	0.78	0.76
S7	1=4	0.96	1.10	1.00	0.92
	2=5	0.92	1.12	0.99	0.91
	3=6	0.90	1.12	0.98	0.90
S8	1	0.79	0.93	0.85	0.89
	2	0.74	0.91	0.81	0.88
	3	0.71	0.89	0.80	0.89
	4	0.81	0.94	0.88	0.86
	5	0.77	0.94	0.87	0.84
	6	0.74	0.92	0.86	0.83
S9	1=4	0.78	0.92	0.85	0.87
	2=5	0.75	0.93	0.85	0.89
	3=6	0.74	0.93	0.87	0.92
S10	1=4	0.79	0.92	0.85	0.85
	2=5	0.76	0.94	0.86	0.86
	3=6	0.75	0.93	0.86	0.87

Table 26. Numerical vs Analytical results: uniaxial combined loading test ratios

Cross-section	Ref. Point	$d_{analytical}/d_{numerical}$			
		CSM(RHS[1])	CSM(RHS[2])	CSM(EN)	EN 1993-1-4 and T&G
S11	1=4	0.80	0.92	0.85	0.80
	2=5	0.77	0.94	0.84	0.80
	3=6	0.75	0.94	0.84	0.80
S12	1=4	0.79	0.93	0.86	0.87
	2=5	0.77	0.95	0.87	0.88
	3=6	0.76	0.95	0.88	0.91
Average		0.79	0.96	0.86	0.85
COV		0.165	0.149	0.141	0.092

As it can be appreciated, the method that provides better results is RHS[2] (Eq. 38) interaction equation with CSM simple resistances (Eq. 33 and 34). However it presents some issues with some cross-sections: S2, S3, S5 and S7 present ratios bigger than one, which means that results are unsafe as the analytical result is higher than the numerical one. For S6, as its slenderness is higher than 0.68 (class 4 limit) CSM can't be applied properly and when there is actuating an M_z, results are too conservative, even though the COV is not too high.

The case that evaluates the EN 1993-1-4 interaction equation (Eq. 11 and 12) with CSM values for the simple resistances (Eq. 33 and 34) provides results with an average that is 10% lower, but results are all more reliable and there is no cross-section with issues to remark. The COV is lower than the RHS[2] case.

4.5 Biaxial bending test

For this loading case, the analytical predicted load result is not possible to be obtained since there are two independent unknown variables in the interaction equation: $M_{y,u}$ and $M_{z,u}$, and no axial force applied (in other cases both moments depend on the axial force, which is the only unknown variable,). Hence, what it has been done is to calculate the result of each interaction equation by using numerical results from 3.4.4 section and normalising them with the ultimate capacities that requires each method being studied. This result will be compared, in the next section, to the unit to see how close each interaction equation is from the numerical one.

The following table 27 presents the results for the different interaction equations that are being studied. For Theofanous & Gardner [25] equations (Eq. 38 and 39, which are represented in table 27 for RHS[1&2]). As the N_{Ed}/N_{csm} term is 0, both (lineal and square) interaction equations provide the same result. EN 1993-1-4 (Eq. 12 and 13) interaction expression will be calculated with two different $M_{u,y}$ and $M_{u,z}$ pairs (bending moments resistant values): one calculated with EN 1993-1-4 (represented on table 27 for EN 1993-1-4) and the other one with CSM (represented on table 27 for CSM), both starting from EN 1993-1-4 slenderness.

The equations that have been used are the following ones but with the particularity that N_{Ed} is 0 for all cases.

For class 1 cross-sections:

$$\left[\frac{M_{y,Ed}}{M_{N,y,Rd}}\right]^{\alpha} + \left[\frac{M_{z,Ed}}{M_{N,z,Rd}}\right]^{\beta} \leq 1 \qquad Eq.14$$

Where $M_{N,y,Rd}$ and $M_{N,z,Rd}$ are defined in Eq. (12/40 and 13/41 above, EN 1993-1-4/CSM)

$M_{y,Ed}\ and\ M_{z,Ed}$ are the design bending moments, for y-y and z-z axis, respectively.

α and β are constants, which may be conservatively be taken as unity, otherwise as follows:

$$\alpha = \beta = \frac{1{,}66}{1 - 1{,}13n^2} \quad \text{but } \alpha = \beta \leq 6$$

$$\text{and } n = N_{Ed}/M_{Ed}$$

For class 3 cross-sections, a linear criterion is applied as follows:

$$\frac{N_{Ed}}{Af_y/\gamma_{M0}} + \frac{M_{y,Ed}}{W_{el,y}f_y/\gamma_{M0}} + \frac{M_{z,Ed}}{W_{el,z}f_y/\gamma_{M0}} \leq 1 \qquad Eq.15$$

Where A cross sectional area

γ_{M0} partial factor for resistance of cross-sections whatever the Class is

$W_{el,y}$ and $W_{el,z}$ are the cross-section elastic resistant modulus referred to the fibre with the maximum elastic, each one referred to y-y and z-z axis, respectively

f_y yield stress, for stainless-steel is considered $\sigma_{0.2}$

N_{Ed}, $M_{y,Ed}$ and $M_{z,Ed}$ are the design values for: the normal force, y-y bending moment and z-z bending moment, respectively.

$$\left(\frac{N_{Ed}}{N_{csm}}\right)^2 + \sqrt{\left(\frac{M_{y,Ed}}{M_{csm,y}}\right)^2 + \left(\frac{M_{z,Ed}}{N_{csm,z}}\right)^2} \leq 1 \qquad Eq.38$$

$$\frac{N_{Ed}}{N_{csm}} + \sqrt{\left(\frac{M_{y,Ed}}{M_{csm,y}}\right)^2 + \left(\frac{M_{z,Ed}}{N_{csm,z}}\right)^2} \leq 1 \qquad Eq.39$$

Where

N_{Ed}, $M_{y,Ed}$ and $M_{z,Ed}$ are the design values for: the normal force, y-y bending moment and z-z bending moment, respectively

N_{csm}, $M_{csm,y}$ and $M_{csm,z}$ are the simple resistant: axial force, y-y bending moment and z-z bending moment, respectively, calculated with the CSM

Table 27. Biaxial Bending analytical results

Cross-section	$M_{y,FEM}$ (kNm)	$M_{z,FEM}$ (kNm)	EN 1993-1-4	CSM	RHS[1&2]
S1-120x80x4	25.8	6.3	2.25	1.49	1.30
	7.7	18.3	2.14	1.66	1.71
	17.8	13.3	2.35	1.55	1.38
S2-80x40x4	7.4	3.2	1.74	1.17	1.11
	3.2	5.1	1.66	1.10	1.14
	7.7	2.9	1.75	1.18	1.12
S3-80x80x4	14.1	3.9	1.72	1.30	1.24
	2.9	14.5	1.71	1.30	1.26
	7.3	12.0	1.69	1.28	1.15
S4-60x60x4	5.9	5.8	2.93	1.97	1.96
	1.8	8.7	3.08	2.06	2.29
	8.5	2.6	3.14	2.10	2.28
S5-100x100x4	21.0	6.0	1.45	1.31	1.32
	4.3	21.5	1.43	1.29	1.33
	9.1	19.3	1.44	1.30	1.26
S6-120x80x3	17.6	4.7	1.98	1.49	2.22
	5.5	12.7	1.94	1.88	7.11
	15.0	7.6	2.11	1.62	3.41
S7-60x60x3	4.1	4.1	1.63	1.18	1.11
	1.2	6.0	1.65	1.20	1.25
	5.9	1.8	1.69	1.22	1.25
S8-70x50x2	4.1	2.5	2.65	260.66	2.37
	1.4	4.3	2.51	611.65	3.44
	5.4	1.3	2.53	91.79	2.39
S9-100x100x3	11.7	11.7	1.99	1.67	1.80
	5.2	16.6	1.86	1.71	1.99
	9.8	13.3	1.96	1.65	1.79
S10-100x100x3.5	13.4	13.4	1.99	1.46	1.47
	9.6	16.7	1.96	1.47	1.52
	4.9	19.7	1.83	1.52	1.69
S11-120x120x5.5	33.2	32.8	1.85	1.48	1.49
	22.7	41.1	1.83	1.46	1.50
	11.1	47.7	1.86	1.49	1.64
S12-80x80x2.5	6.1	6.2	2.01	1.57	1.61
	4.5	7.7	1.99	1.60	1.69
	2.3	9.0	1.84	1.63	1.84

In this case, the method followed to calculate the comparative ratios is the same one used for uniaxial combined loading: a distance two dimensional in the two dimensional space (M_y-M_z). The reason why the numerical results are shown in table 28 is to see which bending moment combination refers to each ratio calculated.

Table 28. Numerical vs Analytical results: biaxial bending test ratios

Cross-section	$M_{y,FEM}$ (kNm)	$M_{z,FEM}$ (kNm)	$d_{analytical}/d_{numerical}$		
			EN 1993-1-4	CSM	RHS[1&2]
S1-120x80x4	25.8	6.3	0.69	0.84	0.88
	7.7	18.3	0.74	0.74	0.76
	17.8	13.3	0.72	0.80	0.85
S2-80x40x4	7.4	3.2	0.72	0.89	0.95
	3.2	5.1	0.74	0.90	0.94
	7.7	2.9	0.71	0.89	0.95
S3-80x80x4	14.1	3.9	0.72	0.87	0.90
	2.9	14.5	0.72	0.87	0.89
	7.3	12.0	0.73	0.88	0.93
S4-60x60x4	5.9	5.8	0.52	0.67	0.71
	1.8	8.7	0.51	0.65	0.66
	8.5	2.6	0.50	0.64	0.66
S5-100x100x4	21.0	6.0	0.80	0.84	0.87
	4.3	21.5	0.80	0.85	0.87
	9.1	19.3	0.80	0.85	0.89
S6-120x80x3	17.6	4.7	0.78	0.63	0.67
	5.5	12.7	0.83	0.37	0.38
	15.0	7.6	0.79	0.51	0.54
S7-60x60x3	4.1	4.1	0.75	0.89	0.95
	1.2	6.0	0.74	0.88	0.89
	5.9	1.8	0.73	0.87	0.90
S8-70x50x2	4.1	2.5	0.63	0.61	0.65
	1.4	4.3	0.62	0.53	0.54
	5.4	1.3	0.60	0.62	0.65
S9-100x100x3	11.7	11.7	0.77	0.69	0.75
	5.2	16.6	0.76	0.68	0.71
	9.8	13.3	0.78	0.70	0.75
S10-100x100x3.5	13.4	13.4	0.78	0.77	0.82
	9.6	16.7	0.77	0.76	0.81
	4.9	19.7	0.76	0.75	0.77
S11-120x120x5.5	33.2	32.8	0.69	0.76	0.82
	22.7	41.1	0.70	0.77	0.82
	11.1	47.7	0.69	0.76	0.78
S12-80x80x2.5	6.1	6.2	0.77	0.73	0.79
	4.5	7.7	0.77	0.72	0.77
	2.3	9.0	0.76	0.72	0.74
Average			0.72	0.75	0.78
COV			0.113	0.166	0.168

Once again, the better results are show by Theofanous [25] equations. For this case there are no problems with any ratio: all are lower than one. All COV are low. S6 presents results too conservative again for RHS1&2 interaction equation, S4 has the same problem for EN1993-1-4 interaction equation and S8 undergoes this problem for all interaction equations.

4.6 Biaxial Combined Loading

The tables below present the results for biaxial combined loading after applying the existent interaction equations. Moreover, it has been done a comparison between these analytical interaction equations and the numerical results obtained from the simulations. The expressions used are from different interaction equations presented in 3.4.2.

Table 29 shows the predicted ultimate loading force that can be applied to a certain reference point (with its respective eccentricity) calculated by four different methods.

Each one of the reference points is defined in 3.4.2.

Table 29. Biaxial Combined Loading Test Analytical Results

Cross-section	Ref. Point	e_z(mm)	e_y(mm)	N_u(kN) EN1993	N_u(kN) CMS(EN)	N_u(kN) CSM(RHS[1])	N_u(kN) CSM(RHS[2])
S1-120x80x4	7	19.3	12.7	342.2	355.63	303.6	371.5
	8	19.3	25.3	281.4	284.57	248.5	312.8
	9	19.3	38.0	234.9	235.85	206.3	262.1
	10	38.7	25.3	250.2	265.02	219.6	284.4
	11	38.7	38.0	218.0	225.30	190.7	245.8
	12	58	38.0	195.4	209.06	172.0	224.7
	13	38.7	12.7	276.5	303.84	248.2	321.4
	14	58	12.7	229.3	258.21	205.9	274.8
	15	58	25.3	215.2	236.70	190.5	252.0
S2-80x40x4	7	12.7	6.0	194.6	224.12	182.3	234.3
	8	12.7	12.0	160.7	186.27	154.6	205.7
	9	12.7	18.0	134.2	156.58	131.2	177.9
	10	25.3	12.0	141.1	166.30	131.8	179.4
	11	25.3	18.0	123.4	145.76	117.7	161.0
	12	38.0	18.0	109.8	130.90	103.2	141.7
	13	25.3	6.0	155.3	182.25	144.2	194.7
	14	38.0	6.0	128.0	151.94	117.5	161.7
	15	38.0	12.0	120.4	143.38	111.3	153.2
S3-80x80x4	7	12.7	12.7	273.6	311.54	251.9	321.8
	8=13	12.7	25.3	223.5	257.00	206.3	274.5
	9=14	12.7	38.0	186.3	215.74	171.4	232.2
	10	25.3	25.3	200.9	232.75	182.5	246.2
	11=15	25.3	38.0	174.1	202.70	158.5	215.4
	12	38.0	38.0	157.3	183.87	143.1	194.4
S4-60x60x4	7	9.3	9.3	149.6	177.50	146.0	189.6
	8=13	9.3	18.7	120.9	145.34	120.0	162.7
	9=14	9.3	28.0	100.0	121.33	100.0	138.4
	10	18.7	18.7	107.8	130.86	106.4	146.5
	11=15	18.7	28.0	93.0	113.54	92.6	128.7
	12	28.0	28.0	83.7	102.67	83.6	116.5

Table 29. Biaxial Combined Loading Test Analytical Results

Cross-section	Ref. Point	e_z(mm)	e_y(mm)	N_u(kN) EN1993	N_u(kN) CMS(EN)	N_u(kN) CSM(RHS[1])	N_u(kN) CSM(RHS[2])
S5-100x100x4	7	16.0	16.0	357.1	371.99	313.5	383.4
	8=13	16.0	32.0	292.5	305.45	256.1	324.6
	9=14	16.0	48.0	244.3	255.54	212.3	272.8
	10	32.0	32.0	263.5	275.65	226.3	289.9
	11=15	32.0	48.0	228.6	239.50	196.3	252.4
	12	48	48.0	206.8	216.82	177.0	227.1
S6-120x80x3	7	19.3	12.7	173.5	201.15	177.6	220.5
	8	19.3	25.3	137.4	139.62	122.6	151.7
	9	19.3	38.0	113.7	106.96	92.8	111.8
	10	38.7	25.3	112.9	133.89	116.5	144.0
	11	38.7	38.0	96.4	104.11	90.3	108.7
	12	58	38.0	83.7	100.08	86.6	104.0
	13	38.7	12.7	136.2	184.07	157.1	197.3
	14	58	12.7	112.1	162.13	136.2	171.8
	15	58	25.3	95.8	125.72	108.2	133.6
S7-60x60x3	7	9.3	9.3	154.6	174.41	141.6	180.1
	8=13	9.3	18.7	126.4	143.83	116.0	153.5
	9=14	9.3	28.0	105.4	120.71	96.3	129.8
	10	18.7	18.7	113.6	130.23	102.6	137.7
	11=15	18.7	28.0	98.5	113.39	89.1	120.4
	12	28.0	28.0	89.0	102.84	80.4	108.6
S8-70x50x2	7	11.3	8.0	69.0	161.22	88.0	106.8
	8	11.3	16.0	54.7	80.05	70.2	87.6
	9	11.3	24.0	45.3	65.50	57.3	71.8
	10	22.7	16.0	44.9	73.79	62.5	79.0
	11	22.7	24.0	38.4	62.17	53.3	67.1
	12	34	24.0	33.3	57.36	48.5	61.0
	13	22.7	8.0	54.2	85.86	72.2	90.9
	14	34	8.0	44.6	72.19	59.8	76.5
	15	34	16.0	38.1	65.45	54.5	69.3
S9-100x100x3	7	16.0	16.0	185.5	259.68	222.4	268.7
	8=13	16.0	32.0	147.7	209.99	179.3	223.0
	9=14	16.0	48.0	122.8	173.73	147.1	184.2
	10	32.0	32.0	122.8	187.27	157.3	196.9
	11=15	32.0	48.0	105.0	161.50	135.5	169.2
	12	48	48.0	91.8	145.30	121.7	151.1
S10-100x100x3.5	7	16.0	16.0	312.1	313.09	267.5	323.3
	8=13	16.0	32.0	255.6	255.67	217.7	271.8
	9=14	16.0	48.0	213.4	213.03	179.9	227.0
	10	32.0	32.0	230.2	229.73	191.9	241.7
	11=15	32.0	48.0	199.7	199.05	166.1	209.5
	12	48	48.0	180.6	179.79	149.6	188.0

Table 29. Biaxial Combined Loading Test Analytical Results

Cross-section	Ref. Point	e_z(mm)	e_y(mm)	N_u(kN) EN1993	N_u(kN) CMS(EN)	N_u(kN) CSM(RHS[1])	N_u(kN) CSM(RHS[2])
S11-120x120x5.5	7	19.3	12.7	574.7	617.93	513.6	638.0
	8=13	19.3	25.3	470.0	508.05	420.0	541.6
	9=14	19.3	38.0	392.1	425.44	348.4	456.2
	10	38.7	25.3	422.9	458.94	371.2	484.5
	11=15	38.7	38.0	366.7	399.01	322.2	422.4
	12	58	38.0	331.4	361.42	290.7	380.5
S12-80x80x2.5	7	12.7	12.7	121.7	175.04	150.0	181.0
	8=13	12.7	25.3	96.8	142.28	121.5	151.3
	9=14	12.7	38.0	80.4	118.15	100.1	125.8
	10	25.3	25.3	80.4	127.40	106.9	134.1
	11=15	25.3	38.0	68.7	110.13	92.3	115.8
	12	38.0	38.0	60.0	99.29	83.1	103.7

Both values under N_u(kN) EN1993 and N_u(kN)CMS(EN) are obtained from EN 1993-1-4 interaction equation (Eq. 14 and 15) but N_u and M_u values (simple axial resistant force and simple bending resistant moment) are obtained from EN 1993-1-4 for N_u(kN) EN1993-1-4 (Eq. 12 and 13) and CSM for N_u(kN)CMS(EN) (Eq. 40 and 41), both with EN 1993-1-4 slenderness (Eq. 29).

Values under N_u(kN)CSM(RHS[1]) (lineal) and N_u(kN)CSM(RHS[2]) (square) are calculated by using Theofanous & Gardner [25] interaction equations: one with the linear term N_{Ed}/N_{csm} (Eq. 39) and the other one with the square term N_{Ed}/N_{csm} (Eq. 39), respectively. N_u and M_u (simple axial resistant force and simple bending resistant moment) are obtained from CSM (Eq. 40 and 41) with EN 1993-1-4 slenderness.

Equations are defined in section 4.5 above.

After presenting all analytical results, the following table 30 shows the ratios that compare these analytical results with the numerical ones. As it has been explained in section 4.1, a three dimensional distance has been defined to define these ratios.

In this case, each type of result presents its different comparison ratio (section 4.4 uniaxial combined loading before, from five types of results, there were only 4 different comparison ratios).

-CSM(RHS[1]): uses RHS1 interaction equation and CSM values for the simple resistances

-CSM(RHS[2]): uses RHS2 interaction equation and CSM values for the simple resistances

-CSM(EN): uses EN 1993-1-4 interaction equation and CSM values for the simple resistances

-EN1993-1-4: uses EN 1993-1-4 interaction equation and EN 1993-1-4 values for the simple resistances

Table 30. Numerical vs Analytical results: biaxial combined loading test ratios

Cross-section	Ref. Point	$d_{analytical}/d_{numerical}$			
		CSM(RHS[1])	CSM(RHS[2])	CSM(EN)	EN1993-1-4
S1-120x80x4	7	0.79	0.94	0.90	0.86
	8	0.78	0.97	0.88	0.87
	9	0.77	0.97	0.87	0.87
	10	0.78	0.97	0.91	0.85
	11	0.78	0.97	0.89	0.86
	12	0.89	1.11	1.04	0.95
	13	0.80	0.98	0.93	0.84
	14	0.80	0.99	0.93	0.83
	15	0.80	1.00	0.94	0.85
S2-80x40x4	7	0.94	1.12	1.07	0.93
	8	0.97	1.19	1.08	0.93
	9	0.98	1.22	1.08	0.92
	10	0.92	1.15	1.07	0.90
	11	0.95	1.19	1.08	0.91
	12	0.94	1.17	1.08	0.91
	13	0.87	1.08	1.01	0.86
	14	0.85	1.07	1.00	0.84
	15	0.90	1.13	1.06	0.89
S3-80x80x4	7	0.88	1.04	1.01	0.89
	8=13	0.87	1.07	1.00	0.87
	9=14	0.87	1.09	1.01	0.87
	10	0.86	1.07	1.02	0.88
	11=15	0.87	1.09	1.02	0.88
	12	0.88	1.09	1.03	0.89
S4-60x60x4	7	0.69	0.82	0.77	0.65
	8=13	0.69	0.84	0.75	0.63
	9=14	0.69	0.85	0.75	0.62
	10	0.69	0.86	0.77	0.63
	11=15	0.69	0.87	0.77	0.63
	12	0.70	0.88	0.77	0.63
S5-100x100x4	7	0.87	1.04	1.00	0.96
	8=13	0.86	1.06	1.00	0.95
	9=14	0.85	1.07	1.00	0.95
	10	0.84	1.05	0.99	0.95
	11=15	0.84	1.05	1.00	0.95
	12	0.84	1.05	1.00	0.96
S6-120x80x3	7	0.56	0.70	0.64	0.83
	8	0.47	0.58	0.54	0.83
	9	0.43	0.52	0.50	0.84
	10	0.50	0.62	0.57	0.83
	11	0.44	0.53	0.51	0.82
	12	0.48	0.58	0.56	0.84
	13	0.61	0.77	0.71	0.83
	14	0.61	0.76	0.72	0.78
	15	0.55	0.68	0.64	0.84

Table 30. Numerical vs Analytical results: biaxial combined loading test ratios

Cross-section	Ref. Point	$d_{analytical}/d_{numerical}$			
		CSM(RHS[1])	CSM(RHS[2])	CSM(EN)	EN1993-1-4
S7-60x60x3	7	0.91	1.08	1.04	0.93
	8=13	0.90	1.11	1.04	0.92
	9=14	0.90	1.13	1.05	0.91
	10	0.90	1.12	1.06	0.92
	11=15	0.90	1.13	1.06	0.92
	12	0.91	1.14	1.08	0.93
S8-70x50x2	7	0.77	0.93	0.88	0.91
	8	0.73	0.90	0.82	0.88
	9	0.71	0.89	0.81	0.88
	10	0.72	0.90	0.84	0.87
	11	0.70	0.87	0.81	0.87
	12	0.73	0.90	0.85	0.88
	13	0.75	0.93	0.88	0.87
	14	0.73	0.92	0.87	0.84
	15	0.75	0.93	0.88	0.89
S9-100x100x3	7	0.76	0.91	0.88	0.92
	8=13	0.74	0.92	0.86	0.91
	9=14	0.72	0.90	0.85	0.91
	10	0.74	0.92	0.87	0.93
	11=15	0.72	0.90	0.86	0.91
	12	0.72	0.89	0.86	0.92
S10-100x100x3.5	7	0.76	0.91	0.88	0.88
	8=13	0.74	0.92	0.86	0.86
	9=14	0.74	0.92	0.86	0.87
	10	0.73	0.91	0.86	0.86
	11=15	0.73	0.91	0.86	0.86
	12	0.73	0.90	0.86	0.87
S11-120x120x5.5	7	0.75	0.90	0.87	0.81
	8=13	0.74	0.92	0.86	0.80
	9=14	0.74	0.93	0.87	0.80
	10	0.73	0.91	0.87	0.80
	11=15	0.74	0.92	0.87	0.80
	12	0.74	0.92	0.88	0.81
S12-80x80x2.5	7	0.77	0.92	0.89	0.90
	8=13	0.75	0.93	0.88	0.90
	9=14	0.75	0.93	0.88	0.90
	10	0.75	0.94	0.89	0.92
	11=15	0.74	0.92	0.87	0.90
	12	0.74	0.92	0.88	0.91
Average		0.77	0.95	0.89	0.86
COV		0.192	0.194	0.195	0.111

Again CSM(RHS[2]) (Eq. 38) provides us the better average (which is closer to the one referred to uniaxial bending test) results, but again there are presented ratios higher than one for sections: S2, S3, S5 and S7. S6 presents results more conservative as more eccentricity has the

axial force, this is because of this section has the slenderness higher than 0.68 (class 4 limit) and CSM can't be applied properly. The COV is low even being the higher of the methods studied.

For biaxial combined loading test, both CSM (EN) and EN 1993-1-4 methods have better averages than they have for uniaxial bending test. For EN 1993-1-4 there are no ratios higher than one, and the COV is very low. However, for CSM (EN) there is the same problem as for CSM (RHS2) with the same sections and it presents the same COV values. Even though ratios are very closer to one and only exceed this limit narrowly.

4.7 Global Valorations

The ultimate numerical resistance of ferritic stainless steel RHS under combined loading has been studied by analysing the interaction equations proposed in EN 1993-1-4 [4] and expressions found in the literature [22 and 25], in order to determine the most appropriate approach. The ratios by which each design interaction curve exceeds or falls short of the corresponding FEM data, denoted as $d_{analytical}$ /$d_{numerical}$, have been calculated and the mean and coefficient of variation (COV) of the $d_{analytical}$ /$d_{numerical}$ values are presented in Table 31. From this preliminary analysis it can be concluded that Eurocode proposals are considerably conservative for the studied cross-sections because they do not consider material strain hardening.

On the one hand, the numerical ultimate loads have been normalized by the CSM predictions and plotted in Fig. 37, 38 and 39 together with the aforementioned interaction expressions in order to assess their applicability. These figures demonstrate that the consideration of the CSM fundamental capacities in the expressions proposed in EN 1993-1-4, Eq. 15 (CSM in EN in Fig. 37, 38 and 39), is the best approach for the prediction of the combined loading capacity of the studied cross-sections, providing safe and accurate results.

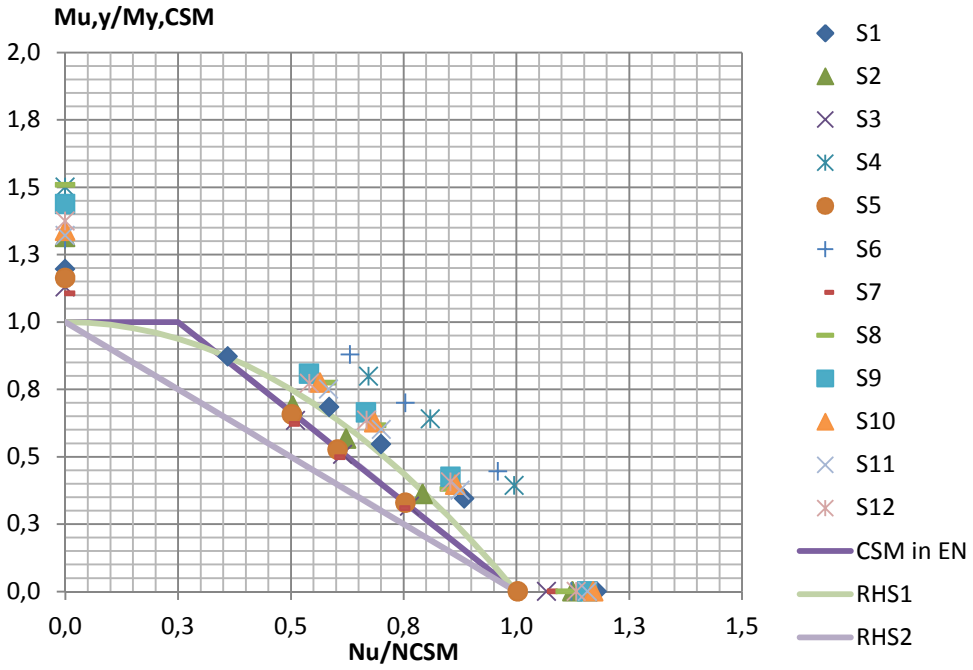

Figure 37. Axial compression-major axis bending interaction, normalised with CSM values

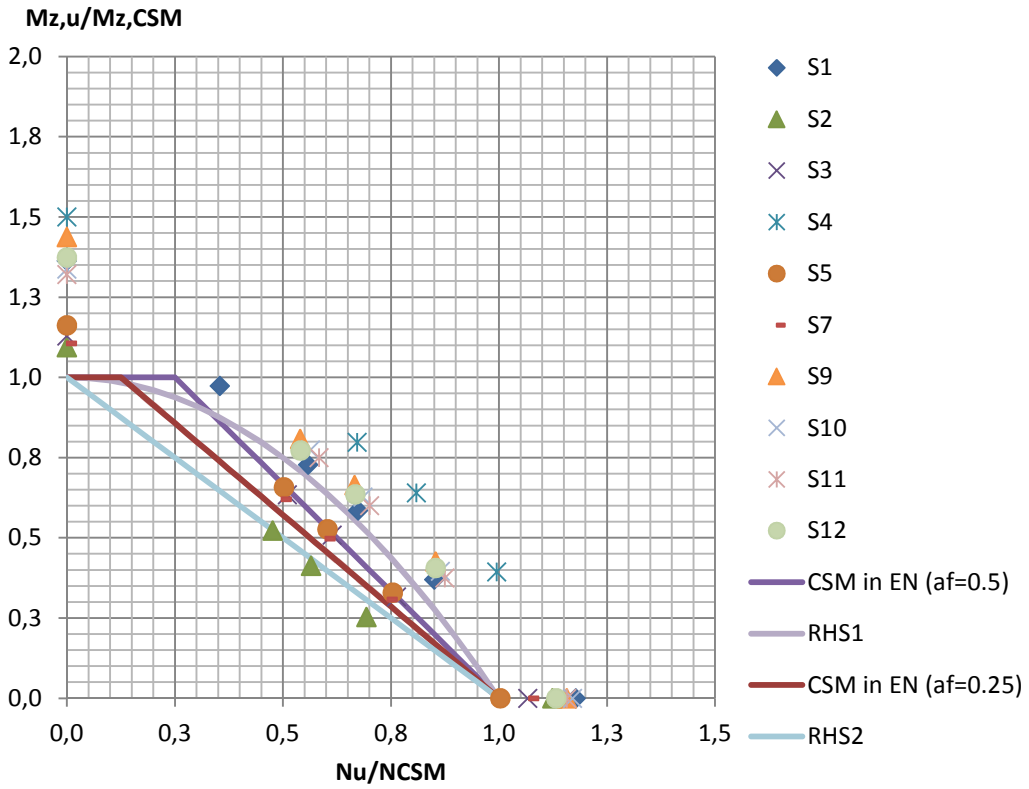

Figure 38. Axial compression-minor axis bending interaction, normalised with CSM values

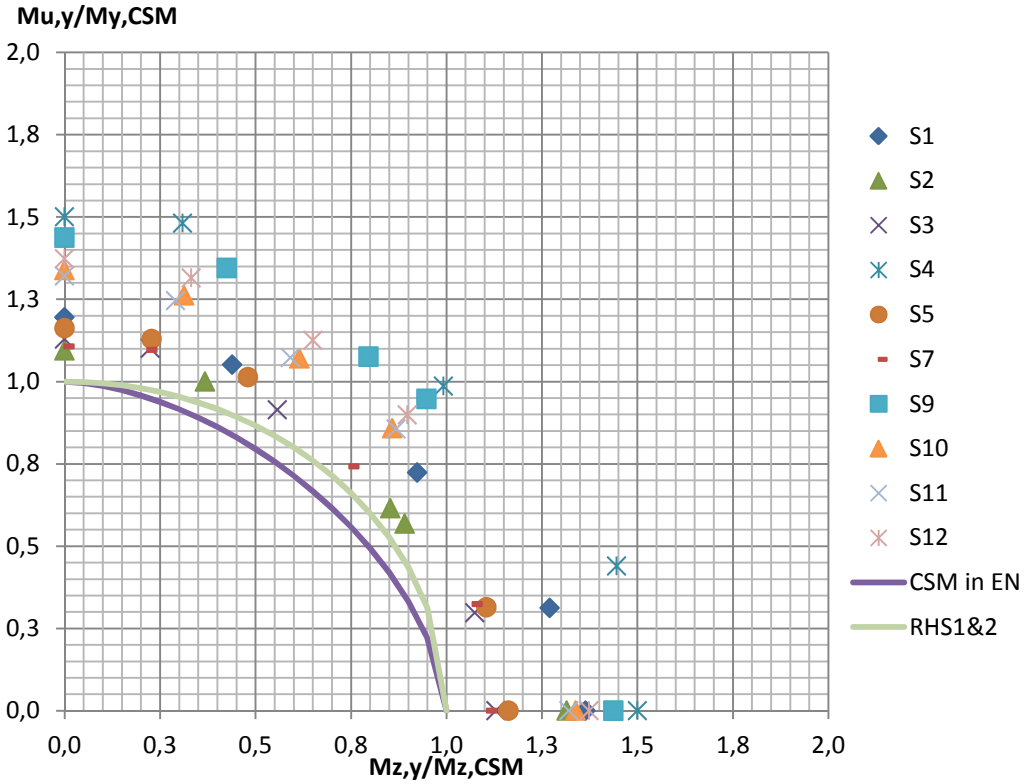

Figure 39. Major and minor axis bending interaction, normalised with CSM values

On the other hand, the numerical ultimate loads have been normalized by the EN 1993-1-4 basic resisting predictions and plotted in Fig. 40, 41 and 42 together with the aforementioned interaction expression in order to assess its applicability. These figures demonstrate that using

this method results are too conservative (far away from the interaction equation) in comparison with Fig. 37, 38 and 39 above.

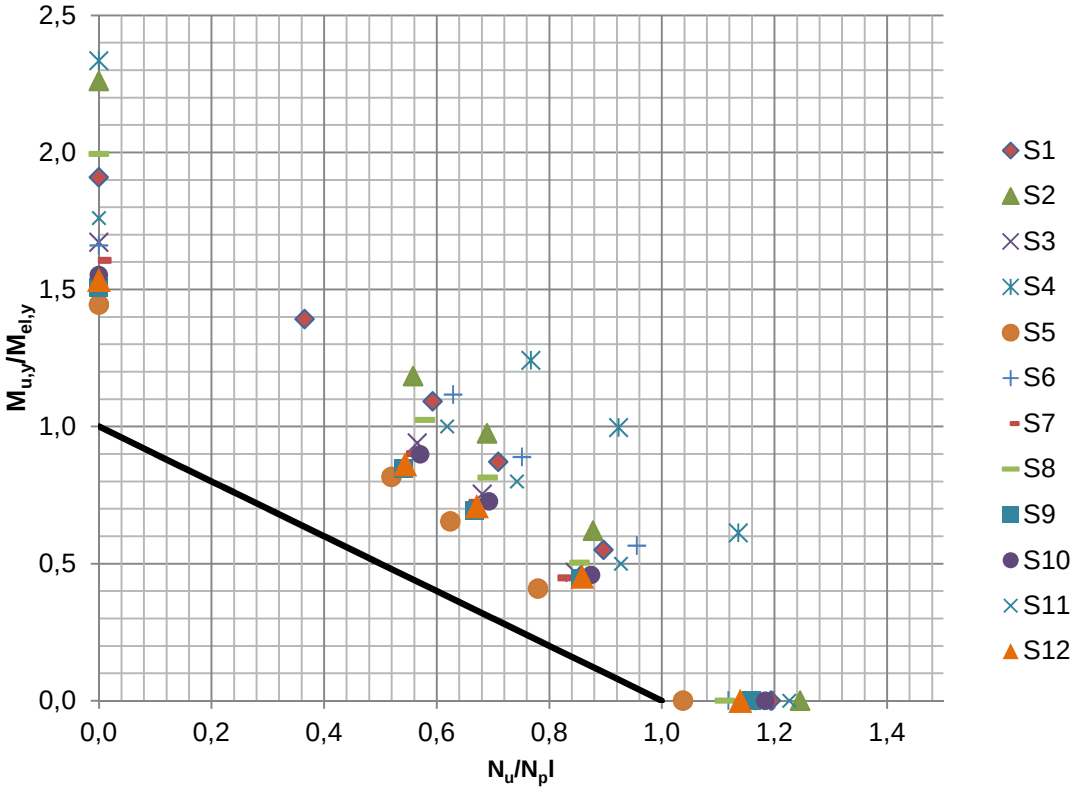

Figure 40. Axial compression-major axis bending interaction, normalised with EN 1993-1-4 values

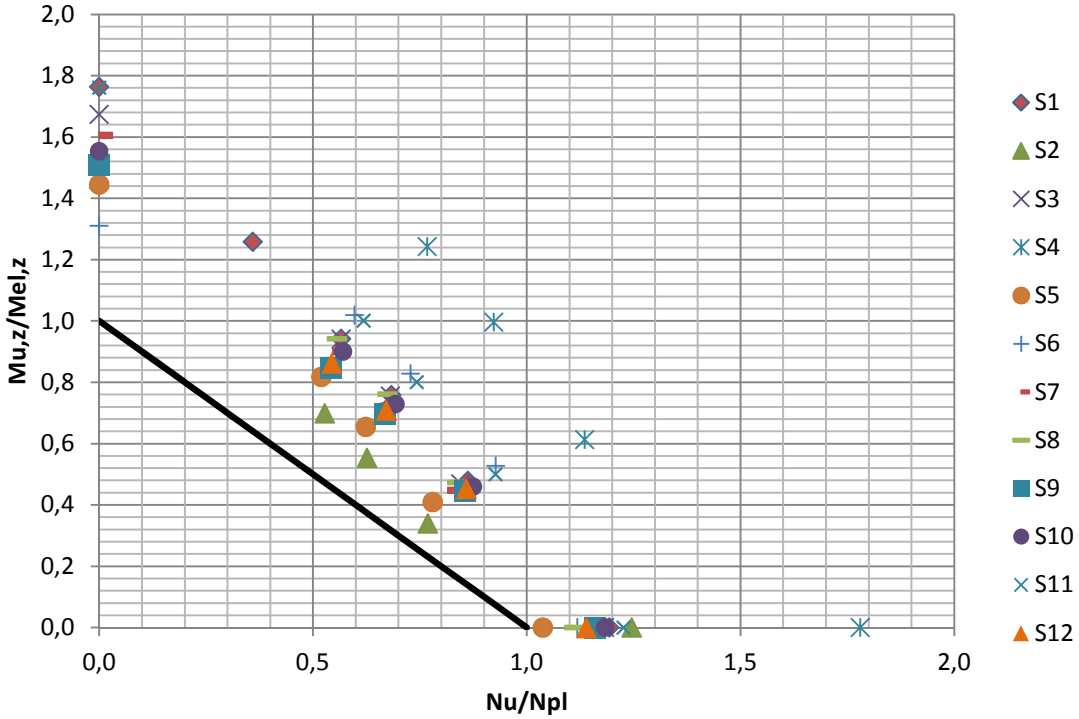

Figure 42. Axial compression-minor axis bending interaction, normalised with EN 1993-1-4 values

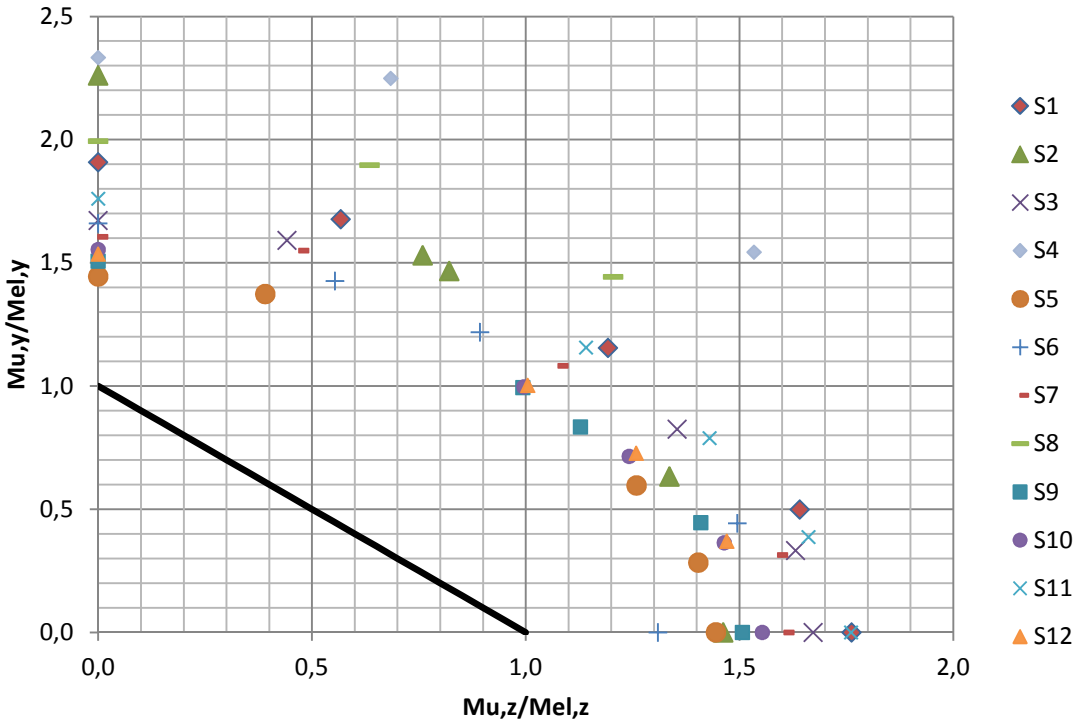

Figure 42. Major and minor axis bending interaction, normalised with EN 1993-1-4 values

Although Table 31 suggests that Eq. 38 provides the most accurate results on average, it is not a suitable solution because it overestimates the ultimate capacities for a large number of cases, as shown in Figs. 37 and 38. On the other hand, Eq. 39 provides safe results for all the studied cases, though with more conservative predictions than Eq. 14 and 15 (CSM in En).

Table 31. Comparison of different proposals with FEM data

EN 1993-1-4 (Eq. 14 and 15)		CSM in EN (Eq. 14 and 15)		RHS[1] (Eq. 39)		RHS[2] (Eq. 38)	
Mean	COV.	Mean	COV.	Mean	COV.	Mean	COV.
0.81	0.152	0.86	0.163	0.91	0.163	0.79	0.144

5. Cross-section analysis: Experimental Programme

An experimental programme is more than just obtaining the ultimate loading data after testing all elements. This is only the last step. Before, it is necessary to think the correct procedure that will be followed to test each element (it will depend on the kind of test that is wanted to be done: stub-column, bending, etc.) and prepare this element properly in order to get the more reliable results as possible. In addition to this, it is important to measure the geometrical properties of each element: imperfections, width, depth, thickness, etc. It is important to verify material properties too. The experimental programme has been done only for stub-column test (ultimate axial load).

This experimental programme took place in the "Structure Technology Laboratory Luis Agulló" (LTE Luis Agulló) which is mainly a research laboratory appointed to the Construction Engineering Department where experimental works of the research and technology transfer projects are developed. Most of the work done consist of applied research, heavily focusing on technology transfer to the construction industry.

5.1 Material testing

In order to verify the material properties of the material supplied, a material testing was carried out. The basic stress-strain properties of the investigated stocky cross-sections were obtained through tensile coupon tests (TCT). These tests were conducted in accordance with EN 10002-1 (1990) and EN ISO 6892-1 [31]. These tests consist of two different specimen types: flat coupon tensile tests and corner coupon tensile tests.

5.1.1 Preparation of coupons

There were a total of twenty specimens: ten were used for flat tensile coupon tests and ten for corner tensile coupon tests. For flat tensile coupon tests five different cross-sections were analysed (two elements of each cross-section) and for corner tensile coupon test five different ones (two elements of each cross-section too). Table 32 presents the number of elements analysed of each cross-section.

Table 32. Number of tensile tests conducted

Cross-Section	Corner TCT	Flat TCT
80x80x4	2	2
60x60x3	2	2
80x40x4	2	2
120x80x3	2	2
70x50x2	2	2

Flat coupons were machined from the face opposite to the weld. Corner coupons were also extracted and tested for each of the five cross-sections. Fig. 43. shows the location of the flat and corner coupons extracted from the element for this study, together with the adopted dimensioning and labelling system. The nominal length was 280mm for all cross-sections.

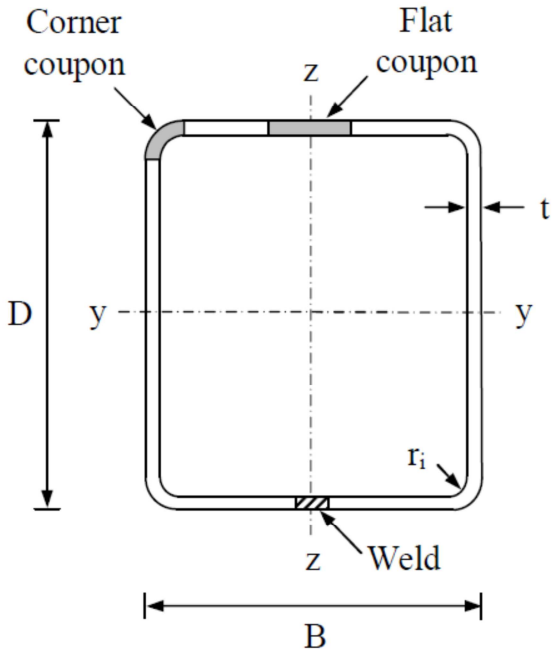

Figure 43. Section labelling convention and locations of flat ant corner tensile coupons

The tested coupons where cut in the rolling direction and mechanized with the geometries presented in Figure 44. The total length of all the specimens is 280mm, and the tested gauge length of 80mm for the flat coupons and the one corresponding the specifications gathered in ISO 6892-1 [31] for the corner specimens. The corner coupons consisted of the corner region plus an adjacent flat part of 2t, where t is the cross-section thickness. Figure 45 shows the different specimens prior to testing.

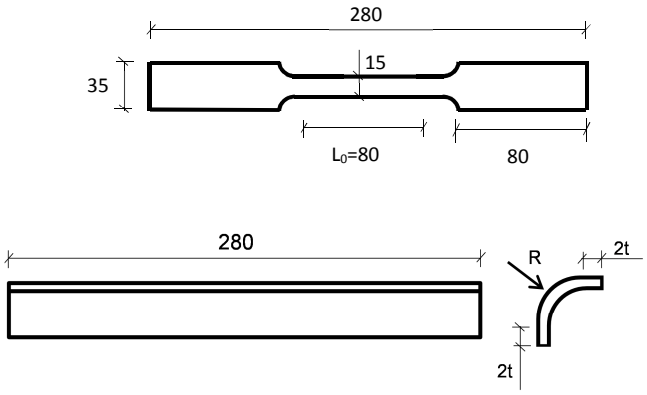

Figure 44. Definition of flat and corner coupons for tensile testing.

Figure 45. Tensile coupon specimens: necked flat coupons and straight corner coupons

5.1.2 Instrumentation and testing

All tensile tests were performed using an Amsler 350 kN hydraulic testing machine. The adopted testing rates are according to the specifications gathered both in ISO 6892-1 [31] and ASTM: $0.00025s^{-1}$ for the initial part of the test and increased to $0.008s^{-1}$ after the yield point is reached to fracture. Figure 46 shows the testing of both a flat and a corner coupon, and the typical failure modes of both types of coupons are shown in Figure 47.

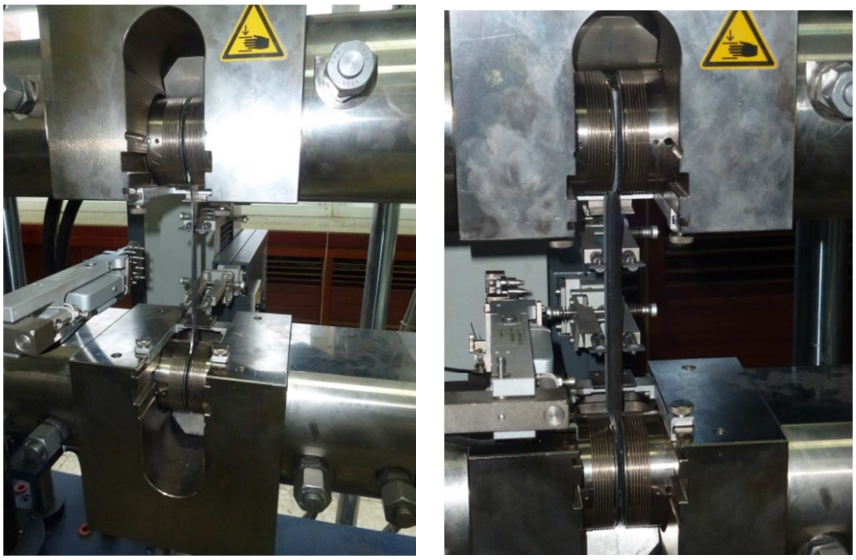

Figure 46. Tensile test configuration in flat and corner coupons.

Figure 47. Typical failure modes for flat and corner coupons after testing.

Load, strain, displacement and input voltage were all recorded using the data acquisition equipment and logged using the computer packages.

5.1.3 Results

In this section the results obtained after testing all twenty flat and corner tensile coupons are shown. Fig. 48 and 49 presents the results of corner and flat tensile coupon tests, respectively, as measured stress-strain curves.

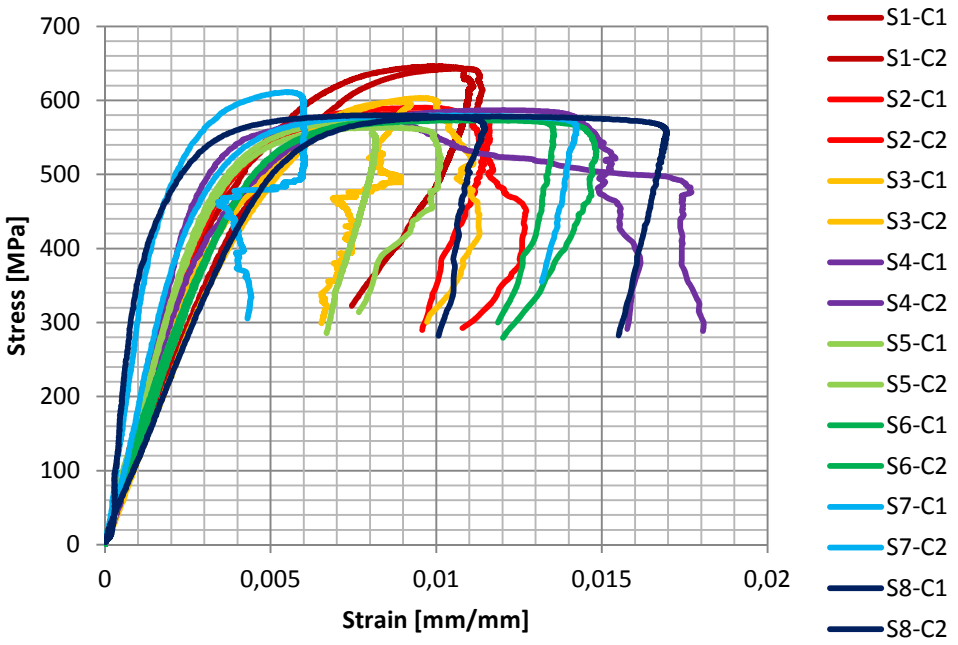

Figure 48. Corner tensile coupon tests results

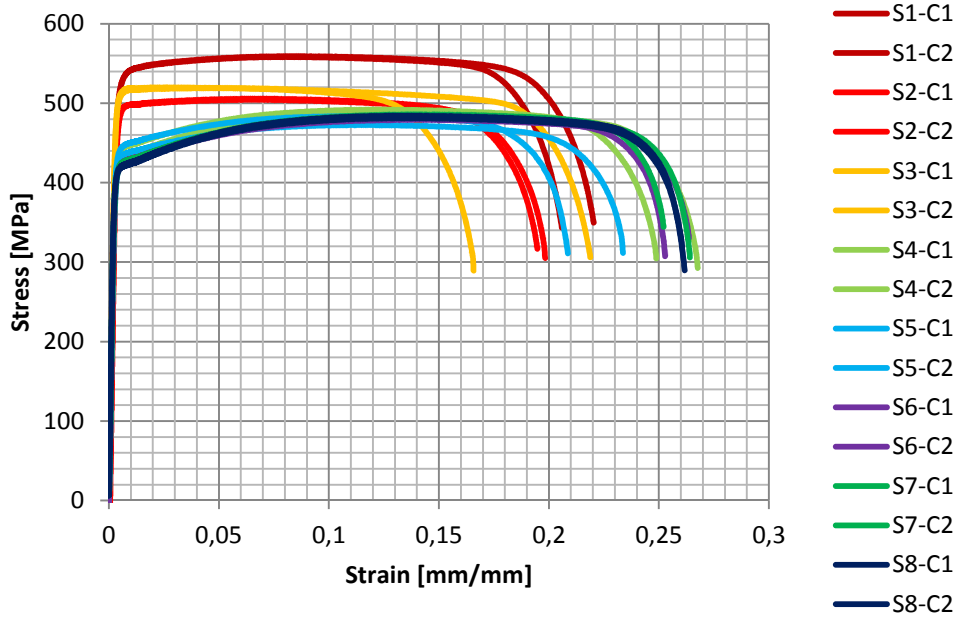

Figure 49. Flat tensile coupon tests results

The following table 33 presents some values that can be of interest for later analysis: $\sigma_{0.2}$ (proof stress corresponding to a 0.2% plastic strain), σ_u (ultimate strength) and ε_u (ultimate strain).

Table 33. Measured tensile material properties of test specimens

Cross-Section	Corner tensile coupon test			Flat tensile coupon test		
	$\sigma_{0.2}$ (Mpa)	σ_u (Mpa)	ε_u (mm/mm)	$\sigma_{0.2}$ (Mpa)	σ_u (Mpa)	ε_u (mm/mm)
S1-80x80x4-C1	310	646	0.0100	291	558	0.0803
S1-80x80x4-C2	240	643	0.0107	271	559	0.0846
S2-60x60x3-C1	310	583	0.0100	337	504	0.0682
S2-60x60x3-C2	328	590	0.0095	250	506	0.0691
S3-80x40x4-C1	225	603	0.0096	340	519	0.0482
S3-80x40x4-C2	279	598	0.0086	350	520	0.0242
S4-120x80x3-C1	357	578	0.0076	325	487	0.1261
S4-120x80x3-C2	305	587	0.0120	333	492	0.1252
S5-60x60x2-C1	330	571	0.0075	327	484	0.1076
S5-60x60x2-C2	327	564	0.0086	297	473	0.1170
S6-70x50x2-C1	260	576	0.0113	322	479	0.1372
S6-70x50x2-C2	276	573	0.0113	314	480	0.1379
S7-80x40x3-C1	372	580	0.0105	324	484	0.1385
S7-80x40x3-C2	486	611	0.0055	320	486	0.1473
S8-100x40x2-C1	228	578	0.0117	340	481	0.1344
S8-100x40x2-C2	480	580	0.0081	334	484	0.1316

It is important to highlight that as expected, values for $\sigma_{0.2}$ are higher for the corner coupons than for the flat ones due to the higher level of cold-work present in these areas. However, the ultimate strain ε_u of these corner coupons is also lower than for the flat specimens, showing the typical loss in terms of ductility for these types of cross-sections. For the flat coupons, it is also shown that the ones that showed higher stress-strain curves (80x80x4, 60x60x3 and 80x40x4) are the ones which present a higher level of cold-worked, being the ones with higher thicknesses.

5.2 Measuring the geometry

This section will explain how the different geometric parameters were measured from the elements prior to testing. These geometric parameters include: dimensions of cross-sections, dimensions of elements and initial local imperfections. Table 34 shows the different cross-sections that are going to be tested (8 overall). Elements for each type of test have different lengths, but their geometrical measurements were done in the same way.

Table 34. Nominal dimensions of the cross-section

Name	Width (mm)	Depth (mm)	Thickness (mm)
S1	80	80	4
S2	60	60	3
S3	80	40	4
S4	120	80	3
S5	60	60	2

Table 34. Nominal dimensions of the cross-section

Name	Width (mm)	Depth (mm)	Thickness (mm)
S6	70	50	2
S7	80	40	3
S8	100	40	2

When elements arrived to the laboratory had not been cut yet, they only had the cross-section dimensions that had been looked for. Although elements were made to be cut by professional technicians, and cross-sections seemed to have the required dimensions, there are always little imperfections and it is a common practice, before carrying out the test, to verify the dimensions and to measure these possible little imperfections.

To measure the lengths of each element was used a measuring tape with an accuracy of +/- 1mm. The elements that were going to be used for stub-column test were supposed to have a length of three times its larger cross-section dimension (see table 35). Two lengths were measured, one on the width face and the other one on the depth face.

Table 35. Nominal stub-column experimental test lengths

Dimensions	SC-Length(mm)	Dimensions	SC-Length(mm)
S1-80x80x4	250	S5-60x60x2	180
S2-60x60x3	180	S6-70x50x2	210
S3-80x40x4	250	S7-80x40x3	240
S4-120x80x3	360	S8-100x40x2	300

To verify the cross-section's dimensions (width, depth, thickness and radius) was used a Vernier caliper with +/- 0.1 mm accuracy. Two measurements were done in order to check each width and depth values (one on each extreme of the element), but for the radius and thickness four measurements were done, one for each face and corner (respectively) of the element. Stub-column elements prior to testing can be appreciated in Fig. 50.

Figure 50. Experimental campaign elements

Once all the dimensions were measured and verified, the next step was to measure the longitudinal imperfections. The result of it can be used to introduce the imperfection's amplitude in the computer simulation model. It can also be used to prove equations or models that try to predict imperfection's amplitude. To measure these longitudinal imperfection was used a machine that had a linear variable differential transformer (LVDT). The element was fixed on the machine adjusting the LVDT (which needed to be calibrated for each beam) on one of the faces of the element. Then, the machine, by moving the element front and rear, stored the longitudinal profile into a digital file that contained all element imperfection data.

Fig. 51 shows the machine for stub-column imperfections measurements. As can be appreciated on the right side of Fig 51, the data obtained from the LVDT was shown through a computer screen in order to verify if the measurements obtained were logical and was no need to calibrate again the LVDT. This process was a bit slow because of the accuracy needed: vibrations or an excess of velocity could make that LVDT did wrong readings.

Figure 51. Stub-column's imperfection measurement

The measured dimensions of all the specimens are gathered in Table 36, where: L is the total length of the specimens defined as at least three times the width of the widest plate element of the cross-section, as established in EN 1993-1-3 (2006)., H is the total depth, B is the total width, t is the thickness, R is the exterior radius and ri is the interior radius.

Table 36. Measured dimensions for the stub columns specimens

Cross-Section	L [mm]	H [mm]	B [mm]	t [mm]	R [mm]	ri [mm]
S1-80x80x4-C1	249.8	79.9	79.9	3.8	8.6	4.8
S1-80x80x4-C2	250.0	79.9	79.9	3.8	8.9	5.1
S2-60x60x3-C1	179.8	60.3	60.2	2.9	6.6	3.8
S2-60x60x3-C2	180.0	60.1	60.1	2.9	6.3	3.4
S3-80x40x4-C1	249.5	39.9	80.0	3.9	7.6	3.7
S3-80x40x4-C2	249.0	40.0	80.0	3.9	7.6	3.8
S4-120x80x3-C1	359.5	79.7	119.7	2.9	7.0	4.1
S4-120x80x3-C2	359.5	79.7	119.9	2.9	6.6	3.7
S5-60x60x2-C1	180.1	60.0	60.1	1.9	5.5	3.6
S5-60x60x2-C2	179.8	59.9	59.9	1.9	5.3	3.3
S6-70x50x2-C1	210.0	49.9	70.1	2.0	4.3	2.3
S6-70x50x2-C2	210.0	49.8	70.0	2.0	4.2	2.2
S7-80x40x3-C1	249.9	39.9	79.9	3.0	7.5	4.6
S7-80x40x3-C2	250.1	40.0	79.9	2.9	7.4	4.4
S8-100x40x2-C1	300.5	40.1	99.9	1.9	6.1	4.1
S8-100x40x2-C2	300.2	40.1	100.1	2.0	6.2	4.1

5.3 Elements instrumentation: strain gauges

Before testing the elements, it is necessary to prepare them by adding some strain gauges where it is thought the local buckling is more likely to occur (it can't be assured where it will happen). The paragraphs below explain what a strain gauge is and how it works.

A strain gauge is a device used to measure strain on an object. The gauge is attached to the object by a suitable adhesive. As the object is deformed, the foil is deformed, causing its electrical resistance to change. This resistance change is related to the strain by the quantity known as the gauge factor (the ratio of relative change in electrical resistance, to the mechanical strain).

The strain gauge takes advantage of the physical property of electrical conductance and its dependence on the conductor's geometry. On the one hand, when an electrical conductor is stretched within the limits of its elasticity such that it does not break or permanently deform, it will become narrower and longer, changes that increase its electrical resistance end-to-end. On the other hand, when a conductor is compressed such that it does not buckle, it will broaden and shorten, changes that decrease its electrical resistance end-to-end.

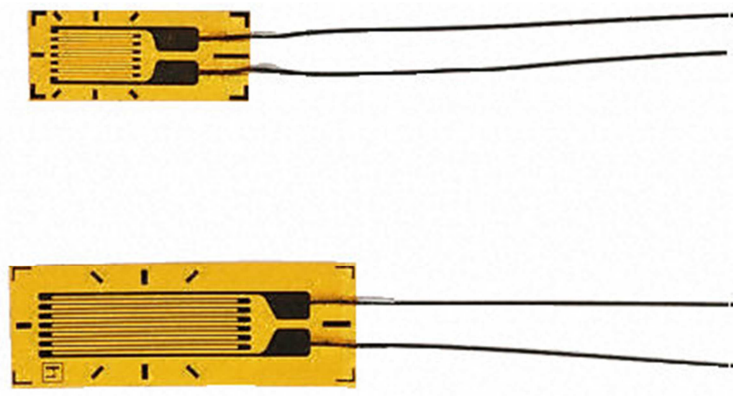

Figure 52. Strain gauges

The positions where gauges are going to be placed are in the middle of each element (see Fig. 53 location of strain gauges). A total of 8 gauges were fixed to square hollow section (Fig. 54) and 4 gauges to the rectangular ones (Fig. 55). For SHS, as is not known a priori in which face the local buckling will occur, every face was covered with two gauges at its middle zone. For RHS, as the buckle is likely to occur in the largest and more slender face of the cross-section, only 4 gauges were necessary, 2 on each face.

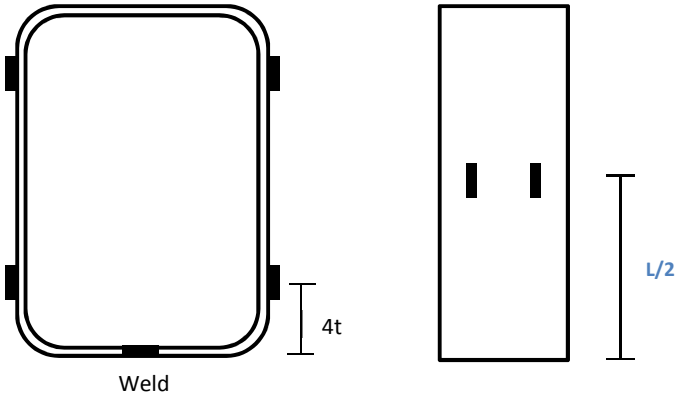

Figure 8. Location of strain gauges for RHS specimens

Before positioning the gauges on the element, it was needed to sand the surface of the element where the gauge was going to be placed on. If the surface where the gauge is fixed is irregular, the lectures will not be realistic.

After the sanding step, it is time to stick the gauges on the element surface. The process followed was first of all to clean the surface with alcohol, spread a little film of adhesive on the rear side of the gauge, and then slowly place it on the surface. To accurately place the gauge in its position, little linear marks were done to the surface of the object. Looking at the lineal references that have all gauges drawn (see Fig. 54 and 55), the aim is to make both lineal marks and references concur.

Once the gauge is placed properly, it is needed to fix the cables that are loose (the stretch of the cables that emerge from the gauge) and protect the cupper part of them from the surface of the element with insulating tape in order to not have problems with the gauges readings.

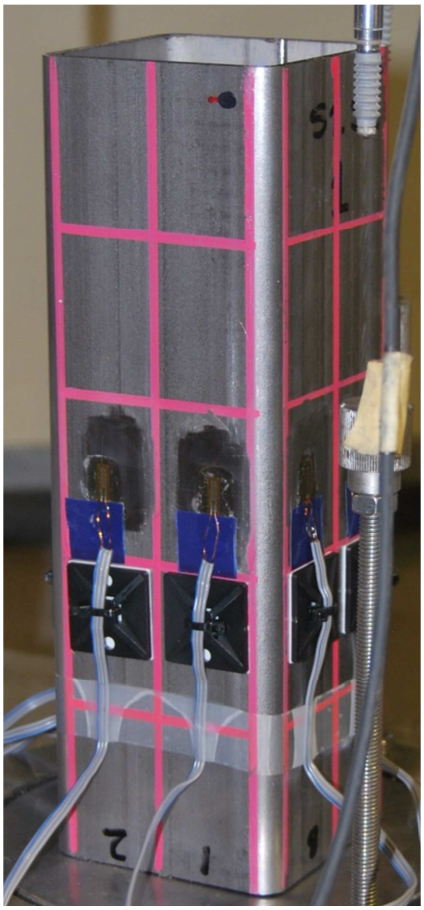

Figure 54. SHS gauges position (8 gauges)

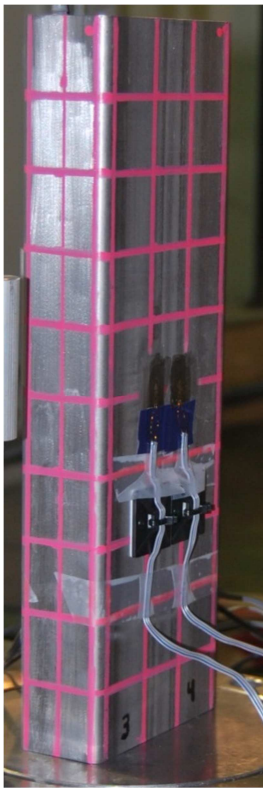

Figure 55. RHS gauges position (4 gauges)

Once all gauges are placed, elements are prepared to be tested.

5.4 Stub-Column: experimental test

The machine used to carry out this test is a dynamic axial test machine with 4 columns frame and +/- 1000 KN actuator, which bran and model are: INSTRON 8805 (Fig. 56). The control system includes two channels for input and control. This device shares with the INSTRON 8803 machine a data acquisition system of 8 channels for dynamic tests.

Figure 56. INSTRON 8805 testing machine

The process to test an element was the following one:

1-The element was put centred on the base of the machine (Fig. 57).

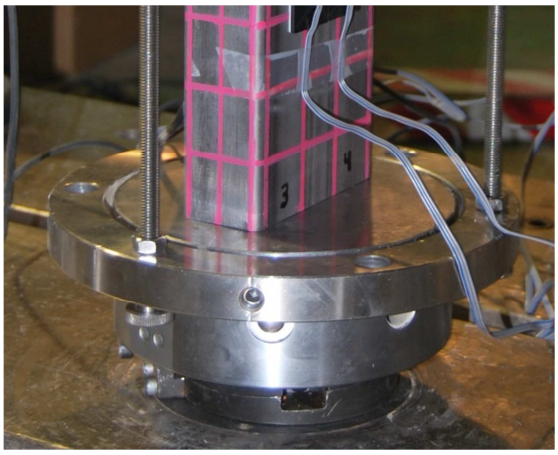

Figure 57. Centring the element on the base of the machine.

2-The upper part of the machine that compresses the element was put closer to the upper face cross-section of the element but without any contact (see Fig. 58).

3-Then, were adjusted the three LVDT in order define the plane (three points) which the machine will work with. It is important to adjust them well because is the reference that the machine uses to push and compress the element. If they were badly adjusted, an accident could happen with the element flying off the original position. Fig. 58 shows two of three LVDT adjusted. The LVDT also permits the measurement of the end shortening of the element.

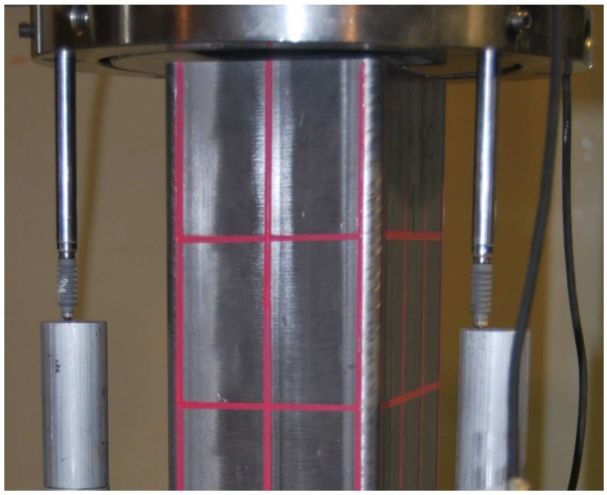

Figure 58. Machine positioning and LVDT adjustment

4-Then, using the computer, the machine was finally adjusted to the upper face of the element. After closing security doors and plugging in cable gauges to the input device, the test was ready to begin.

Before testing any element, it was necessary to prove that the test would work properly. If any element had been tested without making sure it and the test had gone wrong, it would have been lost an element to test. These verifications were done with elements without interest for the programme, which had no strain gauges on them (see Fig. 59).

Figure 59. Check of the functionality of the test

After finishing the test, the element was observed visually in order to contrast with data results. It could happen that there was an error during the process, if we store the test data without contrasting “a priori” them, we could have wrong results. It was observed the part of the element where the buckling took place and was decided if gauges data was or not outstanding. For example, in Fig. 60 the buckle did not happen where the gauges were placed.

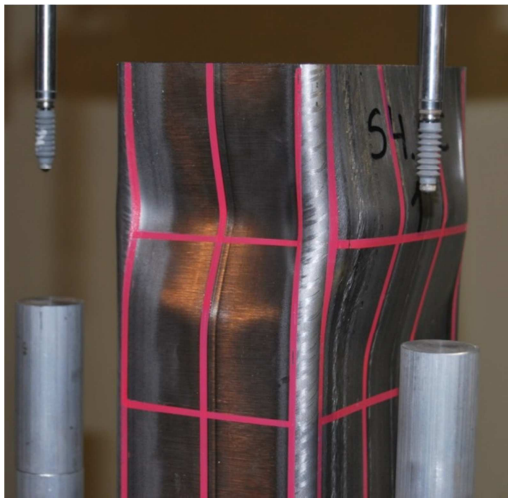

Figure 60. Buckled part of the element

It is important to mention that the tests were done under displacement control: the machine did little increments of deformation per unit of time. The value of this test rate was: 0.5mm/min.

5.5 Experimental Results

After treating obtained data, the following Fig. 61 shows the results obtained:

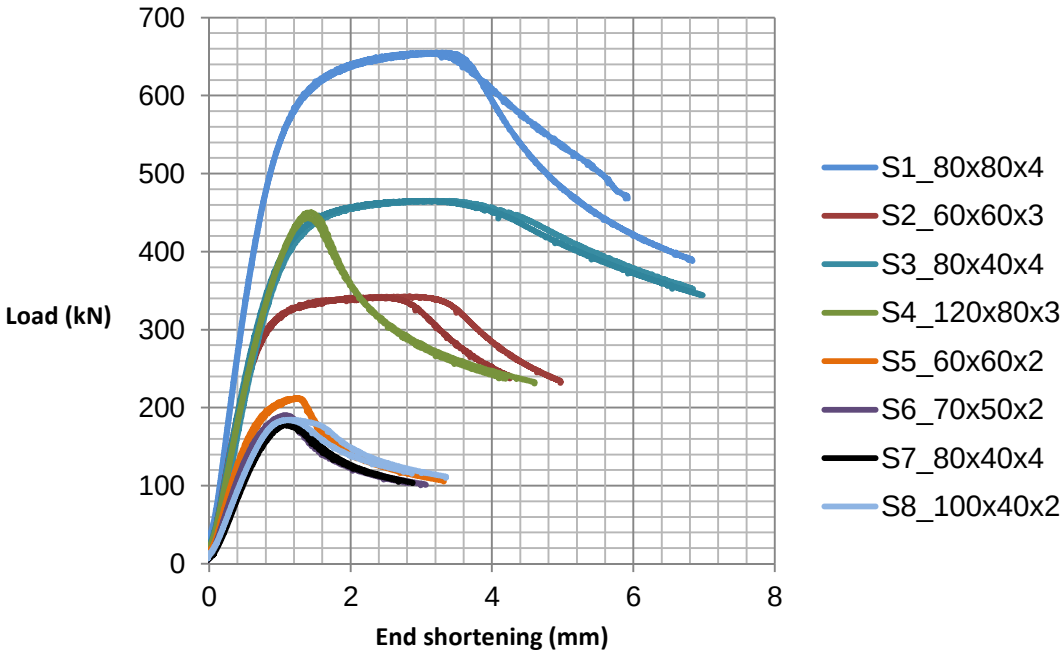

Figure 61. Experimental data results

For each cross-section two tests were conducted. The results are shown above with the same load-end shortening curve colour. Table 37 present the ultimate axial compression load measured in the tests.

Table 37. Stub-column ultimate compression load

Element Dimensions	Ultimate Load (KN)
S1-80x80x4-C1	654.6
S1-80x80x4-C2	655.3
S2-60x60x3-C1	342.6
S2-60x60x3-C2	342.8
S3-80x40x4-C1	465.2
S3-80x40x4-C2	465.1
S4-120x80x3-C1	443.1
S4-120x80x3-C2	450.4
S5-60x60x2-C1	211.3
S5-60x60x2-C2	212.2
S6-70x50x2-C1	190.1
S6-70x50x2-C2	190.1
S7-80x40x3-C1	178.1
S7-80x40x3-C2	179.4
S8-100x40x2-C1	184.4
S8-100x40x2-C2	184.1

The results of the ratios obtained after comparing these experimental results with the numerical and analytical ones are shown in table 38. Only S1, S2, S3, S4 and S6 can be compared since these are the cross-sections that each one has its analogous cross-section studied with the numerical model (S3, S7, S2, S6 and S8, respectively).

Table 38. Stub-column ultimate compression load comparison

Element Dimensions	$N/N_{experimental}$		
	Analytical		Numerical
	EN 1993-1-4	CSM	FEM
S1-80x80x4-C1	0.59	0.63	0.70
S1-80x80x4-C2	0.59	0.63	0.70
S2-60x60x3-C1	0.64	0.68	0.75
S2-60x60x3-C2	0.64	0.68	0.75
S3-80x40x4-C1	0.61	0.67	0.76
S3-80x40x4-C2	0.61	0.67	0.76
S4-120x80x3-C1	0.85	0.84	0.95
S4-120x80x3-C2	0.83	0.83	0.93
S6-70x50x2-C1	0.78	0.78	0.87
S6-70x50x2-C2	0.78	0.78	0.87
Average	0.69	0.72	0.80
Covariance	0.152	0.112	0.116

As it can be appreciated, FEM results are closer to the experimental ones. It is logical because ratios that were calculated in section 4.2 (comparing analytical results with numerical ones) were lower than one. It can be concluded that FEM is conservative referred to experimental ones, and analytical results are conservative referred to numerical ones and so to FEM ones.

6. Conclusions

In this section are gathered all relevant conclusions that have been extracted along this research project.

When it comes to global valorations, in the case that the numerical ultimate loads have been normalized by the Continuous Strength Method (CSM) predictions and plotted together with the aforementioned interaction expressions in order to assess their applicability, it is demonstrated that the consideration of the CSM fundamental capacities in the expressions proposed in EN 1993-1-4, Eq. 15 is the best approach for the prediction of the combined loading capacity of the studied cross-sections, providing safe and accurate results. On the other hand, when the numerical ultimate loads have been normalized by the EN 1993-1-4 basic resisting predictions and plotted together with the aforementioned interaction expression in order to assess its applicability, it is demonstrated that using this method, results are too conservative (far away from the interaction equation) in comparison with the graphs normalized by the CSM predictions.

From the comparative ratios, it can be concluded that the best solution and the more reliable one is to use the CSM for basic resistances and as interaction expression the one included in EN 1993-1-4. Even though the two interaction expressions proposed by Theofanous [25] present better results on average, there are many cases that the ratio exceeds the unit, which means that results are overestimated. More specific conclusions for every of the analysed loading types are presented as follows:

a) For stub-column and uniaxial bending tests, the CSM approaches better the numerical solution than EN 1993-1-4. S4 is the cross-section that presents worse analytical results in both tests. This can be explained by the following reason: as S4 is the only section that does not accomplish the restriction on the normalised deformation capacity and needs to be applied an ε_{csm} modification.
b) For uniaxial combined loading, the case that evaluates the EN 1993-1-4 interaction equation (Eq. 11 and 12) with CSM values for the simple resistances (Eq. 33 and 34) provides the best results. There is no cross-section with issues to remark.
c) For Biaxial bending test, the best results are show by Theofanous [25] equations. S6 presents results too conservative for Theofanous [25] interaction equation, S4 has the same problem for EN1993-1-4 interaction equation (with CSM basic resitances) and S8 undergoes this problem for all interaction equations.
d) For biaxial combined loading tests, the best results are show by EN 1993-1-4 interaction expression (with CSM basic resistances). Even though on average EN 1993-1-4 results are worse than the ones presented by the two Theofanous [25] interaction equations, this last method overestimates the results for some of the cross-sections studied.

With the results obtained during the experimental programme, it can be concluded that FEM stub-column results are conservative referred to experimental ones, which means that numerical models seem to be calibrated properly. Finally, analytical results are conservative referred to numerical ones and so to FEM ones.

7. References

[1] Stainless steel phase diagram figure. Recovered from http://www.gowelding.com/met/diss.html

[2] Stainless steel RHS & SHS figure. Recovered from http://www.alibaba.com/product-detail/MS-ERW-Black-Rectangular-And-Square_523489751.html

[3] American Society of Civil Engineers & Structural Engineering Institute Specification for the Design of Cold-Formed Stainless Steel Structural Members. 2002. Reston, Virginia. ISBN 0-7844-0556-5.

[4] EN 1993-1-4 European Committee for Standardization Eurocode 3. Design of steel structures. Part 1-4: General rules. Supplementary rules for stainless steels. Brussels, Belgium. 2006.

[5] Arrayago, I. Comportamiento estructural de vigas de acero inoxidable ferrítico frente a cargas concentradas. Barcelona 2011. UPC.

[6] Ramberg, W. & Osgood, W.R. Description of stress-strain curves by three parameters. National Advisory Committee for Aeronautics. Technical Note No. 902. 1943. Washington, D.C., USA.

[7] Hill, H.N. Determination of stress-strain relations from "offset" yield strength values. National Advisory Committee for Aeronautics. Technical Note No. 927. 1944. Washington, D.C., USA.

[8] Mirambell, E. & Real, E. On the calculation of deflections in structural stainless steel beams: an experimental and numerical investigation. Journal of Constructional Steel Research 2000, 4, Vol. 54, No. 1, pp. 109-133. ISSN 0143-974X. doi: DOI: 10.1016/S0143-974X(99)00051-6.

[9] Rasmussen, K.J.R. Full-range stress–strain curves for stainless steel alloys. Journal of Constructional Steel Research 2003, 1, Vol. 59, No. 1, pp. 47-61. ISSN 0143-974X. doi: DOI: 10.1016/S0143-974X(02)00018-4.

[10] Gardner, L. & Ashraf, M. Structural design for non-linear metallic materials. Engineering Structures 2006, 5, Vol. 28, No. 6, pp. 926-934. ISSN 0141-0296. doi: DOI: 10.1016/j.engstruct.2005.11.001.

[11] Li, N. & Dong, W. Baosteel Ferritic Stainless Steel B445R for Architectural Applications. Stainless Steel Technology Center, Baosteel Research Institute, Baoshan Iron & Steel Co., Ltd., Shangai 200431, China.

[12] The ferritic solution. Properties, advantages and applications. The essential guide to ferritic stainless stee. International Stainless Steel Forum (ISSF). April 2007. ISBN 2- 930069-51-1.

[13] Price nickel evolution figure. Recovered from http://www.ariva.de

[14] Charles, J., Mithieux, J.D., Santacreu, P.O. & Peguet, L. The ferritic stainless Steel family: the appropriate answer to nickel volatility? ArcelorMittal Stainless, France, ArcelorMittal R&D, France. Helsinki 2008.

[15] EN 1993-1-1. Eurocode 3. Design of Steel Structures: Part 1-1: General rules and rules for buildings. 2005. CEN.

[16] EN 1993-1-3. Eurocode 3. Design of Steel Structures: Part 1-3: General rules - Supplementary rules for cold-formed members and sheeting.

[17] Gardner, L. & Theofanous, M. Discrete and continuous treatment of local buckling in stainless steel elements, Journal of Constructional Steel Research, Special Issue, International Stainless Steel Experts Semenar, Vol 64, No. 11, 2008.

[18] EN 1993-1-5. Eurocode 3. Design of Steel Structures: Part 1-5: Plated structural elements.

[19]Schafer, B. & Ádány, S. Buckling analysis of cold-formed steel members using CUFSM: conventional and constrained finite strip methods. In: The 18th international specialty conference on cold-formed steel structures; 2006. p. 39–54.

[20] Seif, M. & Schafer, B.W. Local buckling of structural steel shapes. Journal of Constructional Steel Research 2010; 66 (10): 1232–47.

[21] Schafer, B.W. Review: the direct strength method of cold-formed steel member design. Journal of Constructional Steel Research 2008; 64 (7): 766–78.

[22] Afshan, S. & Gardner L. The continuous strength method for structural stainless steel design. Thin-Walled Structures 68 (2013) 42–49.

[23] Gardner, L., Wang, F. and Liew, A. Influence of strain hardening on the behaviour and design of steel structures. International Journal of Structural Stability and Dynamics 2011;11(5):855–75.

[24] Liew, A. & Gardner, L. ultimate capacity of structural steel cross-sections under combined loading. Imperial College London, Department of Civil and environmental Engineering. South Kensington Campus, London, SW7 2AZ, UK.

[25] Theofanous, M., Liew, A. & Gardner, L. 2012. Ultimate capacity of stainless steel RHS subjected to combined compression and bending. In: Proceedings of the 14th International Symposium on Tubular Structures, London, UK, 423–430.

[26] S4R mesh element figure. Recovered from http://www.emeraldinsight.com/journals.htm?articleid=1800776

[27] ArcelorMittal. Stainless Tubes Europe. Tubos en Acero inoxidable. Ancerville, France 2008

[28] Stala Tube catalogue. Recovered from http://www.stalatube.com

[29] Gardner, L., Saari, N. and Wang, F.. 2010. Comparative experimental study of hot-rolled and cold-formed rectangular hollow sections, Thin-Walled Structures, Vol:48, ISSN:0263-8231, Pages:495-507.

[30] Talja, A. & Salmi, P. Design of stainless steel RHS beams, columns and beam-columns. Technical research centre of finland. ESPOO 1995.

[31] EN ISO 6892-1. 2009. Metallic materials - Tensile testing - Part 1: Method of test at room temperature. Brussels: European Committee for Standardization (CEN).